

**Genetic cornerstones of grain yield determination
in spike-branching wheat
(*Triticum turgidum* L.)**

Dissertation

zur Erlangung des
Doktorgrades der Agrarwissenschaften (Dr. agr.)

der

Naturwissenschaftlichen Fakultät III
Agrar- und Ernährungswissenschaften,
Geowissenschaften und Informatik

der Martin-Luther-Universität
Halle-Wittenberg

vorgelegt von

Herrn M.Sc. Ragavendran Abbai

Geb. am: 09.12.1993 in Salem, Tamil Nadu, India

Gutachter:

- 1) Prof. Dr. Thorsten Schnurbusch (IPK)
- 2) Prof. Dr. Cristobal Uauy (JIC)

verteidigt am 10.06.2024 in Halle (Saale)

*To my supervisors & fellow scientists who inspired me,
To my family & friends who kept me sane*

Table of contents

Acknowledgments	v
1. Introduction	1
1.1 Evolution of wheat in the wild and under agriculture	4
1.2 Grain yield formation in wheat.....	6
1.3 Major genetic and genomic resources in wheat.....	10
1.4 Principles of recombination-based genetic mapping and fine mapping for studying complex traits	12
1.5 Connecting ecology, evolution and genetics for enhancing grain yield..	15
1.6 Aims of the current thesis	22
2. Materials and Methods	24
2.1 Mapping population	24
2.1.1 TRI 984 x CINRO RILs	24
2.1.2 TRI 19165 x Bellaroi RILs	25
2.1.3 Zavitan introgression lines in Svevo background	25
2.2 Genotyping and linkage map construction (TRI 984xCIRNO RILs)	25
2.3 Examining plant and spike architectural traits	26
2.3.1 Greenhouse conditions	26
2.3.2 Simulated canopy shade (based on our earlier study, Golan et al., 2023).....	26
2.3.3 Field conditions.....	27
2.3.3.1 TRI 984 x CIRNO RILs.....	27
2.3.3.2 Bellaroi x TRI 19165 RILs	28
2.4 Phenotype-based scoring for spike-branching and flag leaf senescence rate.....	30
2.5 Phenotypic and Genetic analyses	30
2.6 Analysis of rachis internode vascular architecture	31
2.7 Data availability	31
2.8 Data contribution by the author and the collaborators for the present thesis.....	31
3. Results	33
3.1 Spike-branching TRI 984 has lower grains per spikelet and thousand-grain weight than CIRNO	33
3.2 Population development, genotyping, and linkage map construction	35
3.3 Grains per spikelet and thousand-grain weight are associated with senescence rate	38
3.4 Grain yield trade-offs in ‘Miracle-Wheat’	40

3.4.1 The <i>bh^t-A1</i> locus underlies sink and source capacity	42
3.4.2 <i>bh^t-A3</i> , a novel spike-branching locus on Chr 5A reshapes source-sink dynamics	42
3.4.3 <i>GPC-B1</i> is the major determinant of senescence rate and thousand-grain weight	47
3.4.4 Specific additive and epistatic interactions may increase yield potential in spike-branching genotypes	50
3.5 The genomic regions associated with spike length affect grain size	52
3.5.1 Re-confirmation of <i>QSL.ipk-4AL</i> in TRI 19165 x Bellaroi recombinants	56
3.5.2 Wild emmer introgressions within <i>QSL.ipk-4AL</i> QTL interval affects spike length	57
3.5.3 High-resolution mapping of the <i>QSL.ipk-4AL</i> QTL	59
3.5.4 The ancestral allele enhanced grain yield per spike in the greenhouse	61
4. Discussion	65
4.1 Balancing Grain yield trade-offs in ‘Miracle-Wheat’	65
4.2 Implications of rachis internode length <i>per se</i> on grain yield determination in wheat	68
5. Outlook	72
5.1 Integrating reductionist approach and genomic selection might improve grain yield gains in spike-branching wheat	72
5.2 Identification and functional characterization of the gene underlying <i>QSL.ipk-4AL</i>	74
6. Summary	77
7. Zusammenfassung	78
8. References	80
9. Appendix	95
10. Abbreviations	127
11. Curriculum Vitae	128
12. Eidesstattliche Erklärung/Declaration under Oath	131

Acknowledgments

I can still vividly remember the day over a decade ago when I discovered my passion for becoming a 'plant doctor (scientist)', making efforts to understand and customize crop plants for human use. Now, it feels more than real that I'm closer than ever before to start realizing this dream.

First and foremost, I express sincere gratitude to my supervisor, Prof. Dr. Thorsten Schnurbusch, for providing me this opportunity to conduct doctoral research in his vibrant Plant Architecture research group (PBP) at the Leibniz Institute of Plant Genetics and Crop Plant Research (IPK), Gatersleben, Germany, since August 2019. His constant encouragement and guidance were instrumental in the successful completion of this project and also in shaping my scientific thinking. Besides, I was trained in peer review of manuscripts, proposal writing, and supervising a Master's student, among others. My last 4+ years at the Plant Architecture group were filled with exciting scientific learnings and wonderful memories that I will cherish for the rest of my life.

Next, I heartfully thank Dr. Guy Golan for all his valuable scientific insights and advice on addressing various challenges during my PhD research; his positive and friendly personality was a source of inspiration and moral support, for which I'm very grateful. My sincere thanks to Prof. Dr. Nils Stein for his guidance and suggestions as my mentor. I would like to thank apl. Prof. Dr. Friedrich Longin and Prof. Dr. Assaf Distelfeld for the productive collaborations that strengthened the outcome of this project. I extend my deepest thanks to all the current and former members of the Plant Architecture research group for the fruitful discussions and their friendship.

As my research involved large-scale field experiments, I especially thank the technicians of the PBP group: Franziska Backhaus, Corinna Trautewig, Kerstin Wolf, Sonja Allner, Ellen Weiss, Ingrid Marscheider, and Angelika Püschel for their excellent support over the years. Special thanks to Roop Kamal, a fellow doctoral student, for her valuable advice in finalizing the field design. I'm very thankful to Peter Schreiber, Enk Geyer, and the team of gardeners for managing the field and greenhouse operations.

Notably, the majority of my research was conducted during the COVID-19 pandemic. I want to thank all those involved in maintaining institutional safety regulations, because of whom it was possible to carry out all the planned experiments in such difficult times.

My heartfelt thanks to Mrs. Bianka Jacobi for helping me with all the administrative requirements. She has a very positive approach to tackling various challenges; in the last 4 years, I always left her office with a smile. Likewise, I'm very grateful to Dr. Britt Leps for her valuable support and advice on conducting productive PhD research at the IPK, organizing various useful workshops that strengthened my soft skills, and also for her help with administrative tasks.

I appreciate the friendship of various people at IPK, including the Indian community, for beautiful memories. I thank my long-time friend, Dr. Nandhakumar Shanmugaraj, who recently completed his PhD in the same group. During the 12 years of our friendship, Nandha has always had my back, providing valuable scientific and non-scientific insights, especially during my PhD time here in Germany.

Finally, I thank my family for their love, unwavering support, and motivation to pursue my dreams. I conclude with a favorite quote that inspires me every day:

“This world is the world of possibilities. There is, of course, every possibility of a possible event, but the most wonderful thing is that there is also the possibility of an impossible event becoming possible.”

- Pujya Shri Ram Chandraji Maharaj of Fatehgarh
(Fondly known as 'Lalaji Maharaj')

1. Introduction

The introduction of semi-dwarf varieties and improved agronomic practices dramatically increased grain yield in wheat and rice during the Green Revolution. Since then, timely advances such as molecular marker systems, genome sequencing platforms, genomic selection, and speed breeding furthered yield gains in various crops (Hickey *et al.*, 2019; Varshney *et al.*, 2021). However, the alarming increase in the global human population from 6.4 billion in 2003 to 7.7 billion in 2019 led to a 10% decrease in the international per-capita cropland area (Potapov *et al.*, 2022). Moreover, about 2.4 billion people (29.6% of the total population) were moderately or severely food insecure in 2022, which is 4.3% more than the pre-COVID-19 pandemic levels in 2019 (FAO *et al.*, 2023). The prevalence of such hunger cases is the most severe in Africa (60.9%), followed by Latin America (37.5%) and Asia (24.2%) (Figure 1.1). With an estimated global population of 10 billion people by 2025, immediate research interventions are necessary to increase the productivity of staple food crops.

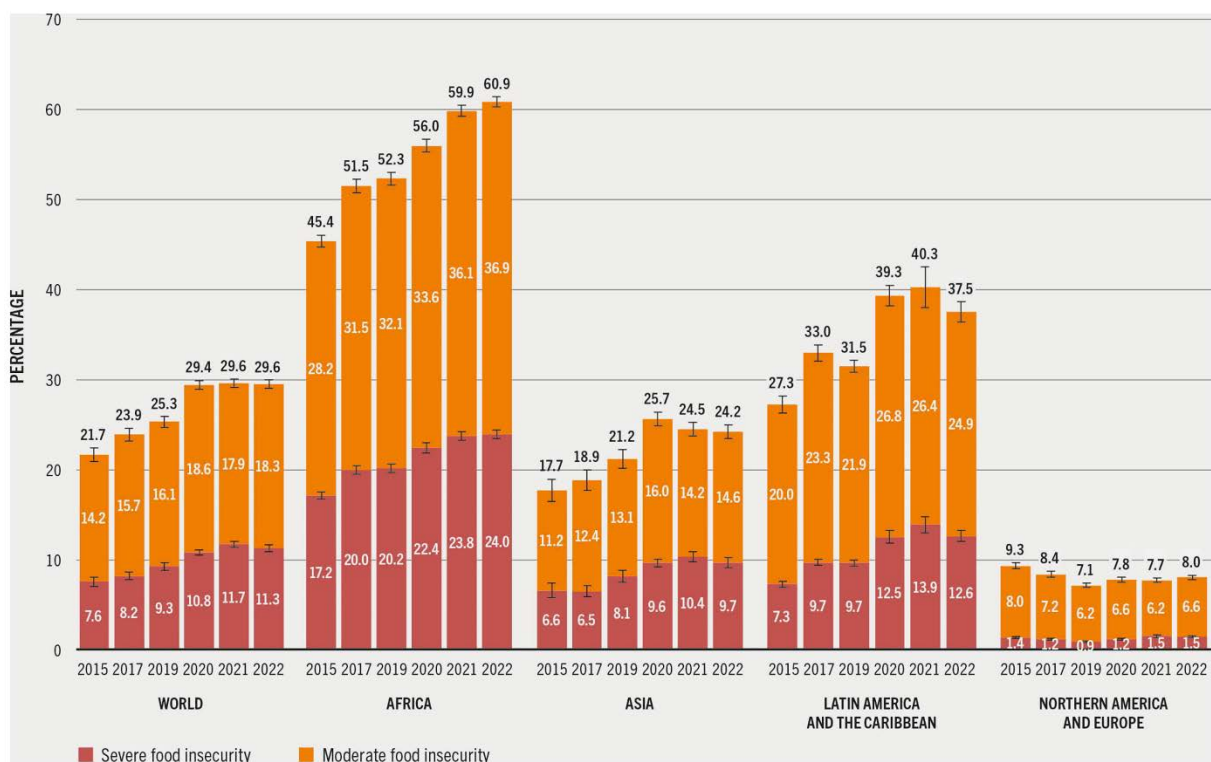


Figure 1.1 Trends in global severe and moderate food insecurity levels from 2015 to 2022. Source: FAO. 2023. FAOSTAT: Suite of Food Security Indicators. In: FAO. 2023. www.fao.org/faostat/en/#data/FS

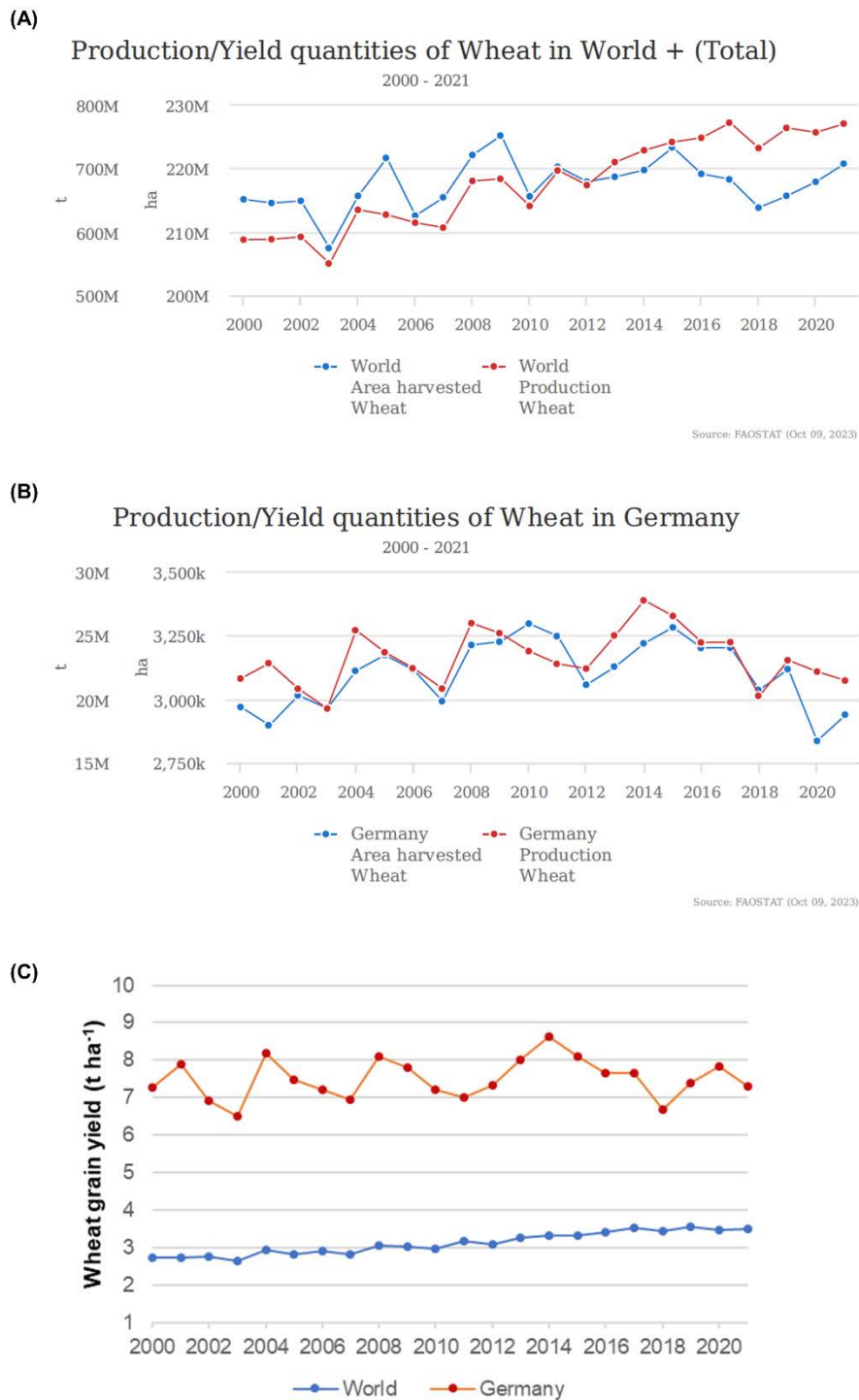


Figure 1.2 Wheat is a global staple food crop. (A-C) Wheat cultivation and production trends worldwide and in Germany.

Source: FAOSTAT 2023: <https://www.fao.org/faostat/en/#data/QCL>

Cereals were the leading type of primary crops produced (32%) in the previous two decades (FAO 2022). Maize (*Zea mays* L.), wheat (*Triticum* sp.), and rice (*Oryza sativa* L.) are the major staple cereal crops that predominantly contribute to global food security. The production of these essential crops has considerably increased from 2000-2021; maize production has doubled since 2000, while rice and wheat had growth rates of +32% and +31%, respectively, since 2000 (FAO 2022). Among these crops, wheat occupied the largest cultivation area, spanning over 220 million hectares in diverse favorable and marginal agroecological zones (Figure 1.2A). Wheat belongs to the Triticeae tribe along with barley (*Hordeum vulgare* L.) and rye (*Secale cereale* L.), and wheat-based products are consumed by over 2.5 billion people across various countries. The hexaploid wheat used for making bread and pastries is the predominantly cultivated wheat, while only 5% constitutes tetraploid durum wheat, which is used for pasta and couscous making (Dubcovsky and Dvorak, 2007; Mastrangelo and Cattivelli, 2021).

Germany was the seventh largest wheat producer in 2021 (21.45 million tonnes) with one of the highest productivity levels viz., 7.3 tonnes per hectare ($t\ ha^{-1}$), which is two times more than the global average (Figure 1.2B, C and FAOSTAT 2023). The global data displayed an increasing trend – from $2.73\ t\ ha^{-1}$ in 2000 to $3.49\ t\ ha^{-1}$ in 2021, while in Germany, grain yield was somewhat fluctuating between 6.5 to $8.63\ t\ ha^{-1}$ over the last 22 years, which might be attributed to the changing climate. Surprisingly, Germany's current wheat productivity level is highly similar to what was recorded in 2000 (Figure 1.2C and FAOSTAT 2023), possibly implying a yield plateau. A similar conclusion pointing to the occurrence of a wheat yield plateau in the high-yielding Northwest European ecosystem, including Germany, was previously indicated (Grassini *et al.*, 2013). Interestingly, (Senapati *et al.*, 2022) estimated the presence of a 51% genetic yield gap in wheat [genetic yield gap is the difference between genetic yield potential (yield of a simulated ideotype based on available genetic diversity) and the potential yield of the leading local cultivar], thus indicating the importance of capitalizing on the untapped diversity from wheat genebanks to break the yield barrier.

The following sections summarize key aspects of wheat's evolution as a global crop, factors affecting wheat grain yield, advances in wheat genetics and genomics, and the concept of agroecological genetics and genomics, among others, finally leading to the objectives of the current thesis.

1.1 Evolution of wheat in the wild and under agriculture

The story of wheat evolution started about 7 MYA (million years ago) with the divergence of A and S+B+T lineage from a common ancestor (Marcussen *et al.*, 2014; Levy and Feldman, 2022 and references therein). Then, A and B genomes combined to give rise to a new diploid species, *Aegilops tauschii*, about 5.5 MYA (Figure 1.3 and (Marcussen *et al.*, 2014)). Before ~0.8 MY, the A and B subgenomes hybridized once again, however, this resulted in an allotetraploid *Triticum turgidum* ssp. *dicoccoides*, the wild-emmer wheat (Figure 1.3 and (Marcussen *et al.*, 2014)). The analysis of successful hybrids derived from *T. turgidum* ssp. *durum* x wild-emmer wheat (Tschermak, 1914; Percival, 1921) and genome sequencing (Avni *et al.*, 2017; Maccaferri *et al.*, 2019) confirmed wild emmer wheat as progenitor of the domesticated tetraploid wheat. Likewise, genetic and cytogenetic experiments confirmed that, *Ae. tauschii* is the D genome donor (Mcfadden and Sears, 1946). Moreover, genomic analysis revealed that hybridization between ancestral donors of the A and B genomes ~5.5 MYA resulted in the D genome (Marcussen *et al.*, 2014; Jia *et al.*, 2013; Luo *et al.*, 2017; Zhao *et al.*, 2017). *Ae. tauschii*, in turn, hybridized with a primitive tetraploid wheat (BBAA) ~9,000-8,500 YA to result in allohexaploid wheat, *T. aestivum* (BBAADD). The knowledge on the actual domesticated free threshing tetraploid wheat that hybridized with *Ae. tauschii* still remains elusive; however, the free threshing *T. turgidum* ssp. *parvicoccum* with non-brittle rachis, which was cultivated ~9,000 YA (Kislev, 1980) in the Fertile Crescent (now extinct), might be a plausible donor of the BBAA genomes (Levy and Feldman, 2022).

Primary components of the domestication syndrome i.e., traits that enabled wheat cultivation, include non-brittle rachis and free threshing habit. (Nalam *et al.*, 2006) reported that homoeologous loci on Chr 3A and Chr 3B affected rachis brittleness in tetraploid wheat; *Brittle Rachis 1* (*Btr-1*) was found to control shattering in wild emmer and its loss of function alleles, *btr-A1* and *btr-B1* gave rise to non-brittle rachis in domesticated wheat (Avni *et al.*, 2017). Mutations in both homeoalleles are required to achieve complete non-brittleness (Avni *et al.*, 2017), consistent with the non-shattering phenotype's gradual evolution (Kislev, 1984; Tanno and Willcox, 2006). However, a wild emmer accession, TD-1320-11 from Southern Levant carried both the nonfunctional *btr-A1* and *btr-B1* alleles that is present in all the domesticated wheat, implying that these non-functional alleles might have possibly originated in the same

population and the importance of southern Fertile Crescent in emmer domestication (Nave *et al.*, 2019).

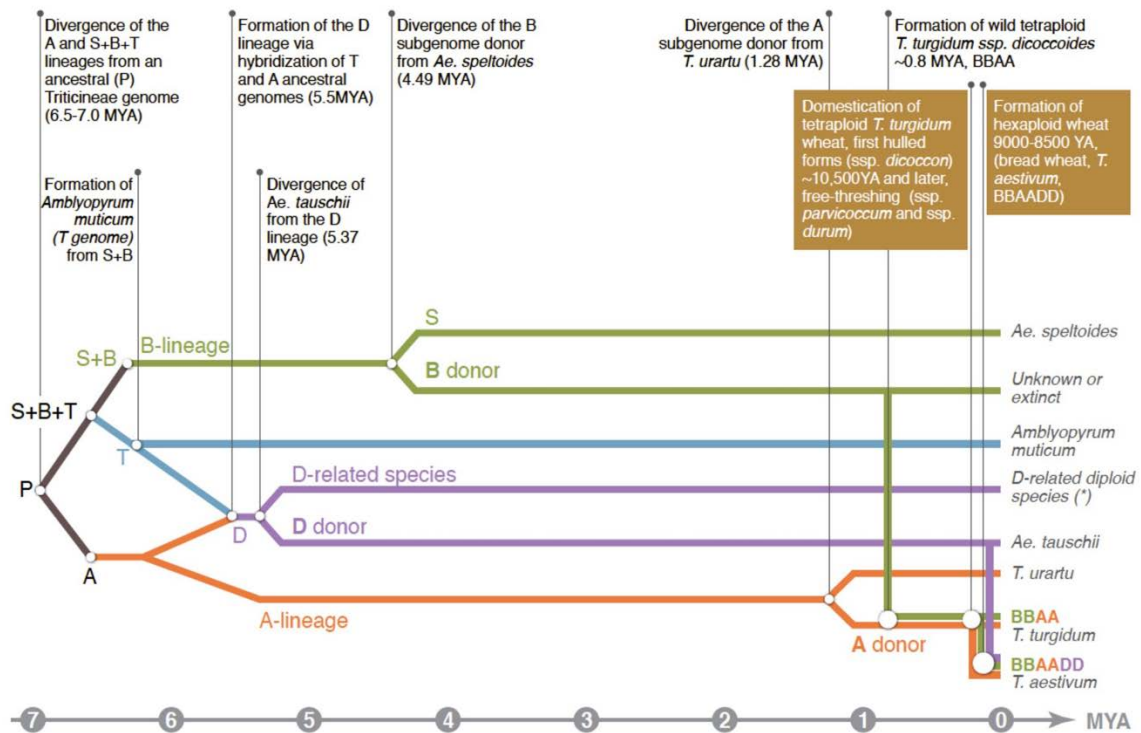


Figure 1.3 Major events in wheat evolution. Hybridization between two diploid species *viz.*, a species very similar to *Triticum urartu* (A genome donor; male) and another which is related to *Aegilops speltiodes* (B genome donor; female) resulted in the formation of tetraploid wild-emmer wheat (*Triticum turgidum ssp. dicoccoides*) about 0.8 MYA. Then, ~9,000 YA *Ae. tauschii* (D genome donor; male) combined with allotetraploid wheat (B and A subgenomes; female) to give rise to the allohexaploid wheat (*T. aestivum*). Source: Image is taken from (Levy and Feldman, 2022).

Q locus mapped on Chr 5 AL was found to be a key contributor to the free threshing attribute, another important domestication trait (Sears, 1954; (Faris *et al.*, 2003). It encodes an AP2-like transcription factor (Simons *et al.*, 2006), and mutation in the miRNA 172 binding site resulted in a relatively abundant transcription of the domesticated Q allele (Debernardi *et al.*, 2017; Greenwood *et al.*, 2017). The Q locus also has pleiotropic effects on many traits, which is detailed in Section 4.2 of the thesis. Apart from Q, *tenacious glume* (*Tg*) locus was also found to contribute to threshability; however, it was previously shown that mutations in Q, *tg-A1*, and *tg-B1* are essential for the completely free threshing phenotype and that Q had the most significant effect among them (Sharma *et al.*, 2019). Thus, the accumulation of these mutations led to the free threshing trait in the modern durum (Q, *tg-A1*, *tg-B1*) and bread wheat (Q, *tg-*

A1, *tg-B1*, *tg-D1*). Other domestication-related changes include transition to relatively erect plant stature and reduction in seed dormancy. Besides, preferential selection of the nonfunctional *grain protein content* (*gpc-B1*) allele (Uauy *et al.*, 2006a; Uauy *et al.*, 2006b) and reduced functional *grain number increase* (*gni-A1*) allele (Sakuma *et al.*, 2019; Golan *et al.*, 2019) may explain the increase in grain size and grain number respectively during wheat domestication and breeding. Although wheat is a recently domesticated crop, faster mutation rates and the buffering action due to allopolyploidy is believed to have played a significant role in its success as a global crop (Dubcovsky and Dvorak, 2007). Moreover, because of the additional subgenome, hexaploid wheat is better adapted to photoperiod *viz.*, *PHOTOPERIOD 1* (*Ppd-A1*, *Ppd-B1*, *Ppd-D1*) (Díaz *et al.*, 2012; Shaw *et al.*, 2012) and vernalization requirements *viz.*, *VERNALIZATION 1* (*Vrn-A1*, *Vrn-B1*, *Vrn-D1*) (Shaw *et al.*, 2012; Trevaskis *et al.*, 2003; Yan *et al.*, 2003), thus, enabling its widespread cultivation. Further, the selection of semi-dwarf *Reduced height 1* (*Rht-B1* and *Rht-D1*) mutant alleles that exhibit reduced responses to gibberellin (Peng *et al.*, 1999) substantially increased grain yield in the 1960s-70s (Green Revolution). But what are the factors that determine grain yield in wheat? The following section provides a brief overview of this aspect.

1.2 Grain yield formation in wheat

Wheat inflorescence – ‘Spike’ is a determinate structure harboring the grain-bearing spikelets on its rachis in a distichous pattern (Figure 1.4). The transition of the shoot apex from vegetative to reproductive phase involves the formation of two ridges on the elongated apex, reaching the double ridge stage *viz.*, the upper ridge is the spikelet primordium that continues to differentiate into various floral organs, while the lower ridge is a leaf primordium that eventually degenerates (Bonnett, 1966; Moncur, 1981; Waddington *et al.*, 1983; Kirby and Appleyard, 1984). Depending on the genotype, vernalization (winter types) and longer day length (photoperiod sensitive) might be necessary for a successful shift to the reproductive phase and subsequent flowering (Hyles *et al.*, 2020 and references therein). Following the double ridge stage, glume primordia appear as ridges (glume primordium stage), flanking the most advanced spikelet meristem at the middle part of the apex (and later in other parts of the spike), after which lemma and floret primordia begin to develop (Kirby and Appleyard, 1984). The formation of the terminal spikelet indicates the completion of the spikelet initiation phase. The duration between the double ridge and terminal spikelet stage affected the

total number of spikelets (Rawson, 1970). After the terminal spikelet stage, the floral organs continue to develop further, resulting in the maximum number of floret primordia close to the green anther stage. However, the tip of the rachilla then starts to degenerate along with a few distal floret primordia, and eventually, the final floret number is determined at about anthesis (Kirby and Appleyard, 1984; Guo and Schnurbusch, 2015; Guo et al., 2016). In summary, during immature spike development, the inflorescence meristem gives rise to multiple spikelet meristems in an acropetal manner; each spikelet meristem (indeterminate) produces florets that potentially form grains (Kirby and Appleyard, 1984; Koppolu and Schnurbusch, 2019).

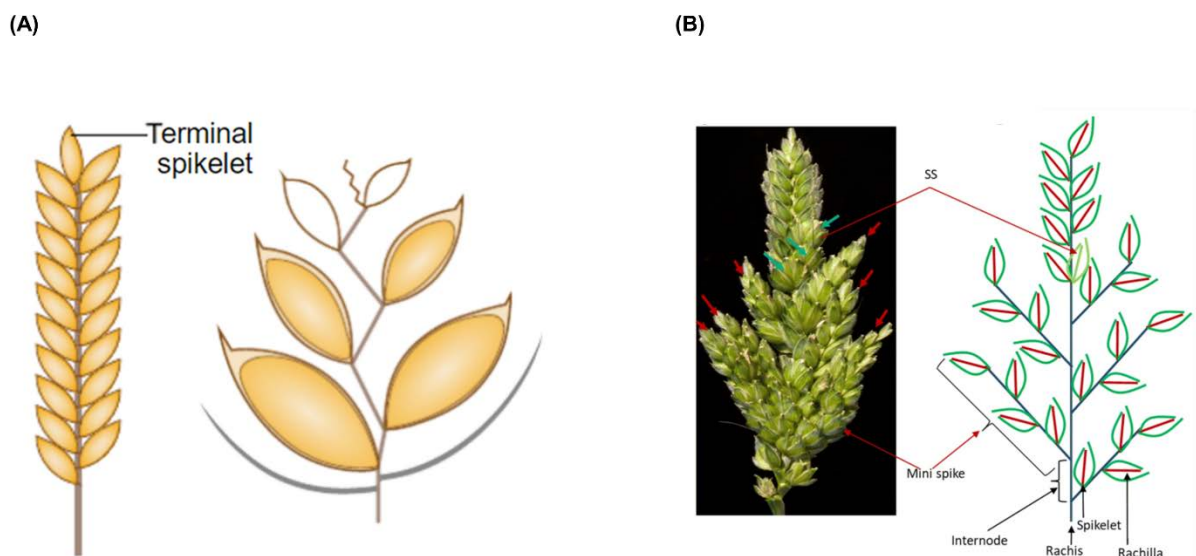


Figure 1.4 Wheat inflorescence architecture. (A) The standard non-branching inflorescence with a terminal spikelet (determinate spike); but indeterminate spikelet meristem leading to multiple florets, some of which produce grains. (B) 'Miracle-wheat' exhibits an altered inflorescence architecture, where the spikelet meristem identity is compromised, leading to lateral branches, significantly increasing the number of spikelets. Source: Images are taken from (A) (Sakuma and Schnurbusch, 2020) and (B) (Wolde et al., 2019a).

However, some exceptions deviate from this standard developmental programme, such as the 'Miracle-Wheat' that produces a non-canonical spike with lateral branches instead of spikelets. In the case of *Triticum turgidum* convar. *Compositum* (L.f.) Filat. accessions, the spikelet meristems lose their identity and determinacy while partially behaving as inflorescence meristems, producing lateral branches or multiple spikelets per rachis node due to mutation in the DNA-binding domain of the *branched head^t* (*bh^t*) allele, encoding an APETALA2/ETHYLENE RESPONSIVE FACTOR (AP2/ERF) transcription factor (Poursarebani et al., 2015). Similarly, in hexaploid wheat, variations for supernumerary spikelet formation were also found for the wheat *FRIZZY PANICLE*

(*WFZP*) (Dobrovolskaya *et al.*, 2015), *Ppd-1* (Boden *et al.*, 2015), *TEOSINTE BRANCHED1 (TB1)* (Dixon *et al.*, 2018), and *HOMEBOX DOMAIN-2 (HB-2)* (Dixon *et al.*, 2022). While branching spikes have considerably higher yield potential, i.e., more spikelet number, they often suffer from grain weight trade-offs, as observed in the tetraploid 'Miracle-Wheat' (Poursarebani *et al.*, 2015). Moreover, despite the increase in overall grain number per spike, spikelet fertility (grains per spikelet) decreased in response to spike-branching (Wolde *et al.*, 2021).

A large body of evidence suggests that wheat grain yield is an outcome of multiple trait-trait interactions (Figure 1.5) mediated by developmental, physiological and environmental factors across the entire lifespan, although some stages are more critical than others (Brinton and Uauy, 2019; Guo *et al.*, 2017; Guo *et al.*, 2018a; Guo *et al.*, 2016; Guo *et al.*, 2018b; Murchie *et al.*, 2023; Reynolds *et al.*, 2022; Slafer *et al.*, 2023). They can broadly be classified as source and sink strength related, which jointly determine a particular genotype's assimilate production and reallocation potential. Typically, green tissues of the plant – both foliar (leaves) and non-foliar (peduncle, spikes) are the photosynthesizing organs that act as 'source' for resource generation (Chang *et al.*, 2022; Molero and Reynolds, 2020). In the pre-anthesis phase, assimilates are partitioned to both vegetative biomass establishment and developing spikes – that determine the overall yield potential (Fischer, 2011; Slafer, 2003). The inflorescence architecture, *viz.*, spikelet number per spike, floret number per spikelet, carpel size, rachis length, etc., are determined before anthesis (Brinton and Uauy, 2019; Kirby and Appleyard, 1984). For instance, the ovary size during flowering regulated floret and grain survival in a panel of 30 wheat genotypes (Guo *et al.*, 2016). Likewise, the duration of leaf initiation, spikelet initiation, and stem elongation period influenced spike fertility in bread wheat (Roychowdhury *et al.*, 2023). The source strength is often characterized by radiation use efficiency (RUE), i.e., the ability for light interception and biomass production (Acreche and Slafer, 2009; Molero *et al.*, 2019). However, the balance between the resources allocated to the 'vegetative vs. reproductive' tissues largely dictates the yield potential (Dreccer *et al.*, 2014; Ferrante *et al.*, 2013), a trait that has been under selection throughout the history of wheat breeding. The deployment of semi-dwarf *Rht-1* alleles ('green revolution' gene) significantly increased the harvest index and the grain number per unit area, possibly by enhancing the flow of assimilates (as the stem length is considerably reduced) to the juvenile spikes (Fischer and Stockman, 1986; Slafer *et al.*, 2023). However, other

strategies might currently be required to further the resource allocation to early spike development as the semi-dwarf *Rht-1* allele is already a selection target (Peng *et al.*, 1999). Increasing the harvest index in the genotypes with high biomass (more robust source) might enhance grain yield (Sierra-Gonzalez *et al.*, 2021). Overall, the source strength from the terminal spikelet stage to anthesis determines grain number and contributes to grain size in wheat.

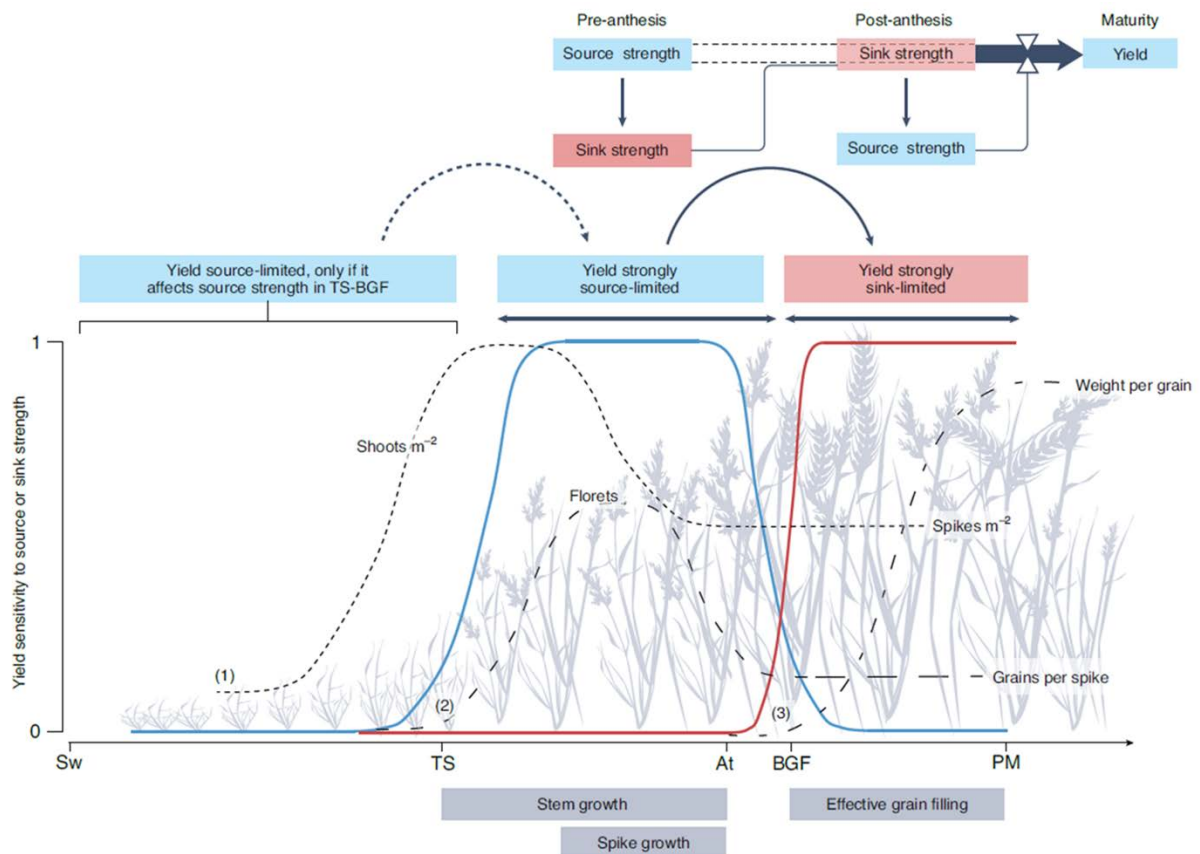


Figure 1.5 The source and sink interplay across development determines grain yield in wheat. The efficiency of source activity before anthesis (yield construction phase) affects resource partitioning to the developing inflorescence, playing a vital role in sink number determination. Then, the sink strength influences the source activity during grain filling (yield determination phase). Sw: sowing, TS: terminal spikelet; At: anthesis; BGF: beginning of grain filling; PM: physiological maturity. Source: Image is taken from Reynolds *et al.*, 2022.

After anthesis, the initiation of senescence in the foliar, but also non-foliar tissues, drives extensive re-mobilization of resources into the developing grains; previous studies indicated that flag leaf and spike photosynthesis contribute to most of the assimilates during the grain filling phase (Distelfeld *et al.*, 2014; Molero and Reynolds, 2020). Hence, a delayed senescence resulted in extended photosynthesis (functional stay-green), leading to higher grain yield (Chapman *et al.*, 2021a; Christopher *et al.*, 2016; Hassan *et al.*, 2021; Kichey *et al.*, 2007; Li *et al.*, 2022; Yan *et al.*, 2023).

Recently, mutation in *CO₂ assimilation and kernel enhanced 2 (cake2)* locus, encoding *ASPARTIC PROTEASE 1 (APP-A1)*, was found to delay senescence rate with a positive effect on grain weight (Niu *et al.*, 2023). However, the effect of delayed senescence in wheat is inconsistent; for instance, prolonged photosynthesis influenced grain yield attributes only under low nitrogen conditions (Derkx *et al.*, 2012; Gaju *et al.*, 2011). The *GPC-B1* locus encoding *NO APICAL MERISTEM (NAM)*, a *NAC* transcription factor that is the primary regulator of senescence rate in wheat (Uauy *et al.*, 2006a); but, despite a 40% increase in flag leaf photosynthesis, the *NAM* RNAi wheat lines had no advantage in grain weight compared to the control plants (Borrill *et al.*, 2015). In addition, the stay-green phenotype of *gpc-A1* and *gpc-D1* mutants did not influence grain yield determinants (Avni *et al.*, 2014). However, (Chapman *et al.*, 2021a) reported that a novel *NAM-1* allele that delayed senescence was associated with a 14% increase in the final grain weight, possibly by enhancing resource remobilization. A plausible explanation for such discrepancies might be that grain yield in wheat is largely sink-limited (Lichthardt *et al.*, 2020; Reynolds *et al.*, 2005); the surplus water-soluble carbons that remain in the stem at physiological maturity supports this hypothesis (Serrago *et al.*, 2013). Thus, a higher sink capacity might be essential to capitalize on the extended photosynthetic period during the grain-filling phase (Lichthardt *et al.*, 2020). In this context, a reductionist approach that focuses on characterizing individual component traits might assist in a more profound understanding of source-sink dynamics but also be integrated to pin-point favorable combinations of alleles/haplotypes for improving wheat grain yield (Brinton and Uauy, 2019; Reynolds *et al.*, 2022). The following section summarizes vital resources developed by the global wheat community that can be used for such functional genetics and breeding research.

1.3 Major genetic and genomic resources in wheat

Recent advances in genome sequencing and assembly methods have resulted in the development of high-quality reference genomes for wild emmer wheat (Avni *et al.*, 2017), durum wheat (Maccaferri *et al.*, 2019), bread wheat (IWGSC, 2018) and a pangenome (Walkowiak *et al.*, 2020). The haplotype diversity across the wheat pangenome can be visualized using the haplotype browser (Brinton *et al.*, 2020); <http://www.crop-haplotypes.com/>), which enables exploring the genomic signatures that were selected during past wheat breeding efforts, but can also be used for the

rational design of future cultivars (Bevan *et al.*, 2017). In addition, the expVIP database (Borrill *et al.*, 2016; Ramírez-González *et al.*, 2018) comprises transcriptome data of 1K+ samples from 36 studies, where the spatiotemporal expression pattern of the gene(s) of interest can be retrieved.

Besides, various genotyping arrays such as the Illumina Wheat 9K iSelect SNP array (Cavanagh *et al.*, 2013), Illumina Wheat 90K iSelect SNP genotyping array (Wang *et al.*, 2014a), Axiom HD Wheat genotyping (820K) array (Winfield *et al.*, 2016), Wheat Breeders' 35K Axiom array (Allen *et al.*, 2017), Axiom Wheat 660K SNP array (Cui *et al.*, 2017) can assist linkage/association mapping and genomic selection experiments in wheat (Sun *et al.*, 2020 and references therein). Moreover, private service providers such as the SGS-TraitGenetics GmbH have developed proprietary (<https://sgs-institut-fresenius.de/en/health-nutrition/traitgenetics/genotyping>; link last accessed on 21.10.2023) Wheat 135K Axiom array, Illumina 25K array (subset of the 90K iSelect array, 35K Wheat Breeders array and 135K Axiom array) and Illumina 7K array (subset of the 25K array) for customized genotyping requirements.

Moreover, exome capture sequencing of 2,735 EMS (ethyl methanesulfonate) induced Cadenza (hexaploid) and Kronos (tetraploid) TILLING (Targeting Induced Local Lesions in Genomes) mutants revealed at least one premature stop codon or a missense mutation in over 90% of the wheat genes (Krasileva *et al.*, 2017). Recently, ~4.3M mutations in the promoter region were documented in the Kronos EMS mutants (Zhang *et al.*, 2023). The sequence information and the seeds of these mutants are publicly available, thus supporting functional analysis of a candidate gene. Furthermore, 50 genotyped (90K iSelect array) wild emmer introgression lines in an elite durum (Svevo) background (Bacher *et al.*, 2021), thousands of wild and domesticated accessions from CIMMYT and ICARDA genotyped by DArT-seq (Sansaloni *et al.*, 2020), global durum wheat panel (Mazzucotelli *et al.*, 2020; genotyped by 90K iSelect array) and tetraploid global wheat collection genotyped using 90K iSelect array (Maccaferri *et al.*, 2019) are some of the major genetic resources available for functional research in tetraploid wheat. Similarly, valuable genetic resources are also available in the case of hexaploid wheat (Adamski *et al.*, 2020 and references therein).

Taken together, effective integration of these resources can now accelerate molecular genetics research to improve polyploid wheat, a crucial crop for food security (Adamski

et al., 2020; tutorials for using major wheat resources are available at <https://www.wheat-training.com/>).

1.4 Principles of recombination-based genetic mapping and fine mapping for studying complex traits

Genome-wide association mapping (GWAS) and linkage-based mapping are the frequently used approaches to explore quantitative variation of complex traits. GWAS capitalizes on the historical recombination and natural genetic diversity, while linkage analysis is based on the recombination within individuals developed from a common set of parental lines (Cortes *et al.*, 2021; Zhu *et al.*, 2008). As linkage-based QTL mapping is a major component of the current thesis, the details on various types of mapping populations, principles underlying linkage map construction, composite interval mapping, and fine mapping are mainly focused here.

The first step of linkage-based QTL mapping is the development of a mapping population. A bi-parental population, derived by crossing two parental lines such as recombinant inbred lines (RILs) comprising of an array of homozygous lines developed via single seed descent method, each representing a unique genetic combination of both the parents and doubled haploid (DH) population derived by chromosome doubling (works only in tissue culture friendly species) are commonly used for genetic mapping. Sometimes, an F₂ population can also assist in mapping; however, a replicated analysis is not possible due to its segregating nature (Collard *et al.*, 2005; and references therein). While a bi-parental population helps map reliable QTLs, it suffers from narrow genetic diversity, i.e., only two alleles segregate at any locus. Hence, a multi-parent population derived by inter-crossing diverse founder lines might be helpful. Nested association mapping (NAM) and multi-parent advanced generation inter-cross (MAGIC) are the widely used methods for developing a multi-parent population (Scott *et al.*, 2020). NAM involves crossing a common (recurrent) founder line with several diverse genotypes, from which RILs are generated; hence, this actually means generating a series of bi-parental populations using a common parent (Yu *et al.*, 2008a). On the other hand, in the MAGIC method, several founder parents are inter-crossed across several generations, after which they are selfed to develop RILs; thus, each MAGIC line consists of alleles from all the parents, creating a unique

genomic pattern of the founder parents (Huang *et al.*, 2015; Scott *et al.*, 2020; and references therein).

Then, the mapping population is genotyped. The molecular marker system continuously evolved, transcending from the laborious RFLP (restriction fragment length polymorphism) based markers to initially the PCR-based system such as RAPD (randomly amplified polymorphic DNA), AFLP (amplified fragment length polymorphism) and microsatellite markers (Schlötterer, 2004); however, the requirement of gel electrophoresis in these PCR based markers made genome-wide screening difficult, especially in a big population. Advances in genome sequencing technologies have enabled large-scale SNP (single nucleotide polymorphism) genotyping using the chip-based system and genotyping by sequencing (GBS) strategy, among others, which are primarily used in the recent times (Amiteye, 2021 and references therein). The availability of various wheat SNP arrays for population scale genotyping was described in the previous section. The third step is the construction of the linkage map. Based on the recombination frequency, the position, the marker order, and the genetic distance between them (measured in centimorgan, cM) is determined in the linkage map; tightly linked markers often co-segregate in the progeny, while a higher recombination rate is observed between the distantly located markers (Jones *et al.*, 1997). This genome-wide data is then used for constructing the linkage map based on the logarithm of odds (LOD) score (Risch, 1992), which is the ratio of linkage versus no linkage. The Haldane mapping function considers that a recombination event does not affect another one, and the Kosambi mapping function that hypothesizes the opposite are the primary methods used for calculating the genetic distance. Various software, such as MAPMAKER (Lander *et al.*, 1987) and JoinMap (Stam, 1993), can be used for developing a linkage map. The earliest wheat linkage maps were based on RFLP (Chao *et al.*, 1989; Liu and Tsunewaki, 1991) and microsatellite markers (Röder *et al.*, 1998), while later dense SNP-based maps (Maccaferri *et al.*, 2015; Wang *et al.*, 2014a) were developed.

Then, the final step involves identifying QTLs by performing genotype-phenotype linkage analysis. A maximum-likelihood method based simple interval mapping (SIM) initially points to a putative QTL position (Lander and Botstein, 1989), after which composite interval mapping (CIM) combines the outcome of SIM with regression analysis to determine the QTL interval (Jansen and Stam, 1994; Zeng, 1994); a typical

CIM outcome indicates the start, peak and end of a QTL based on LOD scores (Figure 1.6). QTL Cartographer (Basten *et al.*, 2002) and GeneStat (VSN International, Hemel Hempstead, UK) are some of the commonly used software for QTL mapping. However, the QTL interval mapped by CIM is generally a large genomic region and, hence, can harbor hundreds of genes. Therefore, individuals with contrasting alleles at the QTL are intercrossed to develop a sizeable segregating population for high-resolution mapping. The availability of reference genome(s) for various major crops, including wheat, has significantly reduced the time required to saturate the QTL interval with new markers to assist in fine mapping (Jaganathan *et al.*, 2020 and references therein). Genotyping the segregating population with additional markers spanning the interval (Figure 1.6) facilitates the identification of recombinants with a reduced interval and their corresponding phenotype, enabling fine mapping the QTL to a much smaller interval (e.g., 10-15 genes). Once the refined interval is established, the various available genomic and genetic resources in wheat can assist in identifying the underlying gene and causal polymorphism (Adamski *et al.*, 2020; also discussed in the previous section).

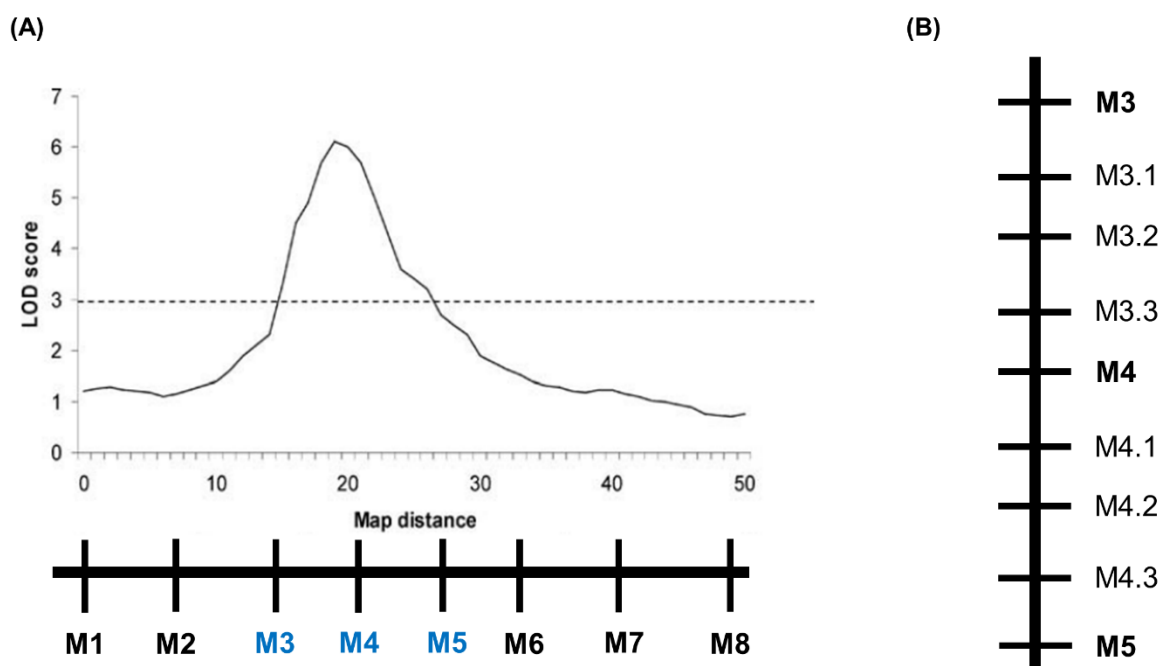


Figure 1.6 QTL mapping and fine mapping. (A) Determination of the initial QTL interval between “M3 and M5” based on composite interval mapping, after which the individuals carrying contrasting alleles at the QTL can be crossed to develop a larger segregating population for fine mapping. (B) Screening the resulting individuals with newly added markers between “M3 and M5” and then linking them with their corresponding phenotypic data can assist in narrowing down the QTL interval. When dealing with quantitative traits, it is crucial to ensure that only the QTL of interest is segregating in the fine mapping population; else, the

noise from the other QTL(s) in the background can affect the interpretation of the genotype-phenotype linkage in the recombinants. Source: The images are modified after ([Collard et al., 2005](#)).

1.5 Connecting ecology, evolution and genetics for enhancing grain yield

(Based on our paper, [Abbai et al., 2020](#), *Trends in Plant Science*)

Enhancing yield potential has always been the cornerstone of crop improvement. In a changing climate, its relevance for ensuring food-nutritional security is now higher than ever before. Over the years, timely technological developments ([Wallace et al., 2018](#)) enabled functional characterization and rapid deployment of key genes in crop breeding. Despite these advances, developing the ideal plant architecture based on target environment(s) and management practices is still largely unexplored. In fact, although proposed more than half a century ago, the ideotype concept (for favorable environment in high-planting density) that defined key attributes of a “communal plant” for a balanced performance, both as an individual and also in an optimized community ([Donald, 1968 and Figure 1.7](#)), has still neither been comprehensively tested nor realized ([Kokubun, 1988](#)). One primary bottleneck hindering further progress may be the presence of trade-offs among major yield component traits. For instance, grain number and thousand-grain weight are negatively related in wheat cultivars ([Sakuma and Schnurbusch, 2020](#)), as are increased panicle branching and reduced tillering in rice (*Oryza sativa*) ([Springer, 2010](#)) and also trade-offs resulting from variations in resource availability ([Weiner, 2019](#)). These scenarios clearly indicate that efforts to solely improve a single trait often risk compromising other traits and negating the desired selection effect. Considering agricultural production as a form of ecological engineering, i.e., the manipulation of populations, communities, and agroecosystems to satisfy fundamental human requirements, may therefore help in this context ([Denison, 2012](#)). Why? Because agricultural production is about populations, communities, and ecosystems. For example, crop yield per unit area is one of the most important quantity measures to determine productivity. This parameter is almost always attributed to the performance of a genetically homogeneous population in the field. For this reason, selection in crop breeding programs should rely largely on field performance under population or group selection, e.g., plot yield. But what are the decisive plant characters that make one population perform better than another? Often, the determinant is the presence or absence of ‘selfish’ plant behavior ([Denison, 2012; Weiner, 2019](#)).

'Selfish' behavior refers to plant traits that confer an advantage, increasing individual plant fitness; whereas the absence of 'selfishness' in a high-density population increases the overall community performance by cooperative use of available resources. Importantly, the loss of 'selfishness' in crop plants is often associated with reduced individual plant fitness, as seen, for example, in the selection of the tough rachis, or semi-dwarf wheat and rice crops during the Green Revolution (Denison, 2012; Weiner, 2019). Many native 'selfish' plant traits are therefore sub-optimal or even disadvantageous in a community context. This may be why the advantages breeding could achieve through selection for "yield" based on single plant (e.g. from F2 families) has plateaued over time. It is also clear that the agricultural plot as a selection environment behaves quite differently from habitats under natural selection (Wallace *et al.*, 2018); yet unconscious selection of less fit individuals may have improved adaptation to this human-customized environment (Denison, 2012; Weiner, 2019).

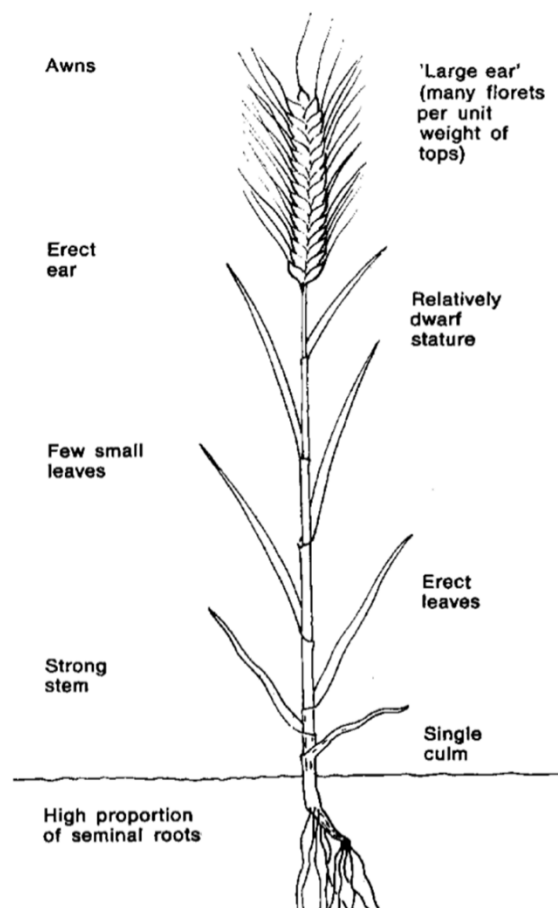


Figure 1.7 The Wheat ideotype as proposed by C.M. Donald, which is expected to perform better as a crop community in high planting densities. The concept of ideotype (ideal plant type with model characteristics) was proposed by Donald in 1967. He hypothesized that developing a semi-dwarf wheat plant type with a strong stem, single culm, few erect leaves, and large and erect ear would result in increased photosynthesis, better source to sink

transition, and, importantly, a weak competitor when planted in high density. Source: Image is taken from [Donald, 1967](#).

Similarly, to how humans have domesticated wolves (*Canis lupus*) to a highly diverse range of dog breeds, from cooperative companions and helpers to cuddly wimps, one might assume that domesticated plants have undergone similar drastic changes. In contrast, however, the overwhelming majority of today's staple cereal crops do not look very different from their wild ancestors (maize being an exception), suggesting that selection was not strong enough or directed incorrectly ([Weiner, 2019](#)), or perhaps most staple crop plant species are more resistant to radical changes.

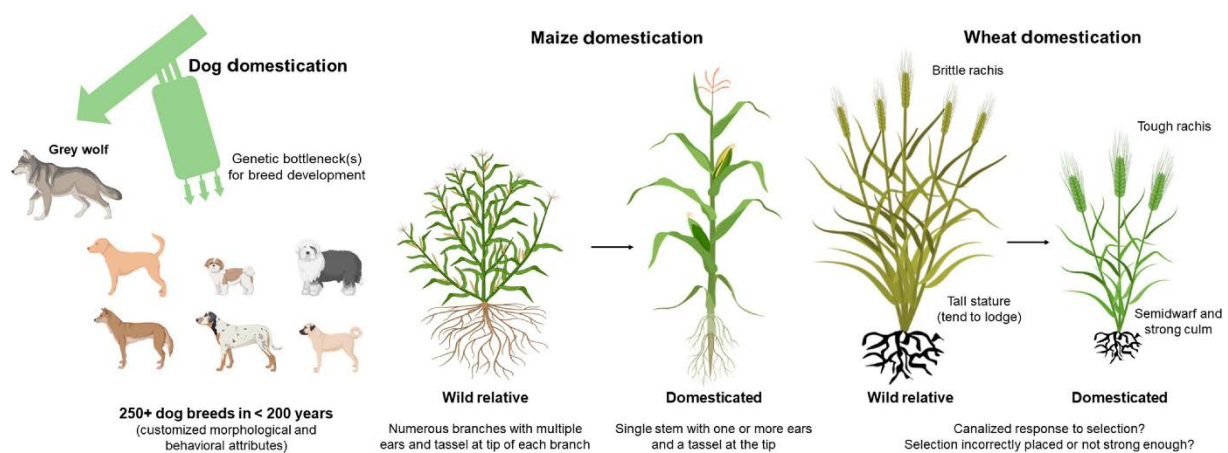


Figure 1.8 Understanding the factors influencing the response to human-induced selection might help in creating new variations and breaking the yield barrier. This figure was partly created using BioRender (<https://biorender.com/>). Source: Image is taken from [Abbai et al., 2020](#).

About two centuries of breeding dogs (domesticated from wolves 15,000-10,000 years ago) resulted in over 250 diverse breeds customized with distinct morphology and behavior to suit various human needs ([Ostrander et al., 2019](#)). To achieve this enormous diversity among dog breeds, strong selection (genetic bottle necks) in combination with inbreeding created pure breeding lines (dog breeds) with large genomic portions being fixed for specific trait combinations (conserved haplotypes), representing their 'genomic ideotypes' ([Ostrander et al., 2019](#)). Most staple food crops (domesticated during a similar timeline or even earlier than dogs) do not exhibit drastic transformations compared to their wild relatives (with few exceptions such as teosinte vs maize; [Figure 1.8](#)). Perhaps in these crops, selection was not strong enough or directed incorrectly. Or, in contrast to animals, plants might be highly developmentally canalized because they are sessile individuals which evolved to cope with erratic, local

environments. This may be why plants expanded their genomes with more genes (including polyploidization) as a consequence of natural selection. Moreover, in large crop plant genomes favorable alleles are often tightly linked to sub-optimal or deleterious alleles in the less recombining genomic regions (Wallace *et al.*, 2018), again favoring the plant's genomic resistance towards change. Precise gene editing, de novo synthesis or customizing meiotic recombination rate(s) might address some of these hurdles. In any case, the dog analogy exemplifies how powerful genetic approaches can work by molding an organism's genetic make-up to human-customized environments. Similarly, strong group selection in crop plants under genuine agroecological growth conditions and introducing new 'drastic' variations may provide useful genotypes with lowered 'selfishness'.

Crop selection since the Green Revolution has been rather tedious and time-consuming, with slow yield progress and frequent tradeoffs with other relevant traits, such as resistances, quality and nutritional value. In the future, recent technological advances may accelerate selection of reduced individual fitness but high field yield. But, what to select for, or against? In this context, one may have to consider two classes of 'selfish characters' that can be roughly defined as exterior or interior. Exterior characters, already well described by C. M. Donald (Donald, 1968 and Figure 1.7) for high-planting densities as well as well-fed growth conditions, reduce plant-plant competition while more efficiently utilizing common resources such as nutrients and light. They relate predominantly to plant architectural traits, such as a less neighbor-invasive root system, sturdy and short culm, low-tillering, erect leaves and a highly-fertile inflorescence. Although exterior characters are inherently measurable, surprisingly little research has been undertaken to create such 'idealized' genotypes for thorough hypothesis testing. Interior characters, on the other hand, are considerably less obvious features of crop plants and hence far less amenable to tracking, e.g. water and nutrient uptake and translocation efficiency – vascular architecture, source-sink and allometric growth relationships, root-to-shoot or organ-to-organ signaling, or radiation use efficiency in a canopy context (Figure 1.9). All of these interior characters are genetically highly complex (quantitative) and have not been resolved in any crop or model plant to date, mainly because this kind of trait behaves like a mechanistic or genetic 'black box'. Clarifying the genetic basis of interior traits might shed light into complex trade-offs such as the hormonal cross-talks that coordinate growth vs defense signaling; uptake and translocation of water vs minerals;

carbon partitioning between sink organs and vegetative parts (Sadras *et al.*, 2020) etc. Ultimately, recombining the exterior and interior characters in a balanced way while selecting under relevant agroecological growth conditions may be the key to high-yielding crop communities.

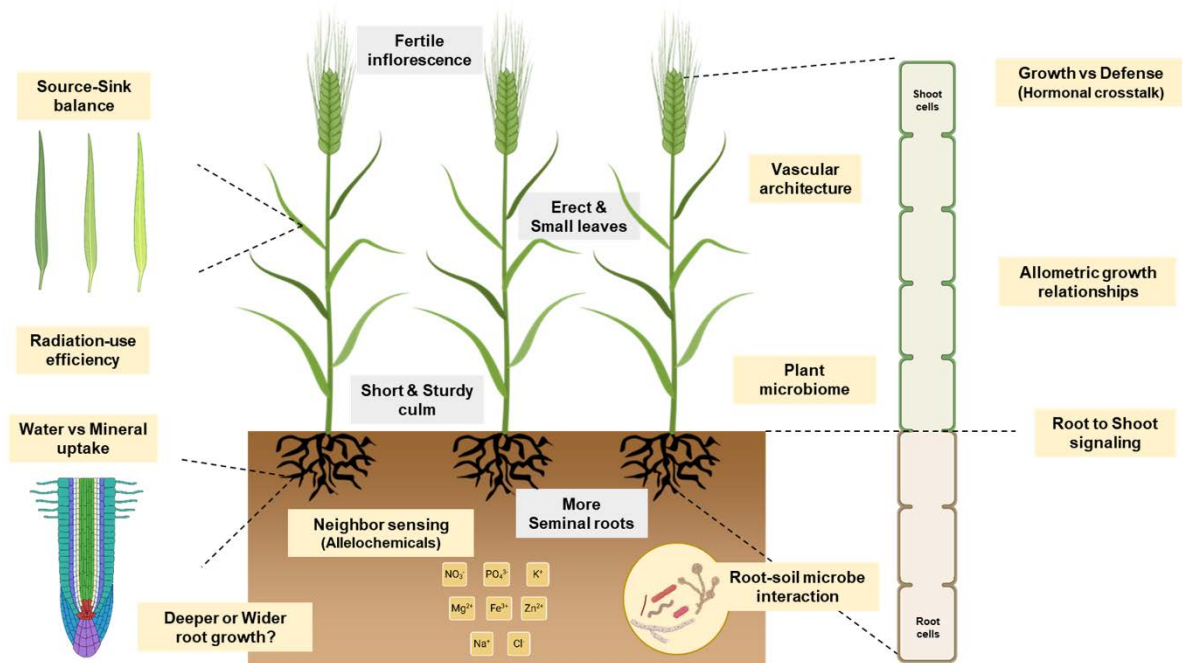


Figure 1.9 Exterior and the less explored Interior traits affect the final communal yield. The exterior traits defined by C.M. Donald are in grey boxes, while the interior traits (golden boxes) are primarily associated with resource production and remobilization including the vascular anatomy and allometric growth relationships of various organs in diverse environments at a community resolution. This figure was partly created by using BioRender (<https://biorender.com/>).

Despite grand progress in recent decades, specifically through basic insights from model plants, we are still only scratching the surface of what repertoire of complex performance and response traits might be considered essential or desirable in crop plants. Nevertheless, first cautious attempts in model plants have demonstrated that ‘selfish’ plant behavior indeed has a genetic basis (Wuest and Niklaus, 2018). Pursuing this in crop plants will require field-phenotyping and selection under relevant conditions in a community context. Thus, connecting genetic principles with ecological and evolutionary concepts by treating agricultural production as an ecosystem or adopting an ecological engineering approach, may open the way towards a more holistic view of “agroecological genetics and genomics” of crop plant populations for enhancing yield. In principle, this viewpoint refers to unravelling the underlying genetics/genomics

of exterior and interior architectural traits of crop plants in their ('unnatural') agricultural environment for maximizing communal yield (either as monoculture or mixture).

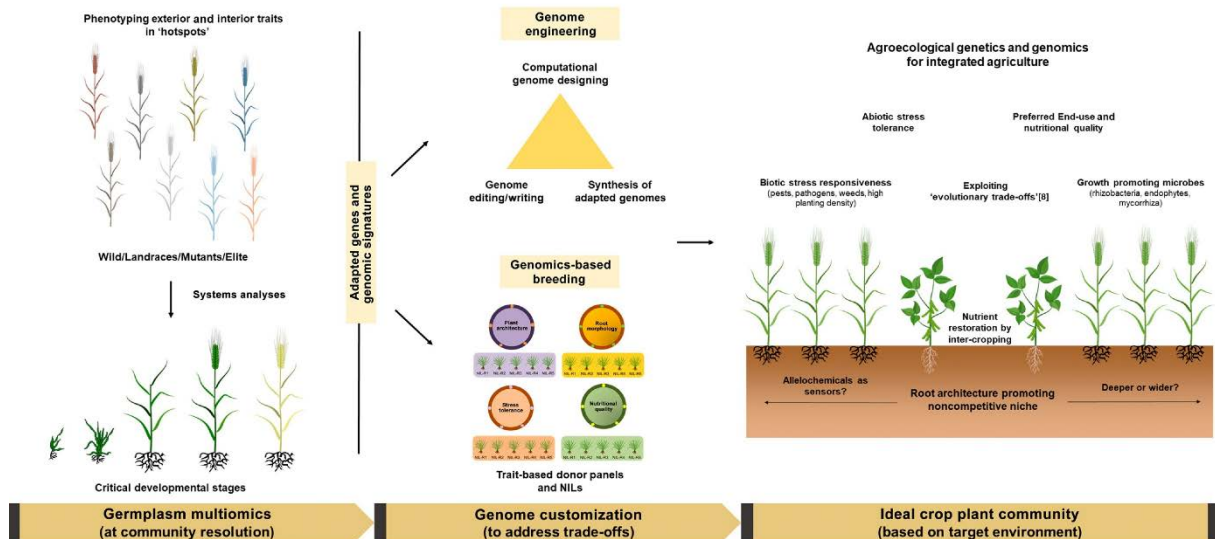


Figure 1.10 Agroecological genomics and genetics for ideal crop plant community. Agriculture, being a function of community performance requires silencing of ‘selfish plant behavior’. Therefore, largely practiced single-plant selection becomes less relevant and it is more expedient to avoid or minimize ‘selfish’ plant behavior through group selection in crop breeding. In this context, embracing an “Agroecological Genetics and Genomics” viewpoint, combining genetic principles with evolution and ecology, might pave the way to unravel key molecular factors that regulate not only well-studied “exterior” traits but also elusive “interior” plant architectural traits at community resolution. Multi-disciplinary research efforts are urgently required in this direction to silence ‘selfish’ traits and maximize communal yield by matching crop genotypes to target environments and management practices. One size doesn’t fit all; for instance, (i.) in water scarce ecosystem drought responsive genes should also be deployed, (ii.) like-wise for biotic stress resistance, (iii.) appropriate intercropping to tackle soil nutrient deficiency, (iv.) biofortification to address malnutrition etc. Note: Superscript indicate reference number. This figure was partly created by using BioRender (<https://biorender.com/>). Source: Image is taken from [Abbai et al., 2020](#).

So, how can we pursue “agroecological genetics and genomics” for balancing the exterior and interior plant architectural traits, and likewise, to better address fitness-versus-yield tradeoffs? Conceivably, recent and future advances in genomics and allied domains may come to the rescue. To this end, multi-omics systems analyses (genome, transcriptome, proteome, metabolome, epigenome, microbiome, etc.) of diverse germplasm across critical developmental stages and large-scale phenotyping for both exterior and interior traits in relevant agroecological contexts can possibly empower research at crop community resolution (Figure 1.10). Deduced trait-responsive network hubs, associated genes and favorable haplotypes (Bevan et al.,

2017) might support computational design of adapted, customized crop genomes (Benes *et al.*, 2020) and will assist in tailoring multiple traits. In principle, genome engineering by multiplexed gene/haplotype editing or synthetic biology routes (Wallace *et al.*, 2018) might facilitate even more rapid development of ideal crop plants in the future. Another promising strategy is the establishment of trait-specific donor panels harboring adapted genomic signatures (Figure 1.10). A ‘First-Generation Ideal Plant Type’ (iGen-IPT) could then be developed by combining superior trait-specific near isogenic lines (NILs) through genomics-based breeding. Multi-omics analyses of these iGen-IPTs could redefine molecular networks and regulators, gene-gene interactions, genetic background effects, high-resolution computational genome and thus an improved iiGen-IPT. Similarly, such recurrent systems analyses might result in better-adapted ‘next-generation Ideal Plant Types’ (nxIPTs) for optimized community performance. It is important to emphasize that these nxIPTs are not universally applicable, but must vary with target-environment and management practices. However, initial investigations of germplasm in ‘hotspots’ representing existing environmental diversity could support rapid and effective generation of multi-omics datasets for simulating customized crop genomes suiting any target-environment, including predicted future climate scenarios; as exemplified from CGIAR’s “Global Rice Array” initiative (see: <http://ricecrp.org/wp-content/uploads/2017/03/Flagship-project-4.pdf>).

Eventually, such human-customized plant communities where caring and sharing is favored over competing may not only provide more resource-efficient, high-yielding, biofortified crop plants; it simultaneously may herald the prospect of more sustainable solutions to future agricultural production systems in a changing climate. Overall, deploying new ‘drastic’ variations in crop breeding and embracing an “Agroecological Genetics and Genomics” viewpoint might maximize communal yield by matching crop genotypes to target environments (Abbai *et al.*, 2020).

1.6 Aims of the current thesis

As elaborated in the previous sections, tremendous progress has been achieved in improving wheat grain yield over the course of domestication and breeding. However, the basic structure of the wheat inflorescence has remained largely similar since domestication – all the modern cultivars have a non-branching spike, where the grain-bearing spikelets are directly attached to the rachis in a distichous pattern. Thus, the observed yield advance was primarily possible because of the increased number, fertility, and size of sink organs (spikelets and florets), while largely preserving the standard spike architecture. This might be one of the important reasons for the detected yield plateau in some of the most highly productive agro-ecosystems, including Germany. Conceivably, altering the inflorescence architecture might pave new paths for yield improvement and possibly assist in overcoming this yield barrier.

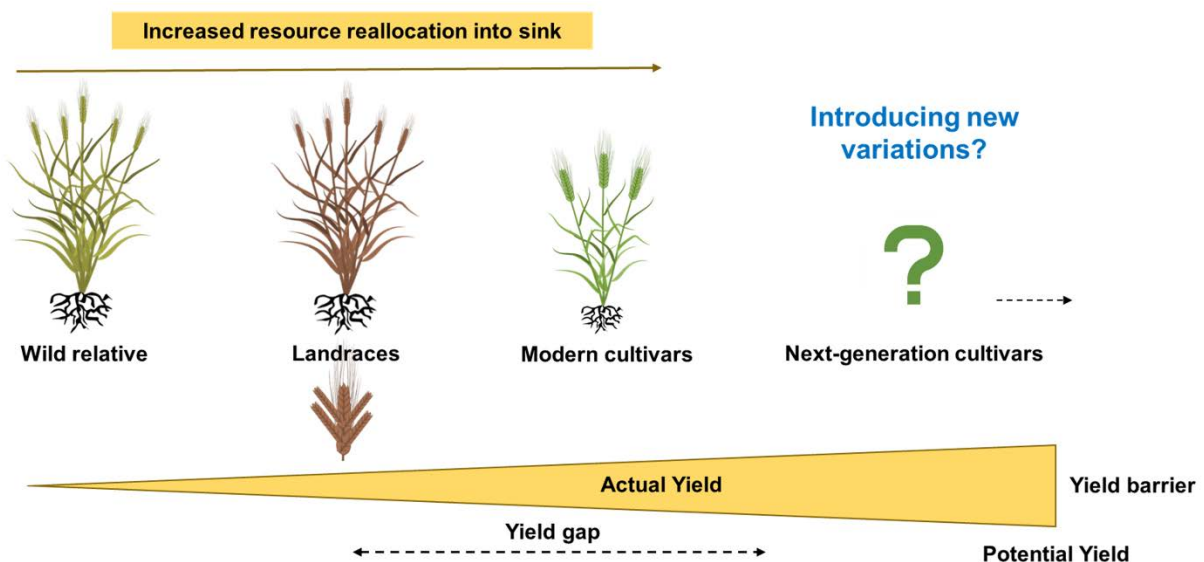


Figure 1.11 Increased resource remobilization into the sink is a key factor that minimized the yield gap during the evolution of wheat under agriculture. One potential strategy that might further yield gains is introducing relevant 'drastic' variations such as the spike-branching phenotype, thus exploring a new path for wheat improvement. This figure was partly generated by using BioRender (<https://biorender.com/>).

Interestingly, 'Miracle-Wheat' (*T. turgidum* convar. *compositum* (L.f.) Filat.) is an exception that deviates from the standard developmental program, producing a non-canonical spike with lateral branches instead of spikelets. But spike-branching wheat suffers from trade-offs on spikelet fertility (lower grains per spikelet) and grain size (shorter grains). Notably, the 'Miracle-Wheat' accessions are landraces with an

exceptionally high number of sink organs and taller plant architecture that has not benefited from decades of breeding progress (Figure 1.11). Therefore, it was hypothesized that delimited post-anthesis source strength might explain the spike-branching induced grain yield trade-offs (Figure 1.12). The major objectives of the current thesis include:

1. Examining the physiological and genetic basis of various ‘exterior’ plant architectural traits, including the (flag leaf, peduncle, and spike) senescence rate, and evaluate their implications on grain yield determination in the spike-branching genotypes under field conditions. For this purpose, 385 RILs derived by crossing the spike-branching landrace, TRI 984 with an elite durum CIRNO C2008, were used.
2. Identification of favorable trait and allele combinations of relevant QTLs to mitigate spike-branching induced grain yield trade-offs in multiple environments.
3. Validation of one of the QTLs affecting rachis length and grain size in multiple genetic backgrounds (including spike-branching types), its fine mapping and finally, uncovering its influence on an ‘interior’ architectural trait – vascular anatomy of the rachis, which might have relevance for resource transport into sink organs.

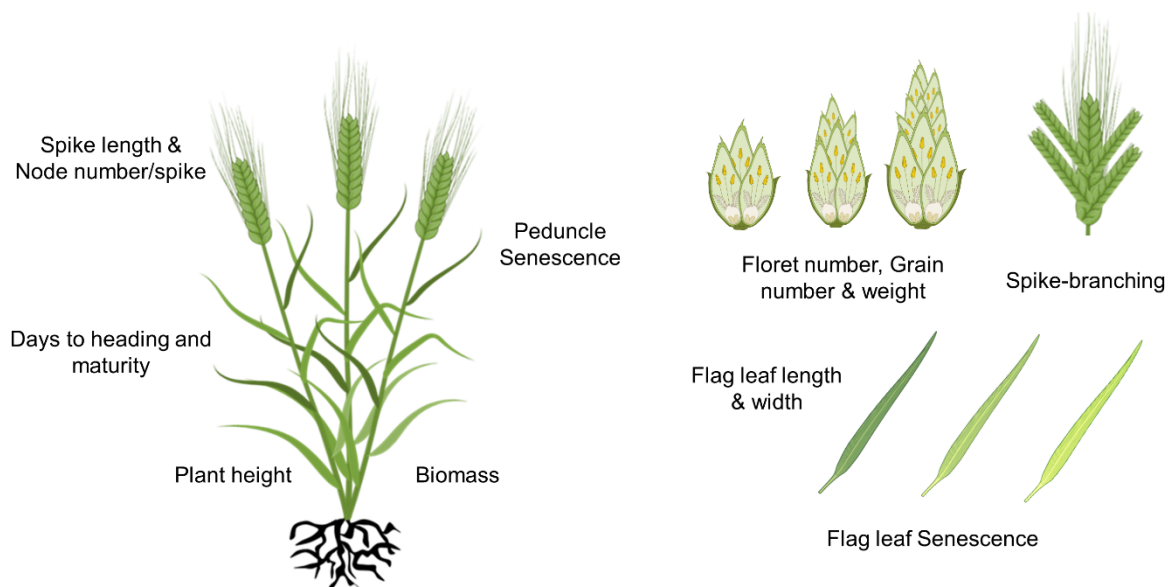


Figure 1.12 Capturing the Source-Sink differences in landrace-elite recombinants that exhibit spike-branching phenotype. This figure was partly generated by using BioRender (<https://biorender.com/>).

2. Materials and Methods

2.1 Mapping population

2.1.1 TRI 984 x CINRO RILs

A bi-parental population comprising 385 RILs was developed by crossing the spike-branching 'Miracle-Wheat' accession, 'TRI 984' and elite durum from CIMMYT, 'CIRNO C2008' (hereafter referred to as 'CIRNO'). A modified speed breeding method (Ghosh *et al.*, 2018; Watson *et al.*, 2018) was used for rapid generation advancement from F₃ to F₅. Initially, the grains were sown in the 96 well trays and grown in standard long day conditions *viz.*, 16h light (19°C) and 8h dark (16°C) for about two weeks. Later, the trays were transferred to speed breeding conditions *viz.*, 22h light (22°C) and 2h dark (17°C) to accelerate the growth. The spikes were harvested at maturity, and a similar method was used for the next cycle. Finally, the obtained F₅ plants were multiplied under field conditions during the spring of 2020, and the resulting F₆ grains (RILs) were genotyped and phenotyped (Figure 2.1).

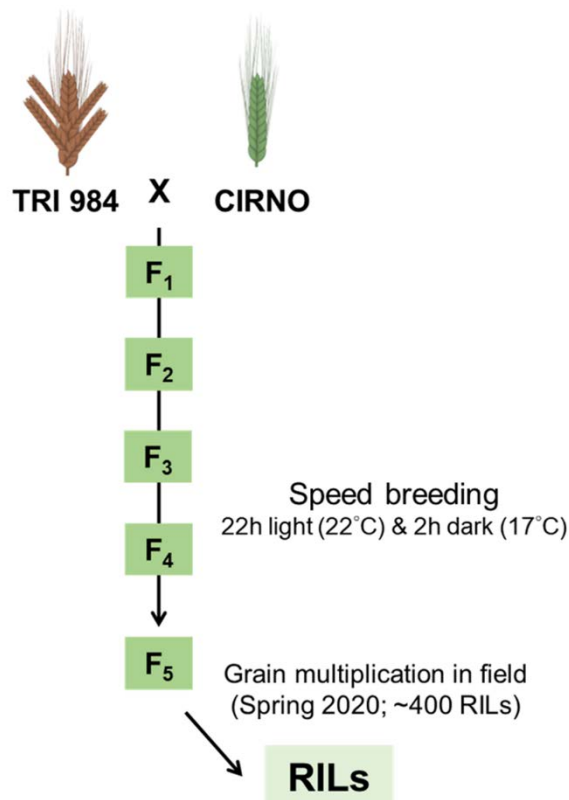


Figure 2.1 Development of mapping population. The 'Miracle-Wheat' landrace TRI 984 was crossed with CIRNO, an elite durum cultivar, to establish a biparental population comprising 385 RILs. Note: The image is partly created using BioRender (<https://biorender.com/>)

2.1.2 TRI 19165 x Bellaroi RILs

The details of the population are described by [Wolde et al., 2019a](#). In brief, about 146 RILs were developed by crossing Bellaroi (elite spring durum cultivar) with TRI 19165 (spike-branching ‘Miracle-Wheat’ with winter growth habit). However, only the spring type F₂s (which were able to complete their lifecycle without vernalization in a greenhouse setup) were forwarded for developing RILs. They were genotyped following two-enzyme genotyping-by-sequencing approach ([Poland et al., 2012](#); [Wendler et al., 2014](#)). Eventually, linkage map was constructed by [Wolde et al., 2019a](#) and the same was used in the current thesis. Here, these RILs were evaluated in greenhouse and field conditions (*Section 2.3*), followed by QTL mapping.

2.1.3 Zavitan introgression lines in Svevo background

In the [Distelfeld lab \(University of Haifa, Israel\)](#), selected number of Svevo x Zavitan RILs ([Avni et al., 2014](#)) were backcrossed three times to Svevo for developing a set of 50 BC₃F₃ introgression lines (ILs) and were genotyped using the 90K array ([Bacher et al., 2021](#)). We obtained these ILs and phenotyped them at IPK-Gatersleben (*Section 2.3*). Besides, we also further backcrossed IL 66 and IL 74 with Svevo to fine map the spike length QTL on Chr 4A long arm (*Section 3.5.3*).

2.2 Genotyping and linkage map construction (TRI 984xCIRNO RILs)

The parental lines and three F₆ grains per RIL were sown in 96 well trays and were grown in standard greenhouse conditions (16h light; 19°C & 8h dark; 16°C) for about two weeks. Leaves were sampled at the two-leaf stage from all the seedlings and stored at -80°C until further use. During the sampling, the leaves from the three replications of a particular RIL were pooled, and genomic DNA was extracted. The DNA integrity was evaluated on agarose gel, after which about 50 ng/μl aliquots were prepared for the genotyping. Eventually, the 25K wheat SNP array from SGS-TraitGenetics GmbH was used for genotyping the 385 RILs along with the parental lines. Then, the polymorphic markers scored to the A & B sub-genome were considered for further analysis and linkage map construction. The linkage map was developed using the regression and maximum likelihood methods in JoinMap v4.1 ([Stam, 1993](#)). These are detailed in *Section 3.2*.

2.3 Examining plant and spike architectural traits

2.3.1 Greenhouse conditions

After collecting the leaves for genotyping (as described in the previous section), the two-week-old seedlings were vernalized at 4°C for one month. Then, the seedlings were transferred to 9 cm square pots, grown in long day conditions (16h light; 19°C & 8h dark; 16°C). In both the parents – TRI 984 and CIRNO, tillers per plant (at booting) and spike number per plant (at maturity) were phenotyped. Besides, flag leaf verdancy was measured at eight different locations along the leaf blade (Borrill *et al.*, 2019) at heading and also at 30 days after heading using the SPAD-502 chlorophyll meter (Konica Minolta). Standard fertilization was performed, and plants were treated with pesticides based on the requirement.

Likewise, the Bellaroi x TRI 19165 RILs (5 plants per RIL) were grown under similar greenhouse (GH) conditions described above (vernalized at 4°C for one month, transferred to 9 cm square pots, grown in long day conditions). At about two weeks after heading, spike length (without awns) and number of spikelets per spike were phenotyped. Rachis node density was derived as the ratio of number of nodes per spike to that of the corresponding spike length.

The two-week-old BC₄F₂ and BC₄F₃ individuals derived by backcrossing IL 66 and IL 74 separately with Svevo were vernalized for two weeks, after which they were transferred to 9 cm square pots and grown in similar long day conditions. Leaf samples were collected for DNA extraction and PCR based genotyping to fine map the QTL interval (Section 3.5.3). The population was also phenotyped for spike length (without awns) during early grain filling stage.

2.3.2 Simulated canopy shade (based on our earlier study, Golan *et al.*, 2023)

The wild emmer introgression lines and the parental lines (Svevo & Zavitan) were grown in sunlight (standard glasshouse) and in another separate glasshouse simulating canopy shade, which was mounted with a green plastic filter (Lee122 Fern green, LEE filters) on the roof inside of the glasshouse. Moreover, both the glasshouses contained natural loamy soil, which had two open, non-glassed sides each with porous metal netting to enable air circulation. The plants grown under green filter experienced a red/far-red ratio from 1.13 to 0.28 (Golan *et al.*, 2023). Likewise, a

comparable reduction in red/far-red ratio of ~0.3–0.4 was reported in high-density wheat canopy (Evers *et al.*, 2006), which declined to 0.1 near canopy closure. The sunlight treatment of the wheat plants was conducted in a glasshouse with identical dimensions but without a green filter and was directly adjacent to the shaded glasshouse. The 50 ILs (eight plants/IL), along with parents (16 plants/parent) were first sown in jiffy pots, and a week later, they were transplanted in incomplete blocks comprising 9 plants each. The plants were grown in a 1-m row (10-15 cm distance between the plants and 20-25 cm distance between the rows). The growth conditions are described in detail in our earlier paper, Golan *et al.*, 2023. Various traits namely, spike length, grains per spikelet, grain length and grain width measured under these conditions are described in the current thesis.

2.3.3 Field conditions

2.3.3.1 TRI 984 x CIRNO RILs

The genotypes were screened at IPK-Gatersleben (51°49'23"N, 11°17'13"E, 112m altitude) under field conditions for two growing seasons *viz.*, the F₆ derived RILs in the spring of 2021, and the F₇ derived RILs in the spring of 2022. They were grown in an α -lattice design with three replications, while each 1.5 m² plot had six 20 cm spaced rows comprising two genotypes (three rows each). Standard agronomic and management practices were in place throughout the growth cycle; however, the experimental trial was completely rainfed. Besides, a subset of genotypes (F₆ derived RILs) in one replication was evaluated at the University of Hohenheim (48°42'50"N, 9°12'58"E, 400 m altitude) in 2022.

Plants from the inner rows (at least five measurements per plot) were considered for all the phenotyping except for grain yield per meter row, where the mean of all three rows of a particular genotype was measured. Days to heading (DTH) was determined at 'Zadoks 55', *i.e.*, when half of the spike has emerged (Zadoks *et al.*, 1974) in about 50% of the plants in a particular plot. Later, this was converted into growing degree days (GDD) to account for temperature gradients (Miller *et al.*, 2001). The distance from the tip of the flag leaf to its base was considered as the flag leaf length, while the flag leaf width was the end-to-end horizontal distance at the middle of the leaf. At heading, flag leaf verdancy was measured using the SPAD-502 chlorophyll meter (Konica Minolta) at eight different locations along the leaf blade (Borrill *et al.*, 2019).

Flag leaf senescence was screened at 30 days after heading using a four-point severity scale from '1' indicating the least senescence to '4' for the highest senescence (described in *Section 2.4*). Days to maturity (DTM) was determined when most spikes turned yellow in a particular plot; later, this was converted to growing degree days similar to days to heading.

Spike weight, spike length (without awns) and straw biomass (dry weight of culm along with leaves) were measured after harvest. In addition, a scoring method was developed for categorizing supernumerary spikelets (two spikelets per rachis node) and spike-branching (true branching with mini-spikes from the rachis nodes) (described in *Section 2.4*). Floret number was measured in from two spikelets at the center of the spike (only in the genotypes without spike-branching) at harvest. Besides, derived traits such as grains per spikelet, grain filling duration ([Chapman et al., 2021b](#)), and harvest index was calculated as follows:

$$\textit{Grains per spikelet} = \frac{\textit{Grains per spike}}{\textit{Spikelet number per spike}}$$

$$\textit{Grain filling duration} = \textit{Days to maturity} - \textit{Days to heading}$$

$$\textit{Harvest index} = \frac{\textit{Grain weight per spike}}{\textit{Straw biomass} + \textit{Spike weight}}$$

'Marvin' digital grain analyzer (GTA Sensorik GmbH, Neubrandenburg, Germany) was used to determine grains per spike, thousand-grain weight, grain length, and grain width. We also recorded the grain width and length of the parental lines manually using a Vernier caliper to reconfirm the observed trend from the 'Marvin' digital seed analyzer ([Appendix Figure 1](#)). All the above-mentioned traits were recorded at IPK-Gatersleben, while only the spike architectural traits were phenotyped from the experiment conducted at the University of Hohenheim.

2.3.3.2 Bellaroi x TRI 19165 RILs

About 135 RILs derived from Bellaori x TRI 19165 were grown at IPK-Gatersleben (51°49'23"N, 11°17'13"E, 112m altitude) in Spring 2020. The plots were of 1.5 m², comprising six 20 cm spaced rows. Each plot had six rows of one genotype

(monoculture), replicated three times in an α -lattice design. Spike length (without awns) was measured in these genotypes couple of weeks after heading and the same was used for QTL mapping.

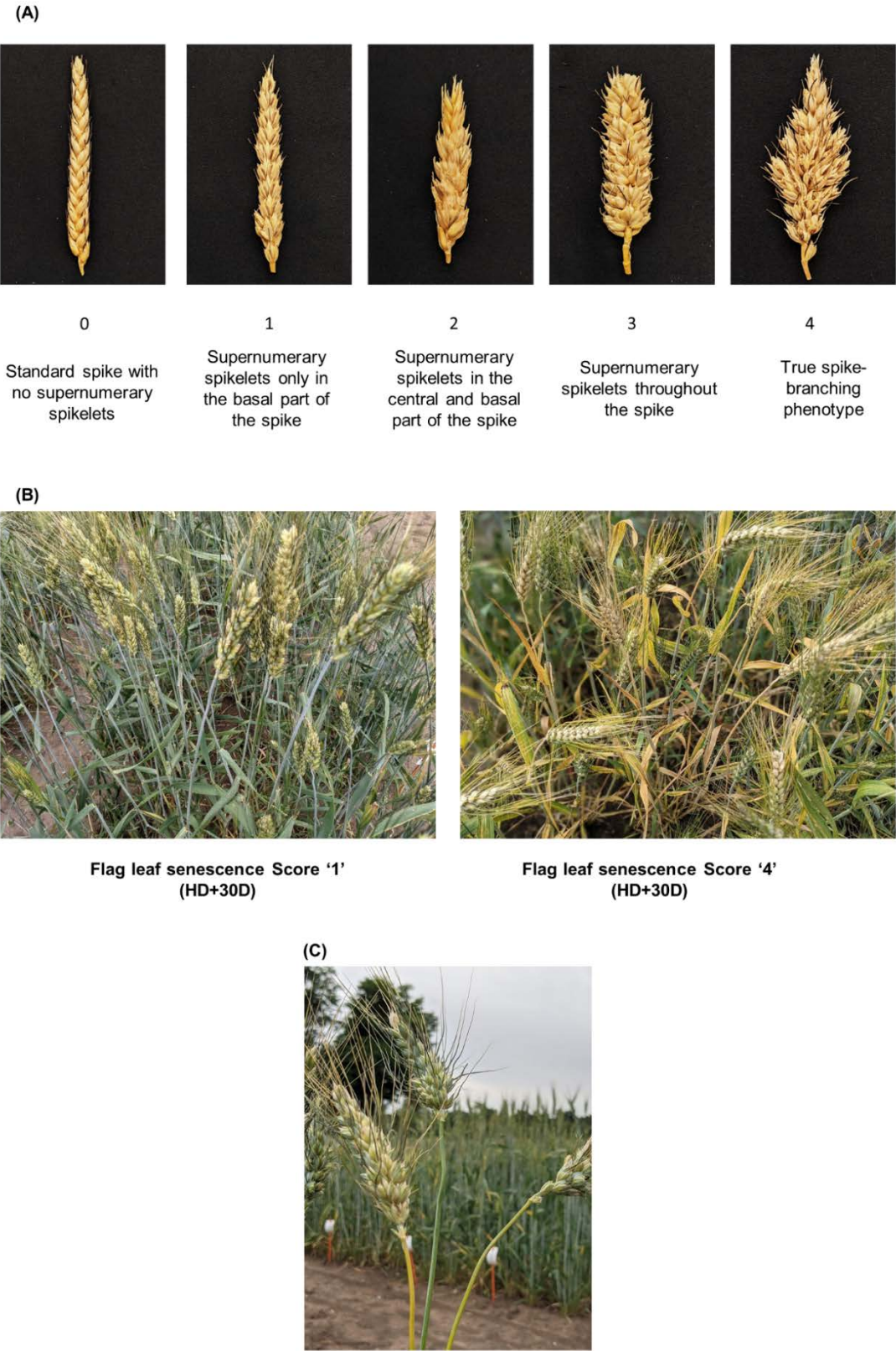


Figure 2.2. Phenotype-based scoring method. (A) 0-4-point scale for supernumerary spikelets and spike-branching phenotypes and tracking the progression of senescence rate at

30 days after heading. (B) Phenotypes of flag leaves with delayed and accelerated senescence. (C) A gradient of peduncle yellowness was observed; however, the population was classified only into two categories in the current study.

2.4 Phenotype-based scoring for spike-branching and flag leaf senescence rate

A scoring method was developed for estimating supernumerary spikelets (two spikelets per rachis node) and spike-branching (true branching with mini-spikelets from the rachis nodes) (Figure 2.2A). '0' (standard spike), '1' (supernumerary spikelets only at the basal part of the spike), '2' (supernumerary spikelets until half of the spike), '3' (supernumerary spikelets throughout the spike) and '4' (proper branching).

Flag leaf senescence was screened at 30 days after heading using a four-point severity scale from '1' indicating the least senescence to '4' for the highest senescence (Figure 2.2B). The number of senesced peduncles per 10 peduncles was counted from the inner rows to determine peduncle senescence (%) (Chapman *et al.*, 2021b). In this context, we found a gradient of yellowness in the peduncle across the RILs; however, in the current study, this was not differentiated, i.e., we had only two classes – green and yellow (Figure 2.2C).

2.5 Phenotypic and Genetic analyses

Genstat 19 (VSN International, Hemel Hempstead, UK) and GraphPad Prism 9.3.1 (GraphPad Software, San Diego, California, USA) were used for all the statistical analyses. Ordinary one-way ANOVA followed by Dunnett's multiple comparisons test was employed for multiple-range comparisons, whereas an unpaired *Student's t-test* was used to compare two groups. Pearson correlation was used to study the relationship among the traits of interest; besides, simple linear regression assisted in understanding the effect of a particular trait (explanatory variable) on another (response variable). The corresponding figures contain all the relevant details, such as P-value, R^2 , and the number of samples compared.

QTL mapping was performed in Genstat 19 using the following criteria: i. step size of 10 cM, ii. minimum cofactor proximity of 50 cM, iii. minimum QTL separation distance of 30 cM and iv. genome wide significance ' $\alpha = 0.05$ '. Simple interval mapping (SIM) was performed as an initial scan to determine the positions of potential candidate QTL(s). These positions were used as cofactors for multiple rounds of composite interval mapping (CIM); CIM was repeated until similar results were obtained at least

three consecutive times. Finally, QTL backward-selection was carried out after CIM to estimate various QTL effects, including the determination of QTL interval, high-value allele, additive effects, and phenotypic variance explained. The QTLs were then visualized using MapChart 2.32 ([Voorrips, 2002](#)).

2.6 Analysis of rachis internode vascular architecture

Spikes from Svevo and the wild emmer introgression lines (IL 34, IL 40, and IL 66) were sampled from field grown plants (inner rows of a 1.5 m² monoculture plot) during early grain filling stage for the microscopic analysis of vascular anatomy. Initially, transverse hand sections were made in the lower half of all the rachis internodes and then the sections were subjected to autofluorescence recordings under the Zeiss LSM780 confocal laser scanning microscope (Carl Zeiss MicroImaging), using 405 nm illumination in combination with a 406-550 nm bandpass. Tissue and vein measurements were carried out using Fiji open-source image software ([Schindelin et al., 2012](#)). Only lateral and central veins were considered for all the measurements.

2.7 Data availability

The phenotypic trait means (field experiments at IPK-Gatersleben) and genotypic data of the TRI 984x CIRNO mapping population are deposited in e!DAL ([Arend et al., 2014](#)) and can be openly accessed here: <http://dx.doi.org/10.5447/ipk/2023/17> and also in Supplementary Dataset S1 and Supplementary Dataset S2 of [Abbai et al., 2023](#).

2.8 Data contribution by the author and the collaborators for the present thesis

Most of the results presented in this thesis were generated and interpreted by the author of the thesis, *Ragavendran Abbai* (RA), under the supervision of *Prof. Dr. Thorsten Schnurbusch* (TS) in the Plant Architecture research group (AG PBP), IPK-Gatersleben. All the data from the TRI 984 x CIRNO population and TRI 19165 x Bellaroi population that are described in this study were generated by RA.

Section 1.4 is based on our article, [Abbai et al., 2020](#):

RA initially prepared a draft of this *Forum* article entitled “Seeking crops with balanced parts for the ideal whole”, emphasizing the importance of studying the genetic and regulatory landscape of the trade-offs affecting resource production and allocation

patterns at a crop community resolution, as a means for customizing crop genotypes to target environments. *TS* added exciting new ideas and substantially reshaped the contents that includes coining the term “Agroecological genetics and genomics”, proposed the classification of “Exterior” and “Interior” architectural traits and the need to clarify their ecological genetic framework; also argued the necessity to bring in radical phenotypic changes to further yield gains in important cereal crops like wheat. Besides, the following data from collaborators enabled designing further experiments and making interpretations explained in *Section 3.5*.

- A set of wild emmer introgression lines (ILs) in Svevo background were originally obtained from *Prof. Dr. Assaf Distelfeld* (University of Haifa, Israel). The *QSL.ipk-4AL* interval in Svevo x Zavitan RIL population was also shared by *Prof. Distelfeld* (*Moran Nave*, Master thesis). ILs within the *QSL.ipk-4AL* interval were identified by *Dr. Guy Golan* (GG), AG PBP; GG and RA evaluated the ILs under sunlight and simulated canopy shade at IPK. RA further developed a segregating back-cross population from selected ILs and fine-mapped *QSL.ipk-4AL*.
- The sectioning of the spike and analysis of vascular architecture was performed by *Dr. Twan Rutten* (TR), Structural Cell Biology research group (AG SZB). The results were further analyzed and interpreted by GG and RA.

3. Results

3.1 Spike-branching TRI 984 has lower grains per spikelet and thousand-grain weight than CIRNO

Consistent with previous findings using different germplasm (Wolde *et al.*, 2021), while the spike-branching landrace TRI 984 had more spikelets and florets per spike, the spikelets contained fewer florets and grains than the elite durum cultivar CIRNO (Figure 3.1A-H). However, we found no difference in grain number per five spikes, but a considerably reduced thousand-grain weight associated with shorter grains was observed in TRI 984 (Figure 3.1I-L). While CIRNO flowered earlier (Figure 3.1M), it had greener flag leaves both at heading (Figure 3.1N) and also after 30 days of heading (Figure 3.1O) along with greener peduncles (Figure 3.1P). Besides, CIRNO had longer but narrower flag leaves (Appendix Figure 2A&B), fewer tillers (Figure 3.1Q), yet spikes per plant remained unaltered (Figure 3.1R), with shorter spikes (Figure 3.1S) and shorter plant stature (Figure 3.1T) as opposed to TRI 984. We found considerable differences in spike-branching expressivity in TRI 984 (Figure 3.1E), which can explain the grain number, grain weight and spike weight variations observed among various replications of TRI 984 (Figure 3.1I-L, Appendix Figure 2C&D). Such inconsistencies in spike-branching have also been reported earlier in another ‘Miracle-Wheat’ – Elite cultivar biparental population (Wolde *et al.*, 2021). Furthermore, there was no difference in the average spike weight (n=5) (Appendix Figure 2C), but CIRNO had more grain yield per five spikes (Appendix Figure 2D).

These observations indicate a clear difference in terms of assimilate production and reallocation patterns between the two genotypes. Variations in tiller number (at booting) might indicate different resource partitioning strategies in TRI 984 and CIRNO during the pre-anthesis phase; however, there was no difference in the total number of spikes at maturity. Importantly, the spike-branching landrace TRI 984 exhibited a shorter grain filling period (quicker senescence), which implies reduced resource production and reallocation compared to CIRNO (delayed senescence) during the post-anthesis phase. Besides, the resources required to maintain the vegetative parts might be higher in the case of TRI 984 because of the taller plant architecture than CIRNO.

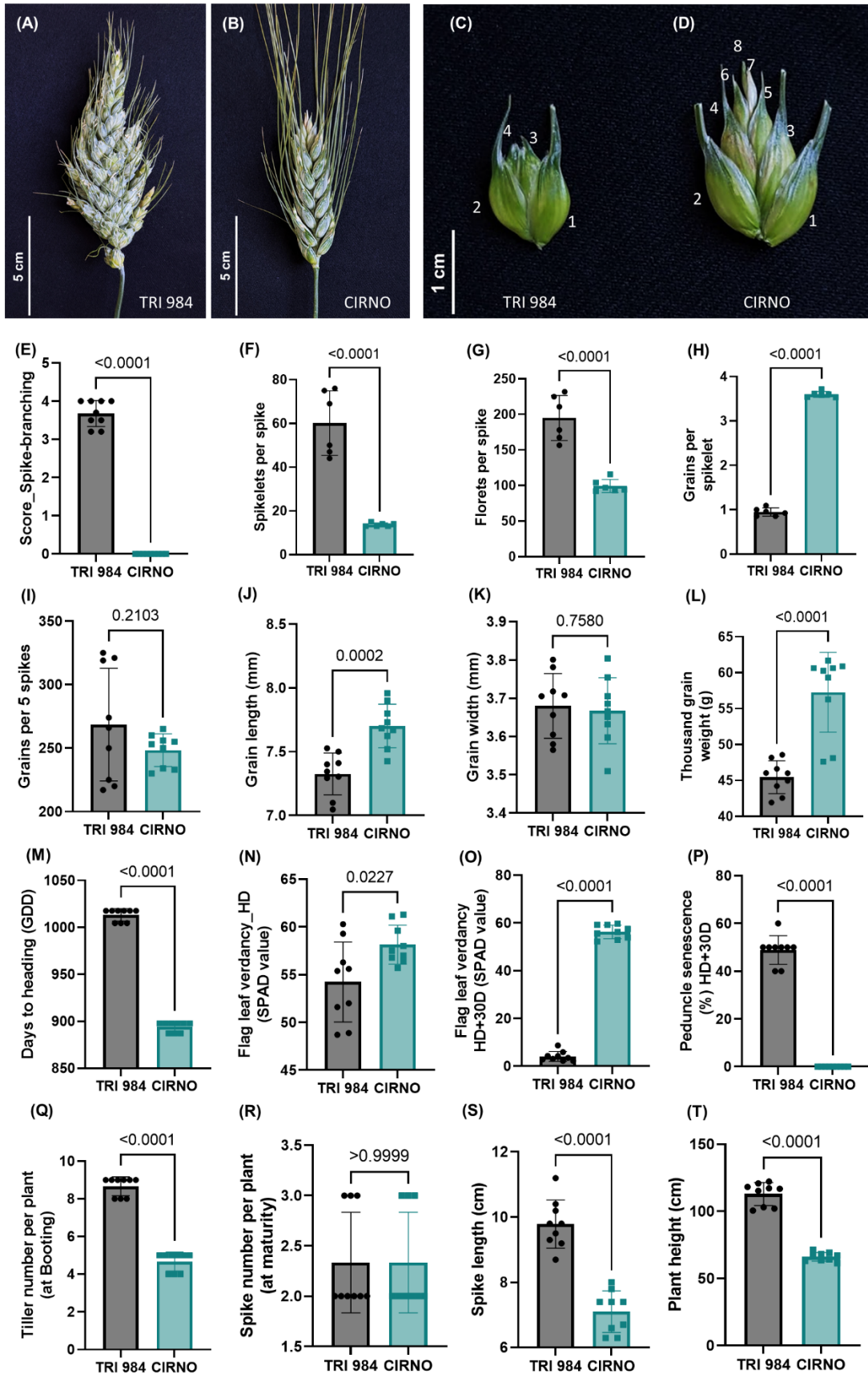


Figure 3.1. TRI 984 has a poor source-sink balance as opposed to CIRNO. (A) Spike-branching phenotype of TRI 984 and (B) Standard spike of CIRNO. (C) Spikelet from the central part of the TRI 984 main rachis shows reduced florets relative to (D) a spikelet from a

similar position in CIRNO. (E) Spike-branching score; (F-I) While having more spikelets and florets per spike, TRI 984 had lower grains per spikelet and there was no difference in grain number per 5 spikes. (J-L) However, the grains are smaller in TRI 984, leading to a reduction in thousand-grain weight. (M) TRI 984 exhibited delayed heading, (N) lower flag leaf verdancy at heading, (O, P) accelerated flag leaf and peduncle senescence. TRI 984 had (Q) more tillers at booting, (R) but final spike number per plant remained unaltered, (V) longer spikes and (W) taller plant architecture. Note: unpaired t-test was performed to determine significance in (E-W) and the resulting P-values (Two-tailed analysis) are displayed. Data represented in (N, O, Q, & R) were obtained from greenhouse experiment, while all the remaining traits were phenotyped from field grown plants.

3.2 Population development, genotyping, and linkage map construction

Based on above mentioned results, it is conceivable that genetic analysis of the corresponding landrace-elite recombinants (TRI 984 x CIRNO) that vary in source-sink balance might provide mechanistic insights into the negative effect of spike-branching on grain number per spikelet and grain weight, two major components of final grain yield. Therefore, a bi-parental population comprising of 385 RILs was developed by inter-crossing TRI 984 with CIRNO to test this hypothesis. Eventually this population was genotyped using the 25K array (SGS-TraitGenetics GmbH). However, only the 21K markers scored to the A & B sub-genome were considered for further analysis; we found that 5,089 markers were polymorphic (Figure 3.2A). A subset of 2,128 markers was prepared after filtering, viz., without segregation distortion (determined based on Chi-squared test), <10% heterozygosity and <10% missing (Figure 3.2B&C). Haldane's mapping function was used in the regression method, while the maximum likelihood method involved the spatial sampling thresholds of 0.1, 0.05, 0.03, 0.02 and 0.01 with three optimization rounds per sample, both available in JoinMap v4.1 (Stam, 1993) was used for the linkage map construction. Outcomes from both these methods were used to determine the 14 linkage groups and final map order (Figure 3.3). The linkage map had about 662 markers, which is a subset of the 2,128 filtered polymorphic markers.

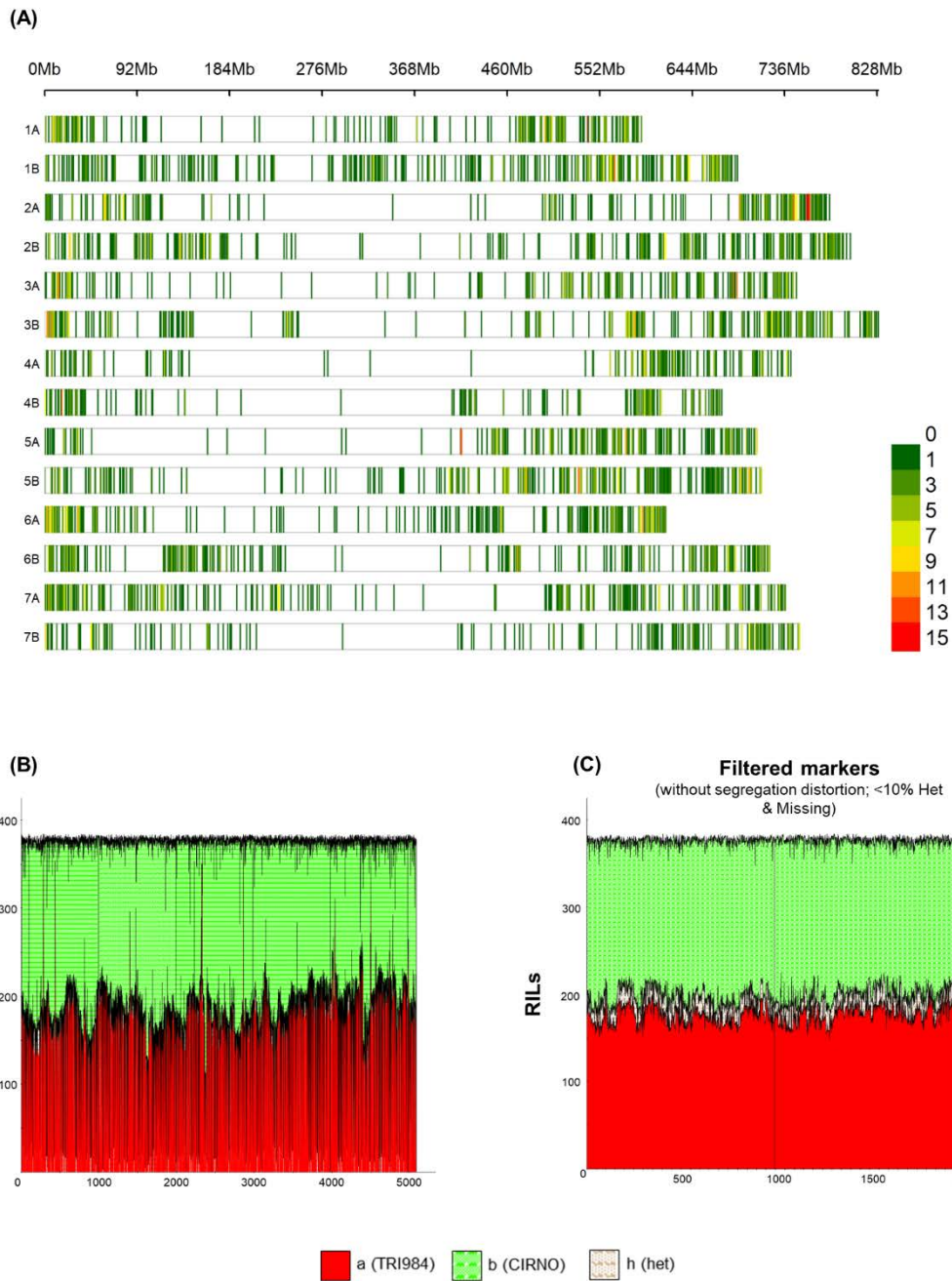


Figure 3.2 The RIL population was genotyped using the 25K array. (A) a total of 5,089 polymorphic markers were found across the genome, (B) but with segregation distortion and (C) eventually, a filtered set of 2,089 markers was developed.

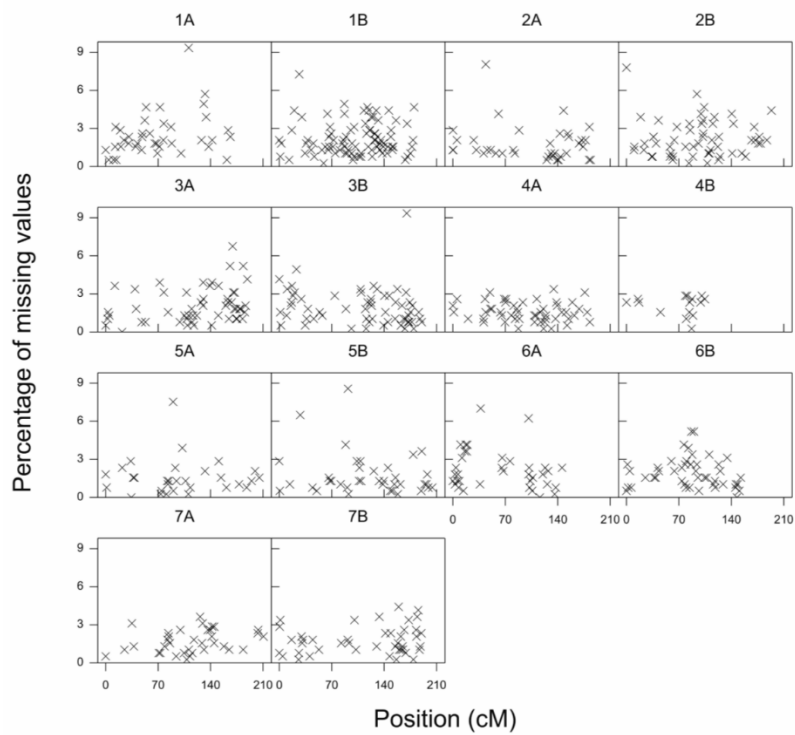
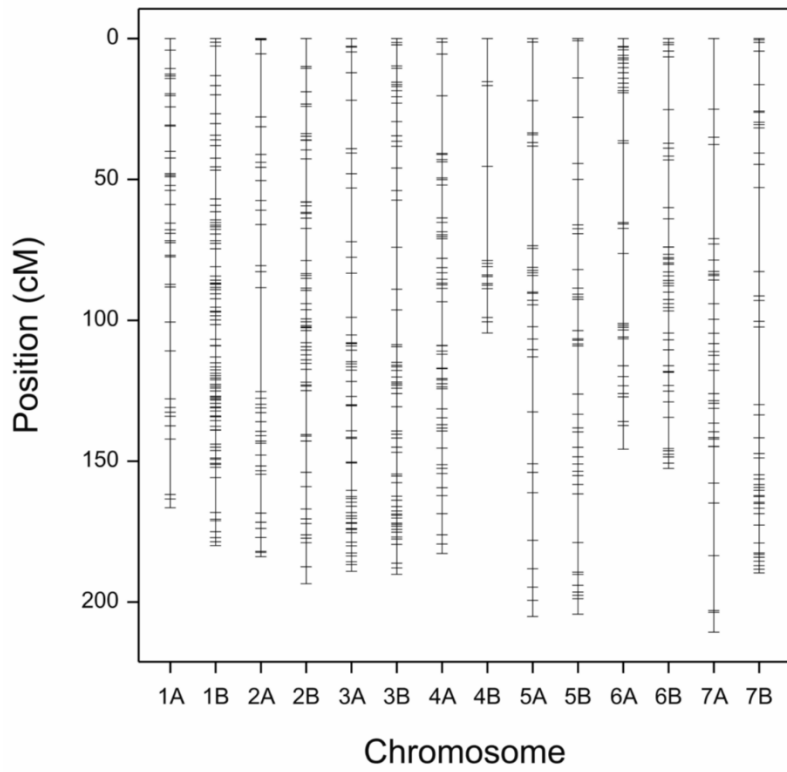


Figure 3.3 The linkage map based on the TRI 984xCINRO recombinants. About 662 markers from the filtered set of polymorphic markers (2089 markers) were categorized into 14 linkage groups, consistent with the previously known chromosome number of tetraploid wheat.

3.3 Grains per spikelet and thousand-grain weight are associated with senescence rate

As expected, we witnessed a considerable diversity for all the plant and spike architectural traits. Importantly, flag leaf and peduncle senescence rates were independent of the heading date; this implies that there is a possibility for the lines that flowered late to senesce early and vice-versa (Figure 3.4A). The lines with delayed flag leaf senescence also had the tendency of retaining green/verdant peduncles for a longer duration (Figure 3.4A). In addition, the intensity of flag leaf greening (SPAD meter value) at heading had no effect ($R^2=0.012$; $p=0.212$) on the progress of senescence (scored at 30 days after heading), indicating that these traits are largely independent (Figure 3.4B). Flag leaf length and delay in senescence were positively related ($R^2=0.045$; $p=0.0034$), while flag leaf width did not influence the same (Appendix Figures 3A&B). Moreover, we observed that the lines with more verdant/greener flag leaves at heading (higher SPAD value) also had a more significant number of florets per spikelet ($R^2=0.085$; $p=0.0014$), in line with the expected consequence of source strength on sink organ establishment before anthesis (Appendix Figure 3C). Intriguingly, the number of florets and grains per spikelet, which is determined earlier, was somewhat associated with senescence rate, i.e., the lines with more florets and grains per spikelet tended to display delayed flag leaf senescence ($R^2=0.071$; $p=0.0007$ & $R^2=0.14$; $p<0.0001$) (Figures 3.4C&D). Likewise, it has been previously reported that higher grain number increased the post-anthesis radiation use efficiency in wheat (Reynolds *et al.*, 2005). Here, we mapped a QTL on Chr 5A (*bht-A3*) influencing grains per spikelet and flag leaf senescence rate (Appendix Table 1). This possibly implies a gene/QTL-mediated pleiotropic association between sink number and flag leaf senescence rate, although these traits might not be physiologically dependent. Besides, the delayed senescence rate had a positive effect on thousand-grain weight ($R^2=0.13$; $p<0.0001$) (Figure 3.4E). We realized that the observed increase in thousand-grain weight is primarily due to the change in grain width ($R^2=0.08$; $p<0.0001$) (Figure 3.4F) and not grain length (Appendix Figure 3D), suggesting that grain width is more plastic, and influenced by resource reallocation compared to grain length. Notably, it became clear that the longer duration of green flag leaf and peduncle was not simply 'cosmetic' – it was associated with grain yield determinants. This vital evidence supports our hypothesis that dissecting the source-

sink relationship might have relevance in balancing the trade-offs that negatively regulate the final grain yield in ‘Miracle-Wheat’ like genotypes.

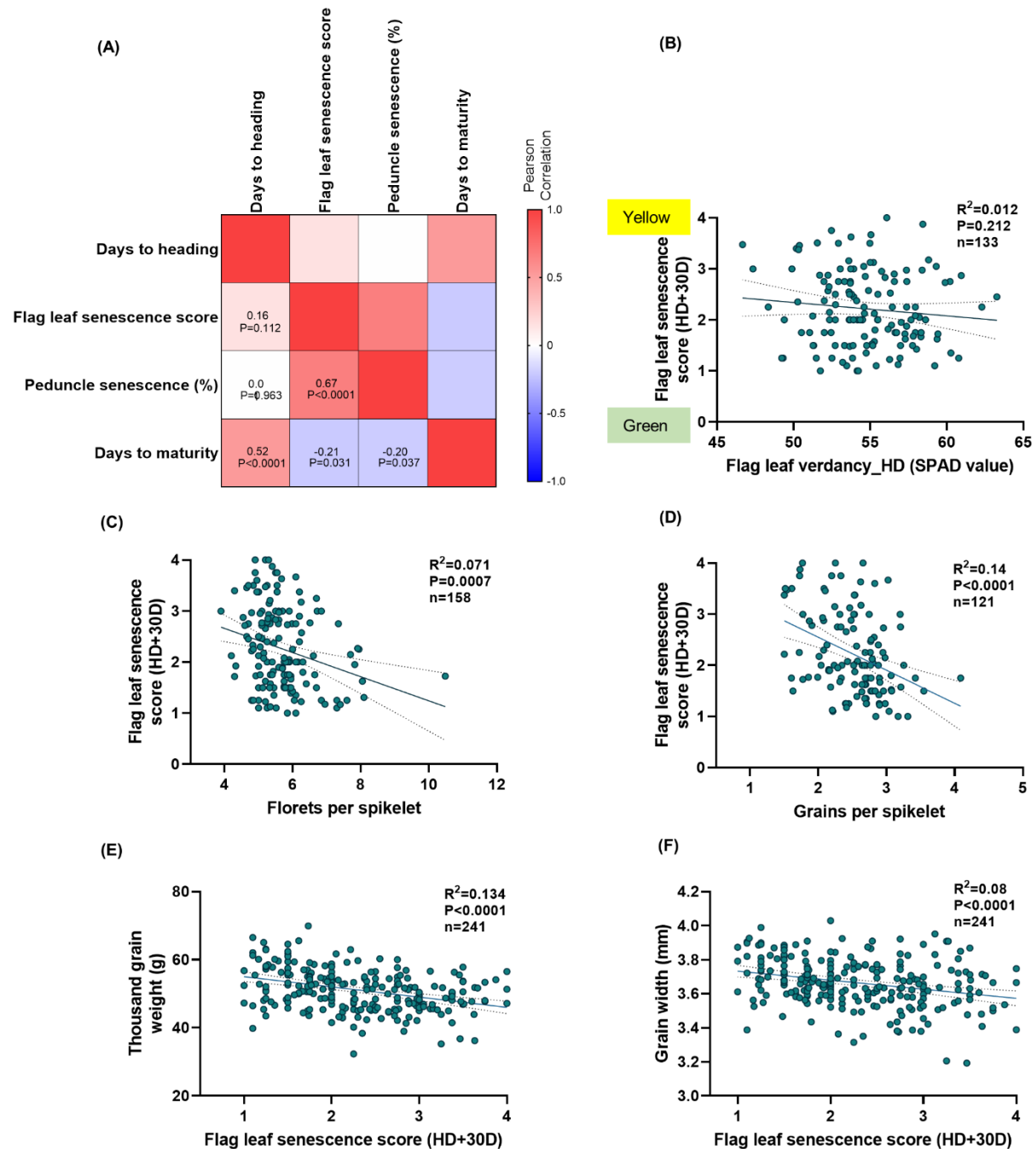


Figure 3.4 Functional ‘Stay-green’ phenotype was observed in the landrace-elite recombinants. (A) Flag leaf and peduncle senescence were positively related, independent of days to heading. (B) Flag leaf verdancy at the heading did not impact the progression of senescence. (C) Florets per spikelet and (D) Grains per spikelet were associated with flag leaf senescence rate and (D) the RILs with delayed senescence had higher thousand-grain weight, due to (E) wider grains. Note: (B-F) are linear regression plots with the explanatory variable on the x-axis, while the y-axis represents the response variable. R^2 is the phenotypic variance explained, and the corresponding P-values of the regression analysis are displayed. The data presented in (A-F) were phenotyped from field grown plants.

3.4 Grain yield trade-offs in 'Miracle-Wheat'

A total of 30 plant and spike architectural traits affecting source-sink dynamics were phenotyped for two field seasons and eventually, 130 associated QTLs were mapped across all the 14 chromosomes (Figure 3.5, Table 3.1). The details of the traits and QTL attributes are summarized in Appendix Tables 1 & 2.

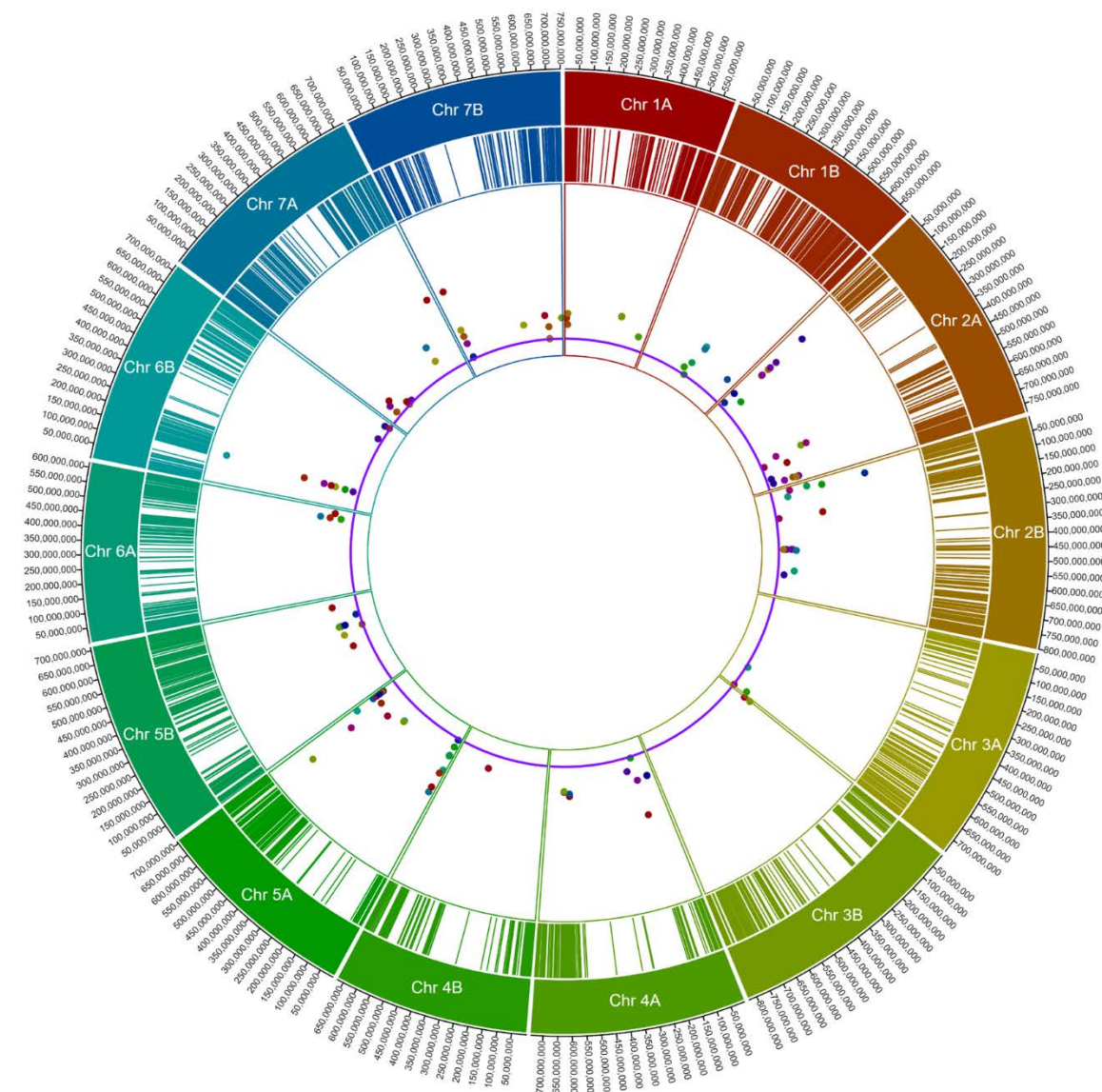


Figure 3.5 Snapshot of QTLs mapped using the landrace-elite RIL population. QTLs for various traits co-localized in certain chromosomes, such as on Chr 2A, Chr 5A, Chr 6B etc., which facilitated to understand trait trade-offs in spike branching genotypes.

Table 3.1 Details of phenotyped traits and mapped QTLs using TRI 984 x CIRNO population

Trait	Number of QTLs	Results
Days to heading (HD)	6	Appendix Figure 4
Days to maturity	2	
Flag leaf verdancy at heading	1	Appendix Figure 5
Plant height	4	
Flag leaf length	5	Appendix Figure 6
Flag leaf width	5	
Flag leaf senescence	4	Appendix Figure 7
Peduncle senescence	4	
Florets per spikelet	5	Appendix Figure 8
Grains per spikelet	4	
Spike length	7	Appendix Figure 9
Grain length	5	
Spike-branching	6	Appendix Figure 10
Thousand-grain weight	5	
Grain width	5	Appendix Figure 11
Grain L/W ratio	6	
Nodes per spike	5	Appendix Figure 12
Spike node density	3	
Average spike weight	4	Appendix Figure 13
Grain weight per spike	4	
Grain area	7	Appendix Figure 14
Grain circularity	8	
Spike chaff weight	5	Appendix Figure 15
Straw biomass	2	
Grains per spike	2	Appendix Figure 16
Fruiting efficiency	6	
Harvest index	4	Appendix Figure 17
Spike harvest index	3	
Grain filling duration	2	Appendix Figure 18
Grain filling rate	1	

3.4.1 The *bh^t-A1* locus underlies sink and source capacity

Using a scoring method based on the phenotype of the spike (Figure 2.2), we mapped a major effect QTL for spike-branching on Chr 2A (Figure 3.6A, Appendix Table 1) associated with the previously known locus *bh^t-A1* (Poursarebani *et al.*, 2015). Regardless of the increase in spikelet number per spike, owing to the lateral branching (Figure 3.6B), there was no difference in the total grains per spike (Figure 3.6C); but, the *bh^t-A1* locus was associated with a reduction in grain length (Figure 3.6D) and thousand-grain weight (Figure 3.6E). While the *bh^t-A1* lines had slightly longer flag leaf blades (Figure 3.6F), the flag leaf verdancy at heading (Figure 3.6G) and spike length (Figure 3.6H) were negatively affected. Thus, the TRI 984 allele induced spike-branching with grain size trade-offs and in addition might also affect the source capacity. Notably, this is not a case of usually observed grain number-grain weight trade-off, but rather the one where grain size is affected because of spike-branching (without a grain number increase).

3.4.2 *bh^t-A3*, a novel spike-branching locus on Chr 5A reshapes source-sink dynamics

Following similar phenotyping (Figure 2.2), we mapped a QTL for spike-branching on the long arm of Chr 5A; here, the CIRNO allele contributed to the spike-branching phenotype (Figure 3.7A, Appendix Table 1). We named the newly identified spike-branching modifier locus as '*bh^t-A3*' following the previously known *bh^t-A1* (Poursarebani *et al.*, 2015) and *bh^t-A2* (Wolde *et al.*, 2021) loci. Importantly, the spike-branching effect of the *bh^t-A3* locus manifests only in the presence of the mutated *bh^t-A1* allele (Figure 3.7A; Figure 3.8A-D; Appendix Table 1). We divided the RILs into two sub-groups for QTL mapping *viz.*, by fixing i. *bh^t-A1*, ii. *BH^t-A1* and the outcome confirmed the epistasis of the *bh^t-A3* to *bh^t-A1* locus (Figure 3.8A). Possibly, this indicates that the plasticity for spike-branching is introduced by *bh^t-A1*, i.e., it might be first essential to have *bh^t-A1* to disrupt the spikelet meristem identity and only then the *bh^t-A3* locus might modify the branching intensity in the spikes. Besides, the grain number increase effect of *bh^t-A3* is only observed in the spike-branching RILs – when *bh^t-A1* is present (Figure 3.8C). Moreover, in this region, we found co-localized QTLs for an array of traits influencing source-sink dynamics. The CIRNO allele was associated with spike-branching (Figure 3.7B), delayed flag leaf senescence (Figure

3.7C), more extended grain filling period (Figure 3.7D), increased grains per spikelet (Figure 3.7E) and grain yield per five spikes (Figure 3.7F).

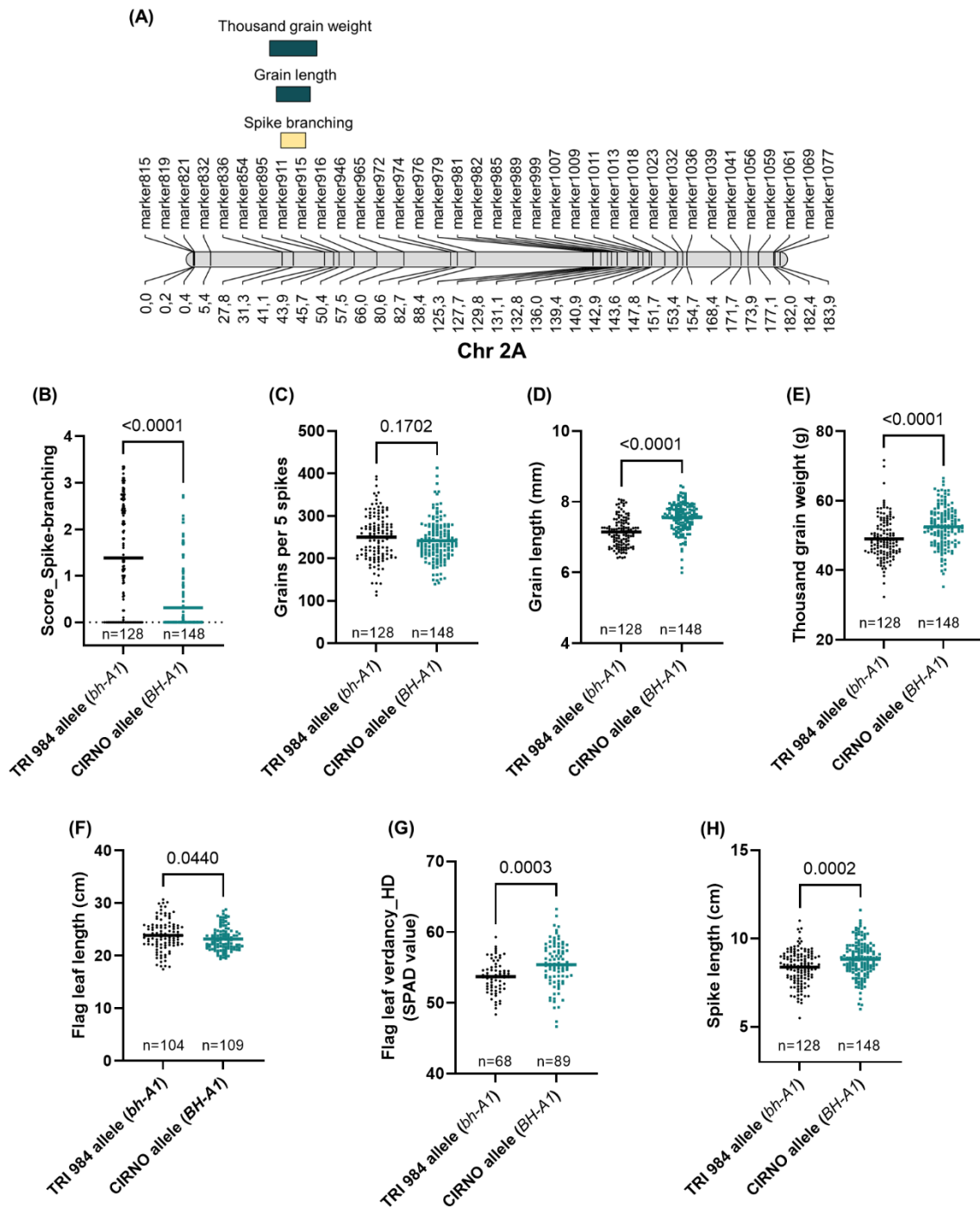


Figure 3.6. *bh^t-A1* induces spike-branching but with a grain weight trade-off. (A) A major effect QTL hotspot for spike-branching, grain length and weight was mapped on the short arm of Chr 2A. (B) RILs with the TRI 984 allele showed spike-branching, (C) no difference in grains per 5 spikes, but a reduction in (D) grain length, (E) thousand-grain weight, (F) flag leaf length, (G) flag leaf verdancy at heading and (H) spike length. Note: In (B-H), 'n' represents the number of RILs that were compared for each allele class, viz., TRI 984 allele data points are in 'black', while 'cyan' colored data points represent CIRNO allele. 'Unpaired t test' was used to determine

the statistical significance, and the resulting P-values (Two-tailed analysis) are displayed for all the comparisons. Data obtained from field grown plants was used for the analysis in (A-H).

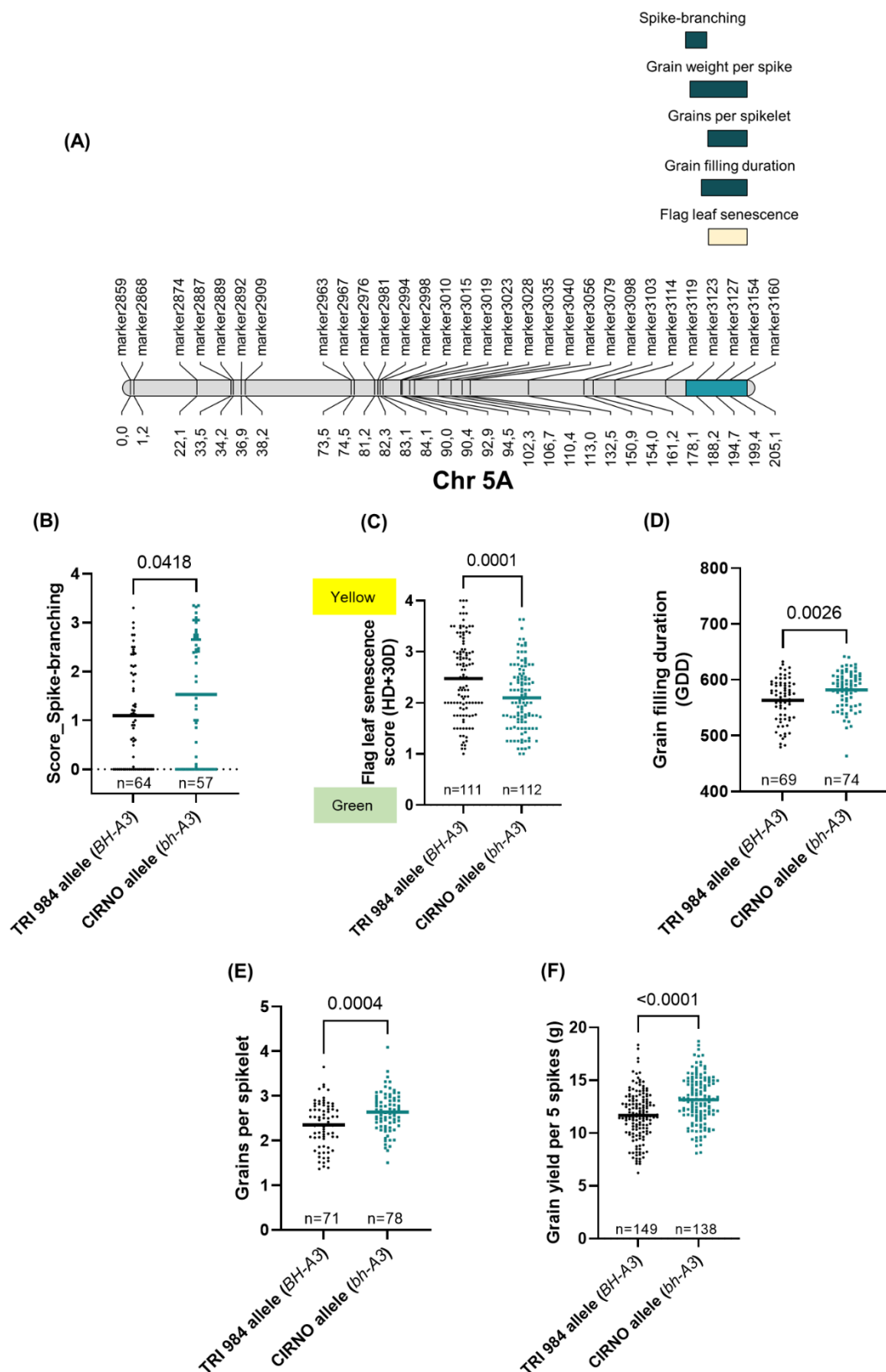


Figure 3.7. bh^t -A3, a new modifier locus for spike-branching. (A) bh^t -A3 mediates spike-branching, flag leaf senescence rate, grain filling duration, grains per spikelet and grain yield per spike. Only when bh^t -A1 is present, the bh^t -A3 CIRNO allele (B) increases the expressivity

of spike-branching, (C) delays flag leaf senescence rate, (D) increases grain filling duration, (E) grains per spikelet, and (F) grain yield per five spikes. In (B-F), 'n' represents the number of RILs that were compared for each allele class *viz.*, TRI 984 allele data points are in 'black', while 'cyan' colored data points represent CIRNO allele. 'Unpaired t test' was used to determine the statistical significance, and the resulting P-values (Two-tailed analysis) are displayed for all the comparisons. Data obtained from field grown plants was used for the analysis in (A-F).

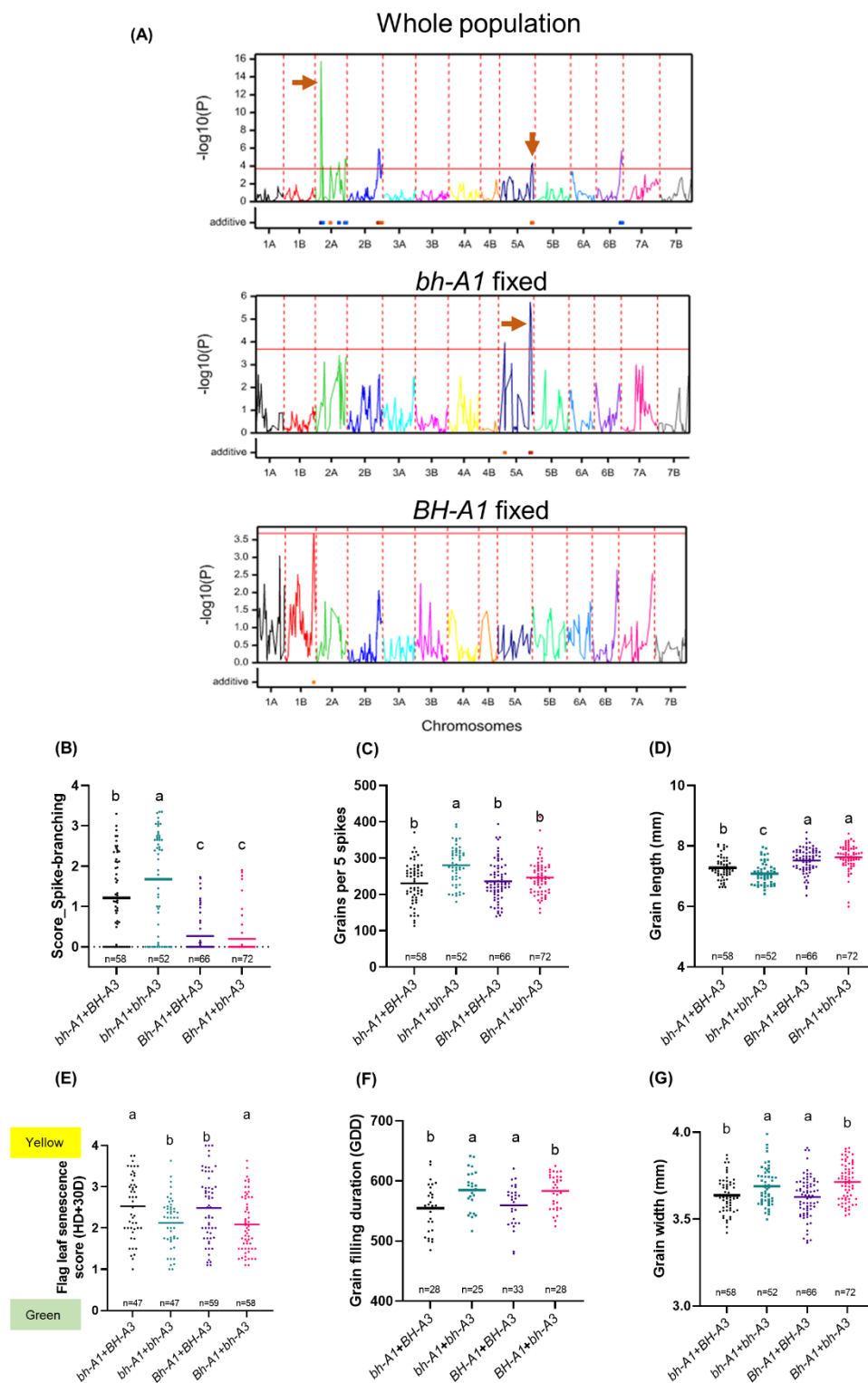


Figure 3.8. Spike-branching effect of *bh^t-A3* depends on the presence of *bh^t-A1*. (A) QTL mapping for spike-branching phenotype using the whole population, but also with two subsets

developed by fixing *bh^t-A1* and *BH^t-A1* revealed epistasis of the *bh^t-A3* to *bh^t-A1* locus. (B) The spike-branching expressivity, (C) grains per 5 spikes and (D) Grain length in various allele combinations of the two QTLs. However, the role of *bh^t-A3* in affecting (E) flag leaf senescence, (F) Grain filling duration and (G) Grain width is independent of *bh^t-A1*. Note: Data obtained from field grown plants was used for the analysis in (A-G).

Besides, we also found that *bh^t-A3* had a subtle, yet positive effect on grain width (Figure 3.9A), florets per spikelet (Figure 3.9B), straw biomass (Figure 3.9C) and harvest index (Figure 3.9D); but, the days to heading were not affected (Figure 3.9E). Interestingly, we found that the effect of *bh^t-A3* on flag leaf senescence, grain filling duration and grain width were not dependent on the presence of *bh^t-A1* (Figure 3.8E-G). This pattern implies that the phenotypic variation explained by the 5A QTL hotspot for spike-branching expressivity and senescence rate might be the outcome of at least two linked genes. Taken together, this trend suggests that the favorable CIRNO allele (*bh^t-A3*) mediates enhanced assimilate production and reallocation of the resources to sink organs, including the lateral branches/supernumerary spikelets because of longer grain filling duration.

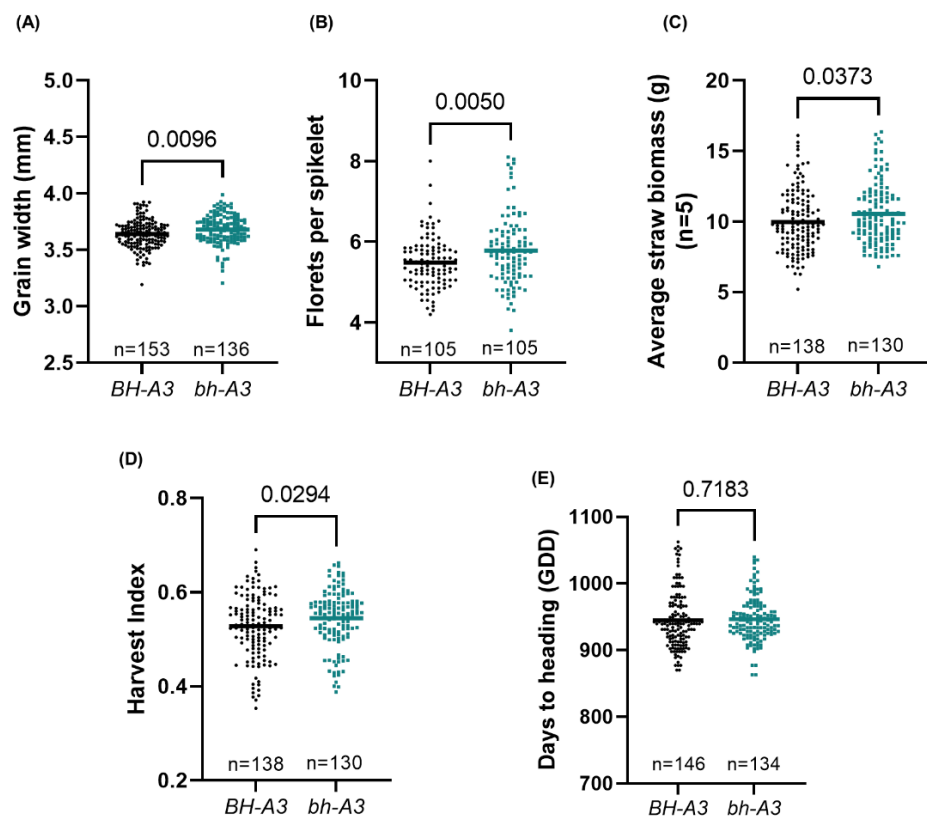


Figure 3.9. *bh^t-A3* influences (A) Grain width, (B) Florets per spikelet, (C) Straw biomass, (D) Harvest index and (E) has no effect on days to heading. Note: Data obtained from field grown plants was used for the analysis in (A-E).

3.4.3 *GPC-B1* is the major determinant of senescence rate and thousand-grain weight

A QTL on Chr 6B, which most likely is associated with *GPC-B1* (Uauy *et al.*, 2006a), explained most of the observed phenotypic variance for the overall plant senescence rate (Figure 3.10A; Appendix Table 1). Likewise, it was found that mutations in the NAC domain of *NAM-A1* (*GPC-A1*) delayed peduncle and flag leaf senescence (Harrington *et al.*, 2019). In the current study, the CIRNO allele ensured delay in the flag leaf (Figure 3.10B), peduncle (Figure 3.10C) and spike senescence (days to maturity) (Figure 3.10D). Therefore, there might be a possibility of more reallocation into the sink organs, leading to an increase in grain width (Figure 3.10E) and grain length (Figure 3.10F). Accordingly, we observed a considerably higher thousand-grain weight in the RILs that senesce late (Figure 3.10G). Besides, there was no meaningful difference in grain number per five spikes (Appendix Figure 19A), straw biomass (Appendix Figure 19B) and harvest index (Appendix Figure 19C). Although flag leaf length was not directly affected by this QTL (Appendix Figure 19D), longer flag leaves, in general, had a positive effect on thousand-grain weight in both allele groups (Figure 3.11A&B) *viz.*, *GPC-B1* ($R^2=0.11$; $p=0.0003$) and *gpc-B1* ($R^2=0.043$; $p=0.041$).

Notably, the relationship between flag leaf length and grain weight was relatively stronger in the early senescing genotypes. In fact, the contribution to thousand-grain weight per unit length of flag leaf was higher in the case of *gpc-B1* allele that is associated with delayed senescence (Figure 3.11C). Furthermore, we also included the effect of the allelic status at *bht-A1*, another major QTL for grain weight, in addition to *gpc-B1*. Here, the RILs with various allele combinations revealed a similar positive relationship between flag leaf length and grain weight (Figure 3.11D-G) *viz.*, *BH^t-A1+gpc-B1* ($R^2=0.113$; $p=0.0118$), *BH^t-A1+GPC-B1* ($R^2=0.164$; $p=0.0032$), *bht-A1+gpc-B1* ($R^2=0.12$; $p=0.0586$), and *bht-A1+GPC-B1* ($R^2=0.136$; $p=0.0048$). Overall, these observations support the importance of source strength *i.e.*, possibly more resource production and reallocation (delayed senescence) enhanced *per se* thousand-grain weight in the current population, including the spike-branching genotypes.

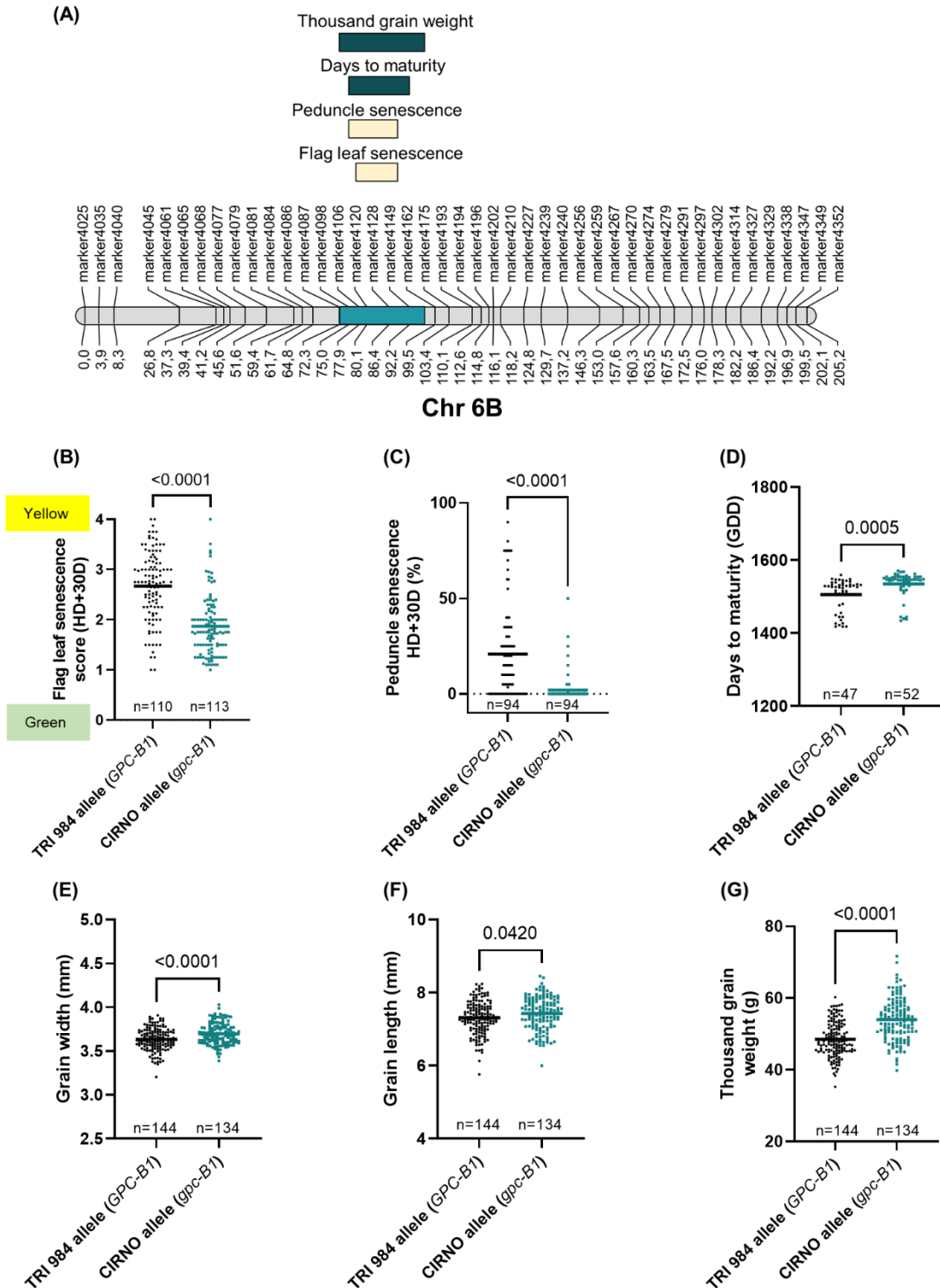


Figure 3.10. *gpc-B1* regulates senescence rate and grain weight. (A) QTLs for overall senescence rate and thousand-grain weight co-localized on Chr 6B. (B) The modern (CIRNO) allele mediated delay in flag leaf senescence, (C) peduncle senescence and (D) days to maturity (spike senescence). The resulting increase in the post-anthesis phase is translated into (E) an increase in grain width, (F) grain length and eventually (G) thousand-grain weight. Note: In (B-G), 'n' represents the number of RILs that were compared for each allele class, viz., TRI 984 allele data points are in 'black', while 'cyan' colored data points represent CIRNO allele. 'Unpaired t test' was used to determine the statistical significance, and the resulting P-

values (Two-tailed analysis) are displayed for all the comparisons. Data obtained from field grown plants was used for the analysis in (A-G).

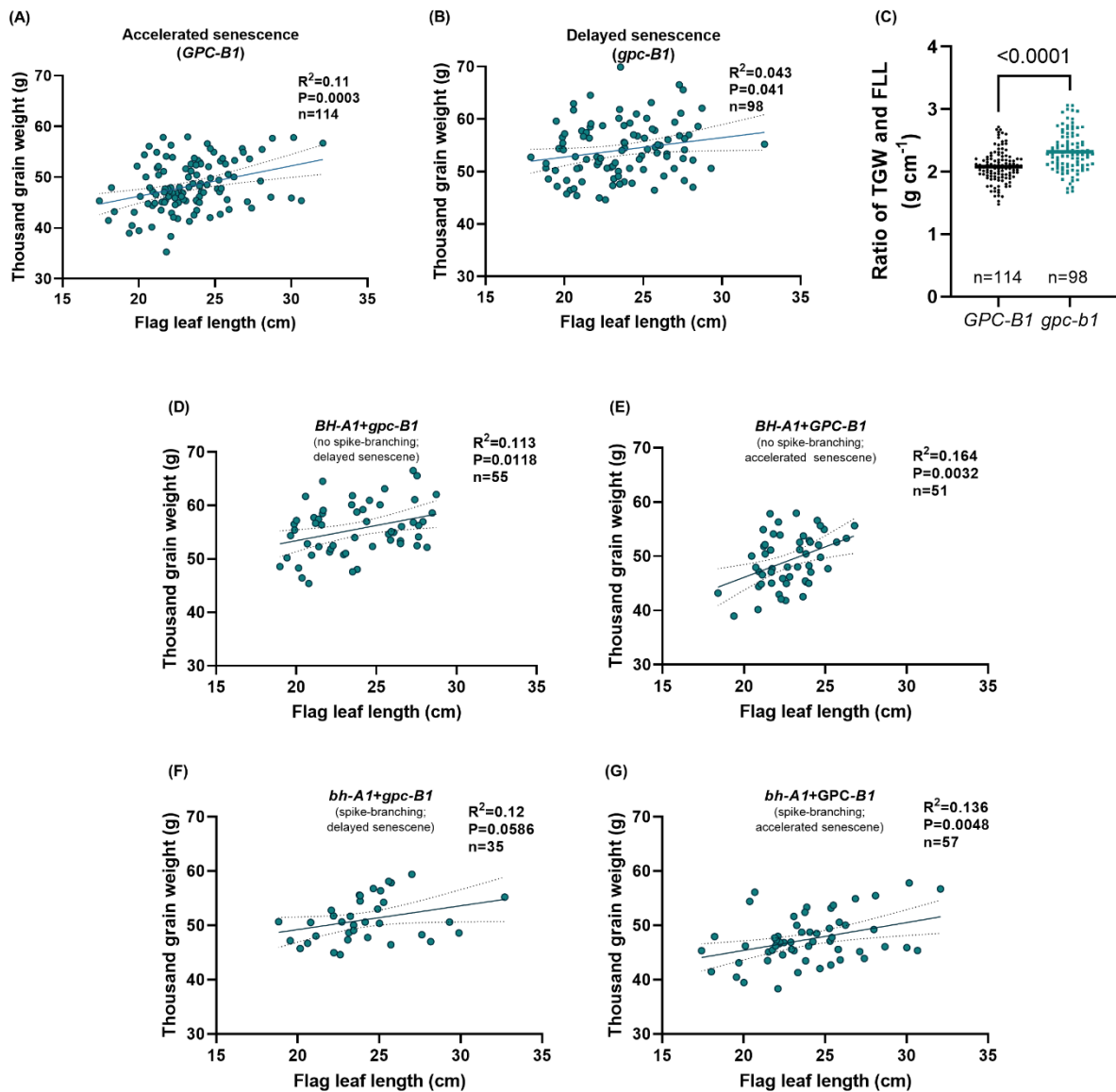


Figure 3.11. Effect of flag leaf length and thousand-grain weight in RILs carrying (A) *GPC-B1* and (B) *gpc-B1*. The contribution to thousand-grain weight per unit length of flag leaves was higher in (C) *gpc-B1* compared to *GPC-B1*. (D-G) Various allele combinations of *gpc-B1* and *bh^t-A1* and their implications on the relationship between flag leaf length and thousand-grain weight. TGW: Thousand-grain weight and FLL: Flag leaf length. Note: Data obtained from field grown plants was used for the analysis in (A-G).

3.4.4 Specific additive and epistatic interactions may increase yield potential in spike-branching genotypes

As the QTLs on Chr 2A, 5A and 6B explain variations in key source-sink attributes, we analyzed their various allelic combinations to better understand the grain yield trade-offs in spike-branching genotypes (Appendix Figure 20A-H, Figure 3.12A-G). Interestingly, the spike-branching lines carrying *bh^t-A1* and *bh^t-A3* loci along with *gpc-B1* had higher grain number per five spikes (Appendix Figure 20A, E) and were associated with a delay in post-anthesis flag leaf senescence. However, the difference in thousand-grain weight was observed only at IPK (Appendix Figure 20B & Appendix Figure 21A, B), while this effect was absent in Hohenheim (Appendix Figure 20F & Appendix Figure 21C, D). Nevertheless, they had higher grain yield per five spikes (Appendix Figure 20C, E) across all the three environments viz., IPK-2021, IPK-2022 and University of Hohenheim-2022 as opposed to the early senescing branched spike RILs (*bh^t-A1+BH^t-A3+GPC-B1*). Moreover, grain yield (per meter row) was also higher in the stay-green spike-branching RILs than the ones that senesced early (Appendix Figure 20G).

Next, we compared the impact of delayed senescence between the spike-branching RILs and those with standard spikes (no spike-branching). Although, the spike-branching RILs carrying the favorable alleles (*'bh^t-A1+BH^t-A3+GPC-B1'*) had higher grain number (Figure 3.12A), they had reduced thousand-grain weight (Figures 3.12B) than the lines with standard spikes having similar senescence rate i.e., *'BH^t-A1+bh^t-A3+gpc-B1'*; nevertheless, the final spike grain yield (Figures 3.12C) was similar in both these cases. Finally, we compared the performance of these spike-branching RILs with both the parental lines. Here, we observed a non-significant increase in grain number, but a slightly reduced thousand-grain weight than CIRNO (Figures 3.12D, E). However, there was an increase in thousand-grain weight and no change in grain number when compared to TRI 984 (Figures 3.12D, E). Eventually, the grain yield per spike of the favorable spike-branching RILs was higher than TRI 984 and similar to CIRNO (Figures 3.12F).

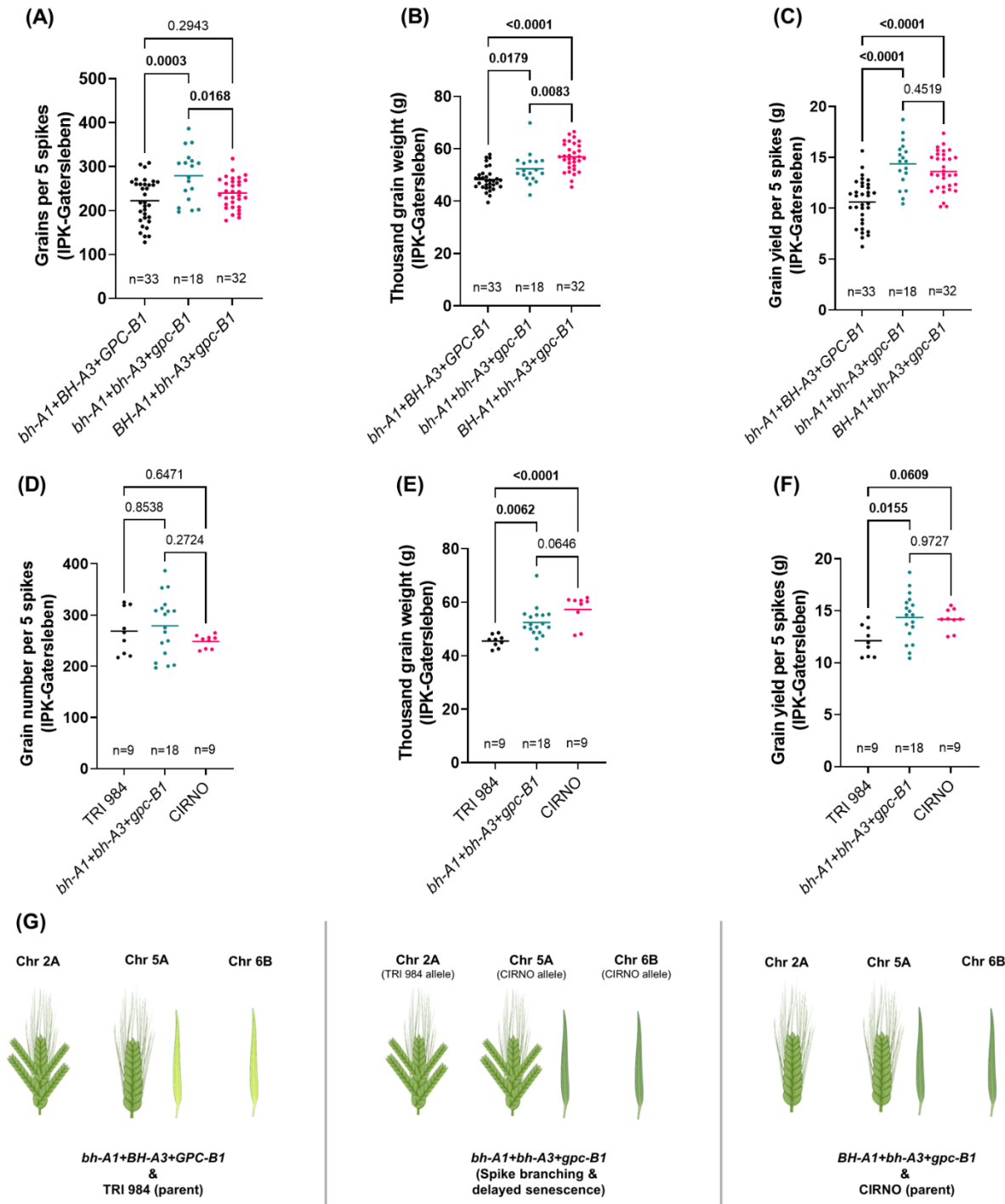


Figure 3.12. The favorable spike-branching RILs (*bh^t-A1+bh^t-A3+gpc-B1*) performed better than TRI 984, but similar to CIRNO. (A) The spike-branching RILs with delayed senescence produced more grains per spike, (B) but with a reduction in thousand-grain weight than the corresponding genotypes with standard spike i.e., no spike-branching (*BH^t-A1+bh^t-A3+gpc-B1*). (C) Further, the spike grain yield was similar among the genotypes that senesce late, irrespective of the presence or absence of spike-branching. (D) However, there was no difference in grain number as opposed to TRI 984 and CIRNO. (E) The favorable spike-branching genotypes had higher thousand-grain weight than TRI 984, whereas a reduction compared to CIRNO. (F) Finally, the spike grain yield was higher than TRI 984, but similar to CIRNO. (G) pictorial depiction of the various allelic combinations that are analyzed in (A-F).

Note: In (A-F), one-way ANOVA followed by Dunnett's test was used to determine the statistical significance. Multiple range comparison was performed, and the corresponding P-values are displayed in all the graphs (significant ones are in bold). Data obtained from field grown plants was used for the analysis in (A-F). The image (G) is partly created using biorender (<https://biorender.com/>). *bh^t-A1+BH^t-A3+GPC-B1*: Recombinants with one locus for spike-branching and two loci for accelerated senescence; *bh^t-A1+bh^t-A3+gpc-B1*: Recombinants with two loci each for spike-branching and delayed senescence. *Bh^t-A1+bh^t-A3+gpc-B1*: Recombinants without any spike-branching alleles but contain two loci for delayed senescence.

This outcome suggests that increasing the grain filling duration can only partially improve the grain yield in the spike-branching RILs. The observed increase in thousand-grain weight in such lines was because of the enhanced grain width. However, it was found that grain length, another important component of grain weight was the least in the RILs with both the spike-branching loci (*bh^t-A1+bh^t-A3*) (Figure 3.8D); this was even lower than those containing only the *bh^t-A1* locus (Figure 3.8D). Hence, to actually have a yield advantage over the genotypes with a standard spike (no spike-branching), it is necessary to address the spike-branching induced grain length trade-off as well. This aspect is explored in the next section.

3.5 The genomic regions associated with spike length affect grain size

In the TRI 984 x CIRNO population, a significant diversity was found for spike length, ranging from 6 cm up to as long as 11.5 cm (Appendix Figure 9). In total, seven QTLs viz., one each on Chr arm 1AL, 2AS, 3BS, 4AL, 5AS, 5AL, and 7BL were identified (Appendix Figure 9). The QTL on 5AL co-localizing with the Q locus explained the majority of the phenotypic variation for spike length (17.66%; high-value allele: TRI 984) (Appendix Table 1). Moreover, the longer spike type from five of these QTLs (except for Chr 1A and 2A) was associated with the TRI 984 allele. Overall, these seven QTLs accounted for about 48.18% of the spike length diversity found in the RILs. Interestingly, the high-value allele from the QTLs on Chr arm 2AS (*BH^t-A1*), 3BS, 4AL, and 5AS also had longer grains, while the QTLs on Chr arm 1AL, 5AL (Q locus), and 7BL did not exhibit such effects on grain size (Figure 3.13A-G).

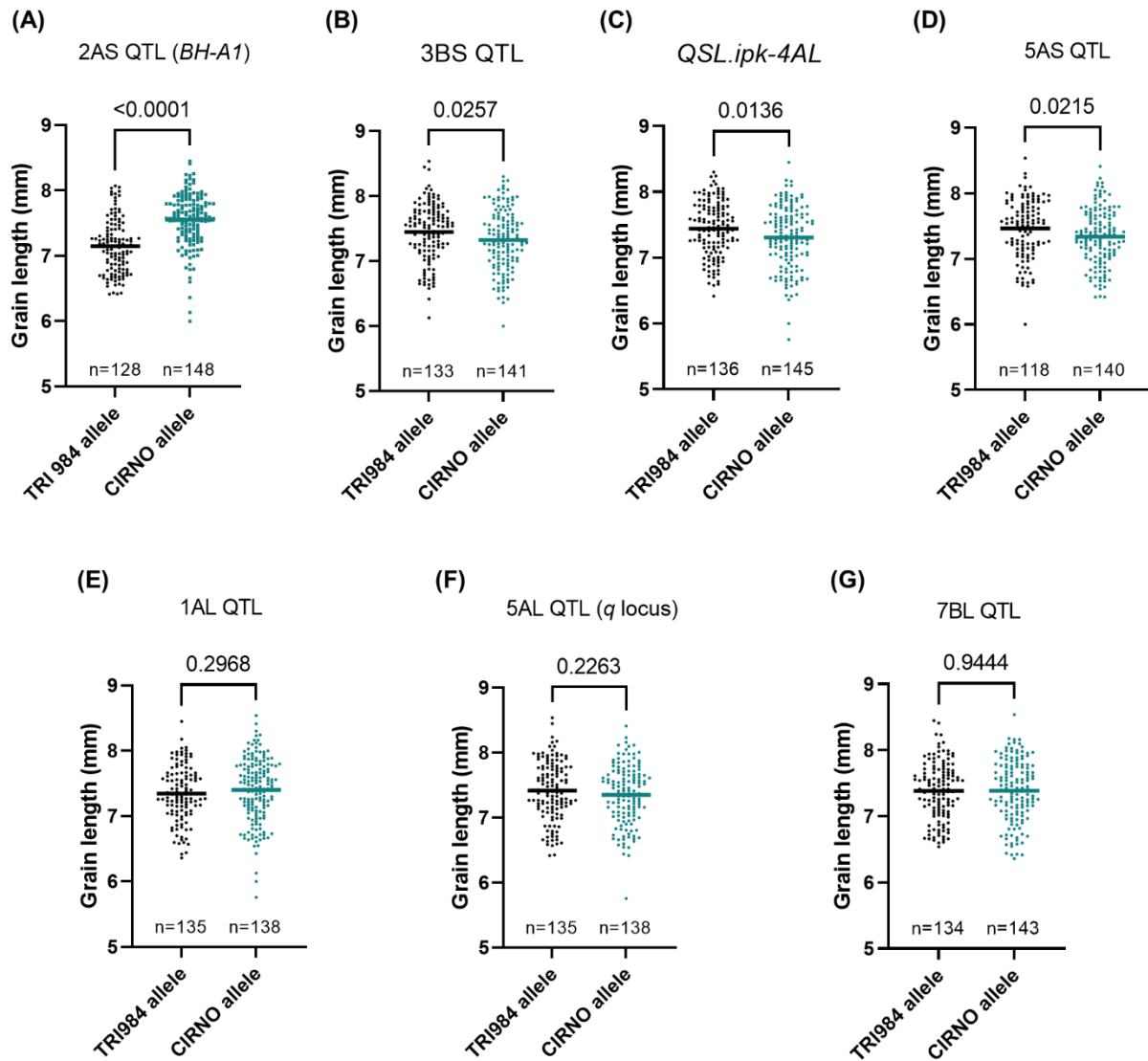


Figure 3.13. Certain spike length alleles associated with the longer spike phenotype can simultaneously increase grain length. Spike length QTLs on (A) Chr 2AS (*BH^f-A1*), (B) Chr 3BS, (C) Chr 4AL and (D) Chr 5AS affected grain length, whereas the QTLs on (E) Chr 1AL, (F) Chr 5AL (*q* locus) and (G) Chr 7BL did not exhibit such a relationship.

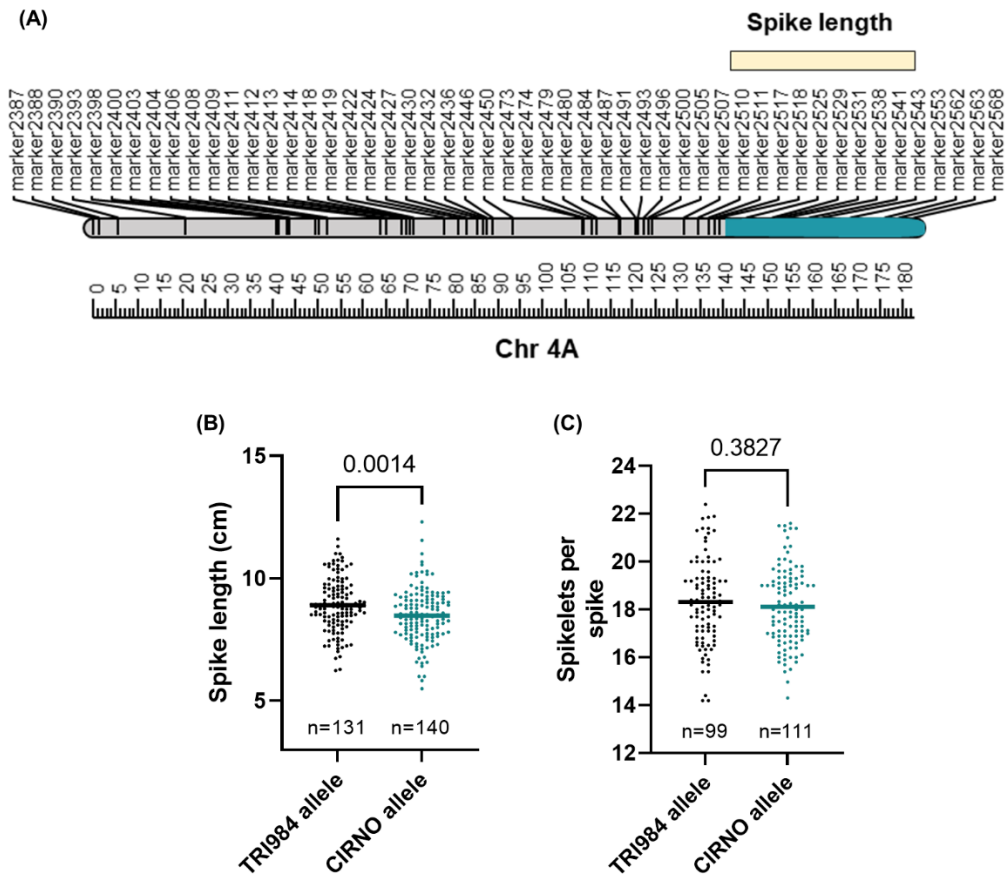


Figure 3.14. (A) *QSL.ipk-4AL* was mapped on the long arm of chromosome 4A for spike length. (B) The TRI 984 allele was associated with longer spikes, (C) however, the spikelet number per spike remained unaltered.

It is conceivable that increasing inflorescence length in the spike-branching genotypes might result in relatively longer grains and eventually higher grain yield per spike in the ‘Miracle-Wheat’ like RILs as opposed to the standard non-branching spike type. In this context, the QTL on Chr arm 4AL (hereafter *QSL.ipk-4AL*) was chosen for further analysis (Figures 3.14A-C & 3.15A-H). While the TRI 984 allele was associated with longer spikes (Figure 3.14B) and grains (Figure 3.15A, E), there was no change in spikelet number per spike (Figure 3.14C), grain width (Figure 3.15B, F) and grain number per spike (Figure 3.15 C, G). Interestingly, the QTL’s effect on grain length was much stronger in the spike-branching genotypes, and in fact, the increase in thousand-grain weight was only observed in spike-branching RILs (Figure 3.15 D, H).

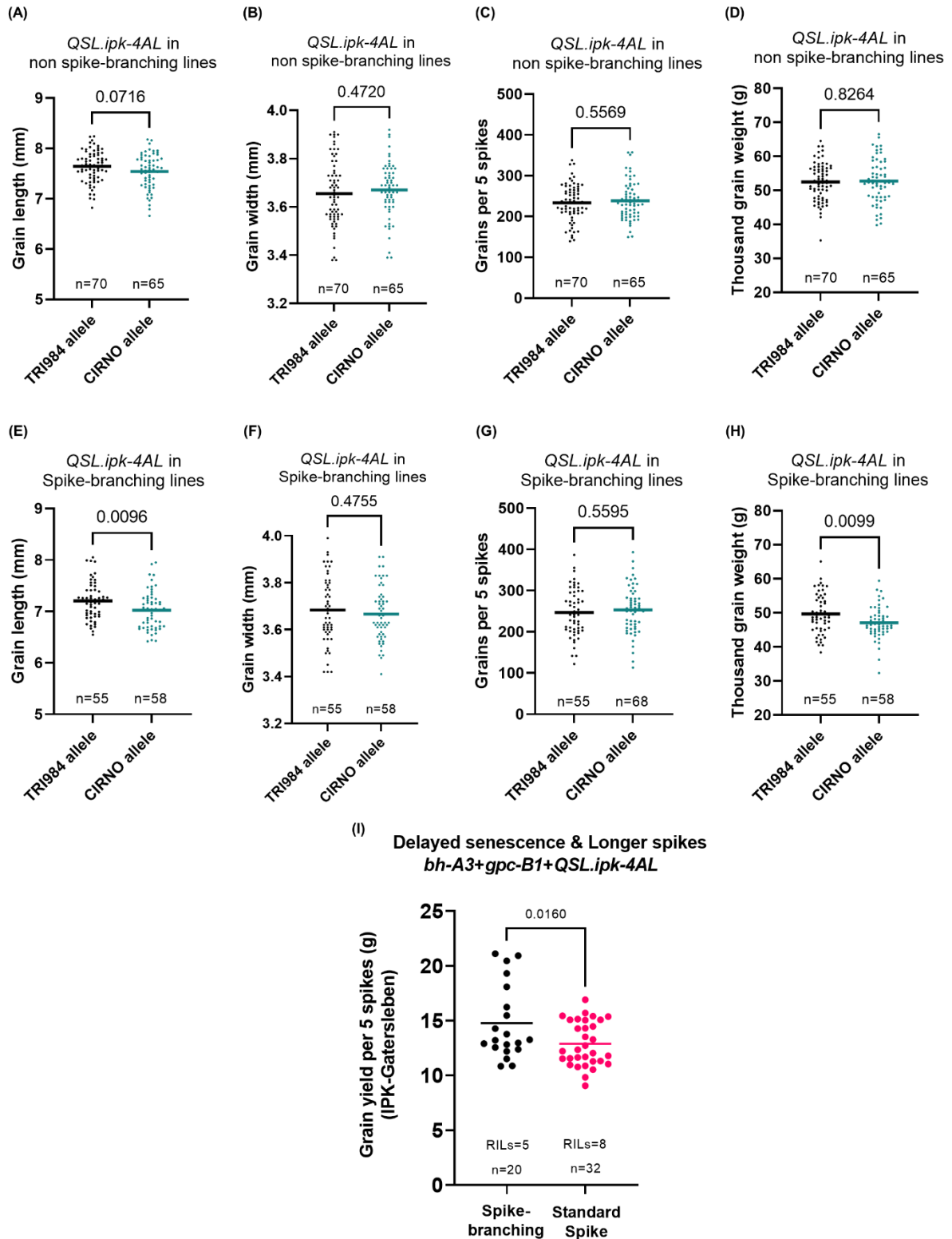


Figure 3.15. The spike-branching RILs with extended post-anthesis source activity (*bh^t-A3* and *gpc-B1*) and longer spike allele at *QSL.ipk-4AL* had higher spike grain yield than the corresponding non-spike-branching RILs. (A) Grain length, (B) Grain width, (C) Grains per 5 spikes, and (D) Thousand-grain weight in non-spike-branching RILs, while (E) Grain length, (F) Grain width, (G) Grains per 5 spikes, and (H) Thousand-grain weight depicts the status of *QSL.ipk-4AL* in spike-branching genotypes. Finally, (I) Spike grain yield in spike-

branching and non-spike-branching RILs with similar alleles for grain filling duration and spike length at *bh^t-A3*, *gpc-B1* and *QSL.ipk-4AL*.

Next, we compared the grain yield per spike in the genotypes with *QSL.ipk-4AL* (TRI 984 allele – longer spike) and delayed senescence (*gpc-B1*, *bh^t-A3*) between the spike-branching (*bh^t-A1*) and standard non-spike-branching (*BH^t-A1*) inflorescence types. The grain yield per spike was higher in the stay-green spike-branching genotypes carrying the longer spike allele (from TRI 984) than the corresponding non-spike branching RILs (Figure 3.15I). This outcome was largely due to the increase in grain length (leading to a further improvement in thousand-grain weight), an effect from *QSL.ipk-4AL*, and grain number increase coming from *bh^t-A3*, which is epistatic to *bh^t-A1*. The following sections of the thesis describe *QSL.ipk-4AL* in two additional genetic backgrounds *viz.*, TRI 19165 x Bellaroi RILs and Svevo x Zavitan introgression lines and further fine mapping.

3.5.1 Re-confirmation of *QSL.ipk-4AL* in TRI 19165 x Bellaroi recombinants

Spike length data was collected from 150 RILs derived from the spike-branching TRI 19165 and the elite durum wheat cultivar, Bellaroi that were grown in greenhouse conditions and likewise, from field grown plants (124 RILs). Composite interval mapping confirmed the contribution of *QSL.ipk-4AL* to the spike length variations under both the conditions (Figure 3.16A).

While the TRI 19165 allele resulted in longer spikes, the total node number per spike (central rachis) remained unaltered in greenhouse conditions (Figure 3.16B, C). This confirmed that the rachis internode length is higher in the genotypes carrying the TRI 19165 allele in *QSL.ipk-4AL* (Figure 3.16D). Likewise, the TRI 19165 allele also had longer spikes when evaluated from inner rows of the field experiment in Spring 2020. The observed results were in line with the previous study, where the QTL was initially mapped using the same population (Wolde *et al.*, 2019a).

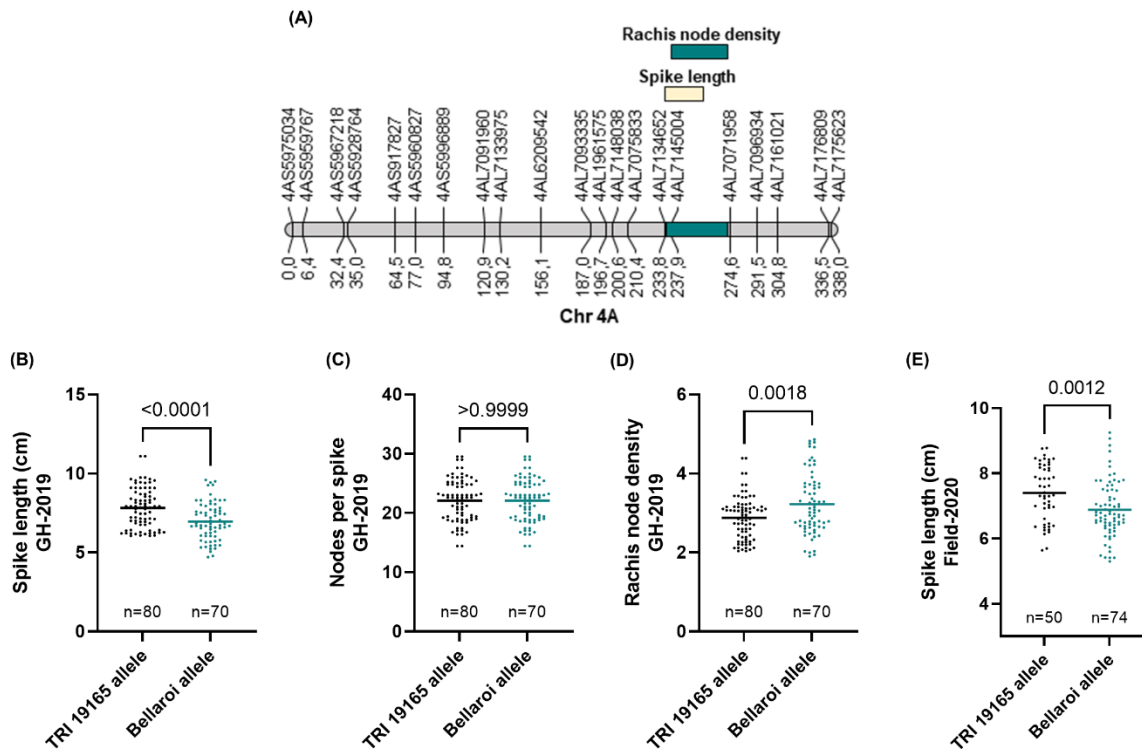


Figure 3.16. (A) Composite interval mapping of *QSL.ipk-4AL* in TRI 19165 x Bellaroi population. (B) Spike-length, (C) Nodes per spike and (D) Rachis node density evaluated under greenhouse conditions. (E) Spike length evaluated from field grown plants in Spring 2020.

3.5.2 Wild emmer introgressions within *QSL.ipk-4AL* QTL interval affects spike length

In an independent study conducted at Prof. Distelfeld's group in Israel, the same genomic region on Chr arm 4AL was mapped for spike length in the Svevo x Zavitan RIL population (Moran Nave, Master thesis). From Prof. Distelfeld's group, we obtained a set of 50 introgression lines (IL), which contain Zavitan introgressions in the Svevo background (BC₃F₄). The ILs were evaluated in IPK-Gatersleben for various traits, including spike length. We found that six ILs carrying the wild emmer introgression within the QTL interval had longer spikes than Svevo, which assisted in narrowing the QTL interval to about 3.52 Mbp region on Chr 4A long arm (Figure 3.17A).

We also screened Svevo and the ILs under control i.e., sunlight – in glasshouse) and simulated canopy shade (described in Golan *et al.*, 2023) i.e., LEE122 filter covering the roof of the glasshouse (Figure 3.17B-F). It was found that ILs showed a non-significant increase in grains per spikelet under control conditions (Figure 3.17B), while displaying a non-significant decrease under simulated canopy shade as opposed to Svevo (Figure 3.17E). Moreover, the ILs had longer grains than Svevo in both conditions (Figure 3.17C, F); the grain width was unaffected in control (Figure 3.17D),

while ILs showed a non-significant increase in grain width under simulated canopy shade (Figure 3.17G).

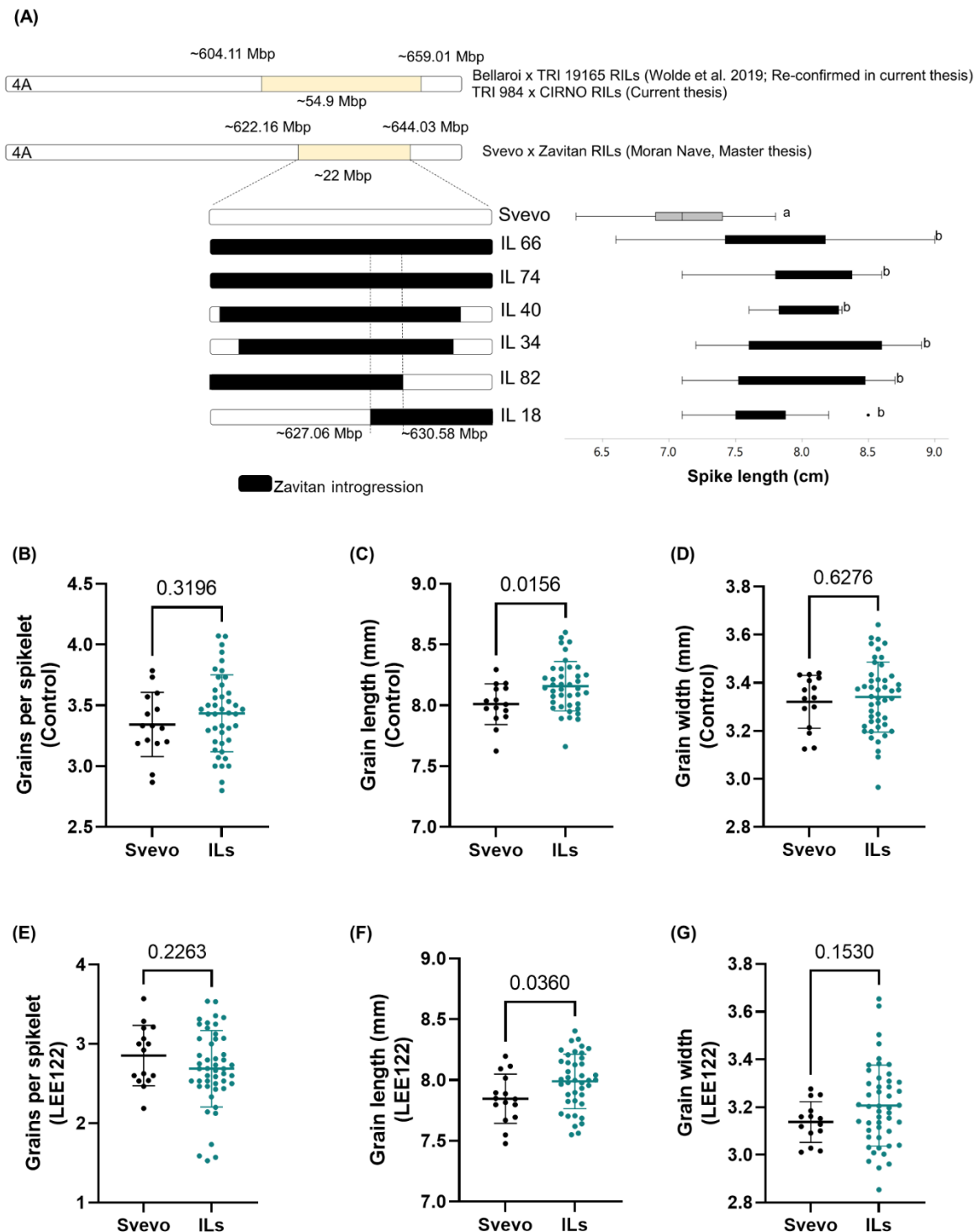


Figure 3.17. The wild emmer introgression in *QSL.ipk-4AL* resulted in longer spikes and influenced grain length. (A) Identification of six wild emmer introgression lines within the QTL interval having longer spike phenotype (Svevo background-BC₃F₄), (B) Grains per spikelet, (C) Grain length, (D) Grain width evaluated under control (sunlight) conditions in glasshouse (field like conditions – no pots). (E) Grains per spikelet, (F) Grain length, (G) Grain width under

simulated canopy shade, where the roof of the glass house is covered with LEE122 filter. Note: In (B-G), ILs indicate the data points from IL 66, IL 74, IL 40, IL 34, and IL 18 that carry wild-emmer introgression within *QSL.ipk-4AL*.

Although these ILs can be considered near isogenic to Svevo, they did contain more than one Zavitan introgression (Appendix Table 3; data based on Bacher *et al.*, 2021). Hence, in order to reconfirm the refined QTL interval, a detailed fine mapping experiment was performed.

3.5.3 High-resolution mapping of the *QSL.ipk-4AL* QTL

Initially, IL 66 and IL 74 were backcrossed to Svevo separately to develop BC₄F₁. Then, the true BC₄F₁s were selfed to obtain about 1000 BC₄F₂ lines. This population was screened using six polymorphic makers covering the QTL interval, leading to the identification of 23 recombinants (Appendix Table 4; Figure 3.18). Eventually, the recombinants were used to derive a BC₄F₃ population comprising 625 individuals.

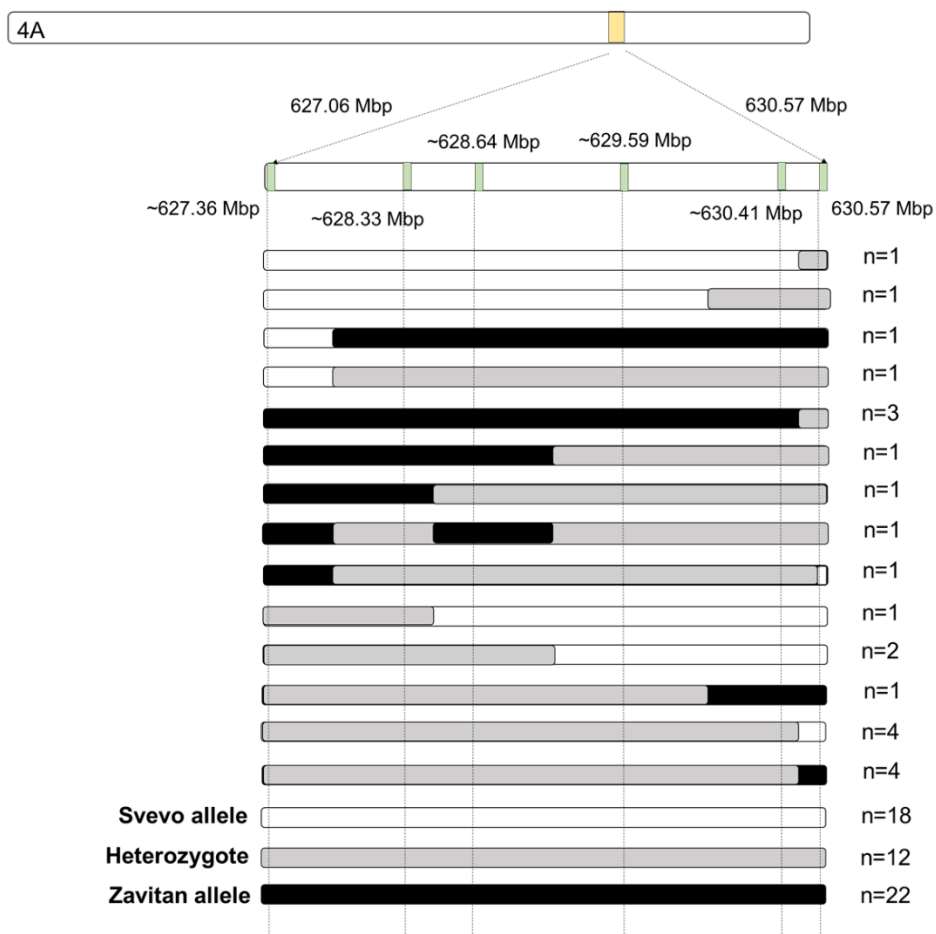


Figure 3.18. A total of 23 recombinants were identified in the BC₄F₂ generation, and the same were forwarded for further fine mapping in the consecutive generation.

All the BC₄F₃ individuals were genotyped with the previously mentioned six markers, and the corresponding spike length data was also collected. However, the genotype-phenotype linkage revealed that the underlying gene is likely more towards the distal end i.e., after 630.57 Mbp. This means that the refined interval of 3.52 Mbp (from 627.06 Mbp to 630.58 Mbp), previously determined based on IL 82, was not accurate, implying that the observed effect in IL 82 might be due to other Zavitan introgressions (totally 14.02% introgressions in IL 82) in the background (Appendix Table 3; data based on Bacher *et al.*, 2021).

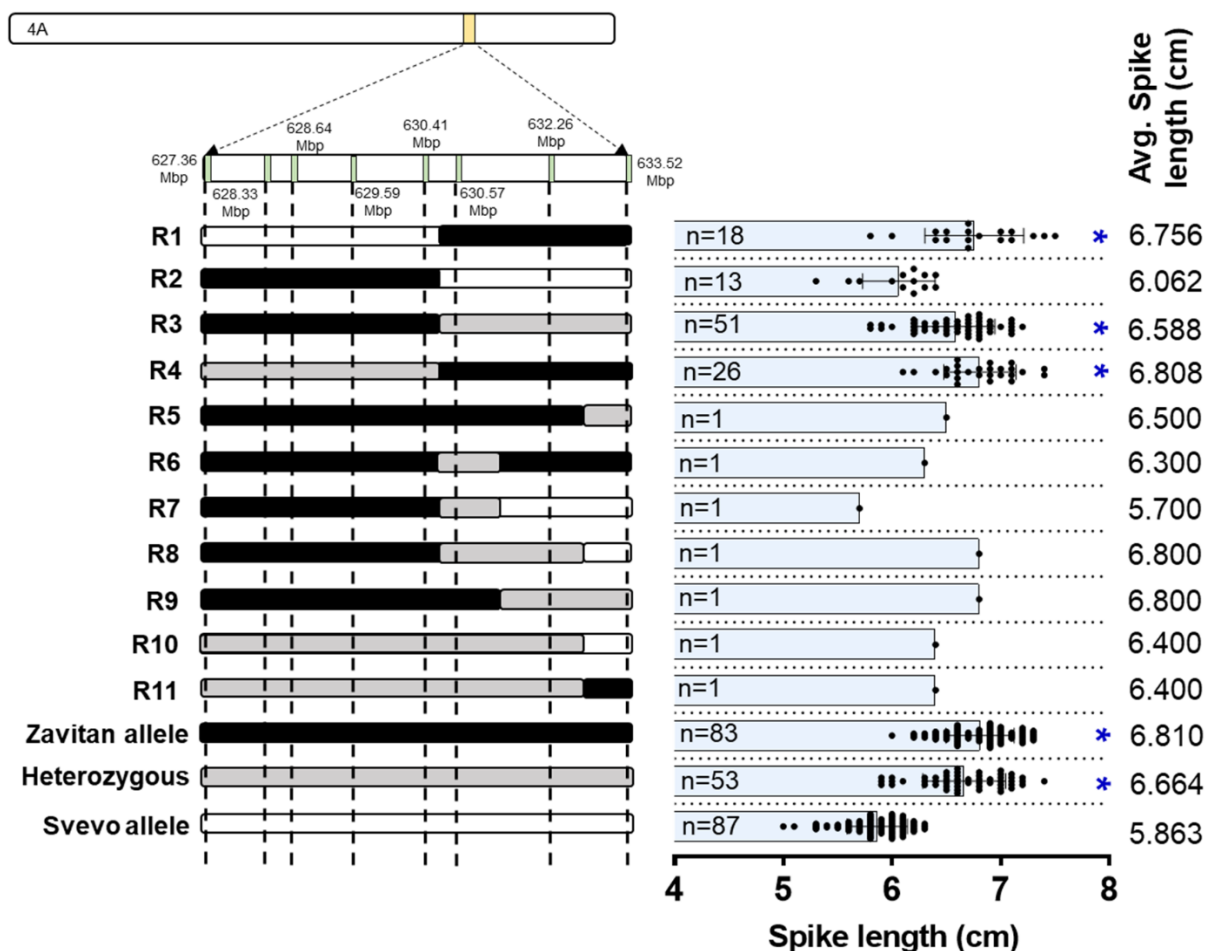


Figure 3.19. High-resolution mapping of *QSL.ipk-4AL*. The BC₄F₃ individuals were screened with eight well-distributed markers within the QTL interval, and the recombinants were related with their spike length data to fine-map *QSL.ipk-4AL*. The QTL showed a semi-dominant mode of action for spike length, as the heterozygous individuals had longer spike phenotype. Note: Blue asterisk indicates statistical significance when compared to Svevo ($p < 0.0001$; one-way ANOVA followed by Dunnett's test).

In any case, we screened the genotypes with two additional markers, the most distal one at 633.52 Mbp (based on wild emmer introgression in IL 34) and another marker

at 632.26 Mbp (Appendix Table 4; Figure 3.19). It was found that the heterozygous individuals had longer spikes than Svevo, but were slightly shorter than Zavitan; thus, suggesting a semi-dominant effect. Based on the spike length of recombinants, R1 (18 plants), R2 (13 plants), and R3 (51 plants), it was clear that the refined QTL proximal position was 630.57 Mbp. Then, seven independent recombinants comprising one plant each viz., R5 to R11 indicated 633.52 Mbp as the QTL end (Figure 3.19). Interestingly, upon comparing R7 (short spike), R8 (long spike), and R9 (long spike), the interval might further be narrowed down to a 1.69 Mbp region between 630.57 and 632.26 Mbp (Figure 3.19).

3.5.4 The ancestral allele enhanced grain yield per spike in the greenhouse

Like the previously described RIL populations, the BC₄F₃ individuals with the ancestral allele (here Zavitan) had longer spikes with unaltered spikelet number per spike (Figures 3.20A, B), thus suggesting its role in affecting rachis internode length. Here, the longer spike was also associated with increased grains per spike (Figure 3.20C), grains per spikelet (Figure 3.20D), and grain length (Figure 3.20E), but with a trade-off on grain width (Figure 3.20F); the thousand-grain weight was not affected (Figure 3.20G). Eventually, the final grain yield per spike (Figure 3.20H) was higher in the genotypes carrying the ancestral allele. It is to be noted that the BC₄F₃ population was evaluated in the greenhouse. In an earlier experiment, we found that the ILs had a non-significant decrease in grains per spikelet than Svevo under simulated canopy shade (Figure 3.17E). Hence, further experiments in genuine field conditions are required to understand the actual grain number effect. Nevertheless, the wild emmer allele had longer grains in all the experiments that we conducted in two different genetic backgrounds in multiple environments.

One possible explanation for the relationship of rachis length with grain number and grain length might be variations in resource allocation within the spike. In this context, we analyzed the vascular architecture from transverse sections of the rachis internodes (lower half of all the internodes), sampled from IL 66, IL 40, IL 34, and Svevo at the grain filling stage. Only the lateral and central veins were considered for all the measurements (Figure 3.21A). In brief, the rachis vascular area, mean vein size, vein number, and total tissue area displayed an acropetal decline in all five genotypes (Figures 3.21B-E). A similar decline in both the central and peripheral bundles towards the tip of the rachis was recorded earlier (Whingwiri *et al.*, 1981).

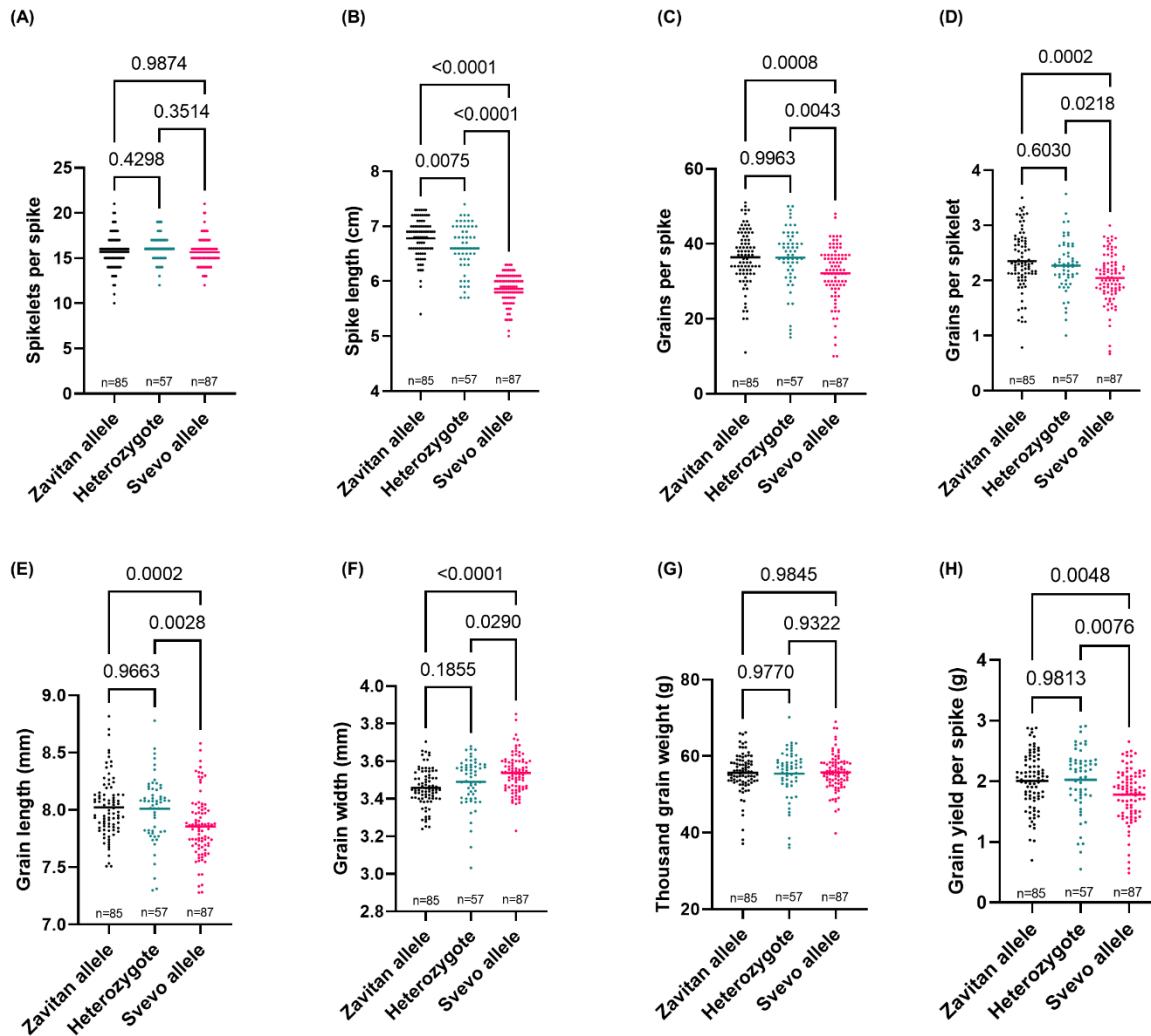


Figure 3.20. Effect of *QSL.ipk-4AL* on grain yield determinants in the greenhouse conditions. (A) Spikelets per spike remained unaltered, the BC₄F₃ lines with Zavitan allele at *QSL.ipk-4AL* and heterozygotes had (B) longer spikes, (C) more grains per spike, (D) more grains per spikelet, (E) longer grains, (F) reduced grain width, (G) no change in thousand-grain weight and eventually, (H) more grain yield per spike. Note: The classification of ‘Zavitan allele’, ‘Svevo allele’, and ‘Heterozygous’ is based on the allele status in all 8 markers depicted in Figure 3.19. For instance, ‘Zavitan allele’ consists of the BC₄F₃ lines carrying the wild emmer allele from 627.36 to 633.52 Mbp; similar is the case for ‘Svevo allele’ and ‘Heterozygous’.

Although we did not notice any drastic differences, the ILs carrying wild emmer introgressions within *QSL.ipk-4AL* showed a trend of more vascular area (Figure 3.21B) and larger vein size (Figure 3.21C) per rachis internode. In addition, the ILs had a greater number of main veins (Figure 3.21D) and a larger tissue area only in the basal part of the rachis (Figure 3.21E). As this region is closer to the peduncle-rachis junction, it was challenging to discriminate the larger veins that would make up the rachis main vascular veins from the smaller veins that may result in the peripheral

network. Hence, this outcome must be further confirmed in serial sections of developing wheat spikes at various time points.

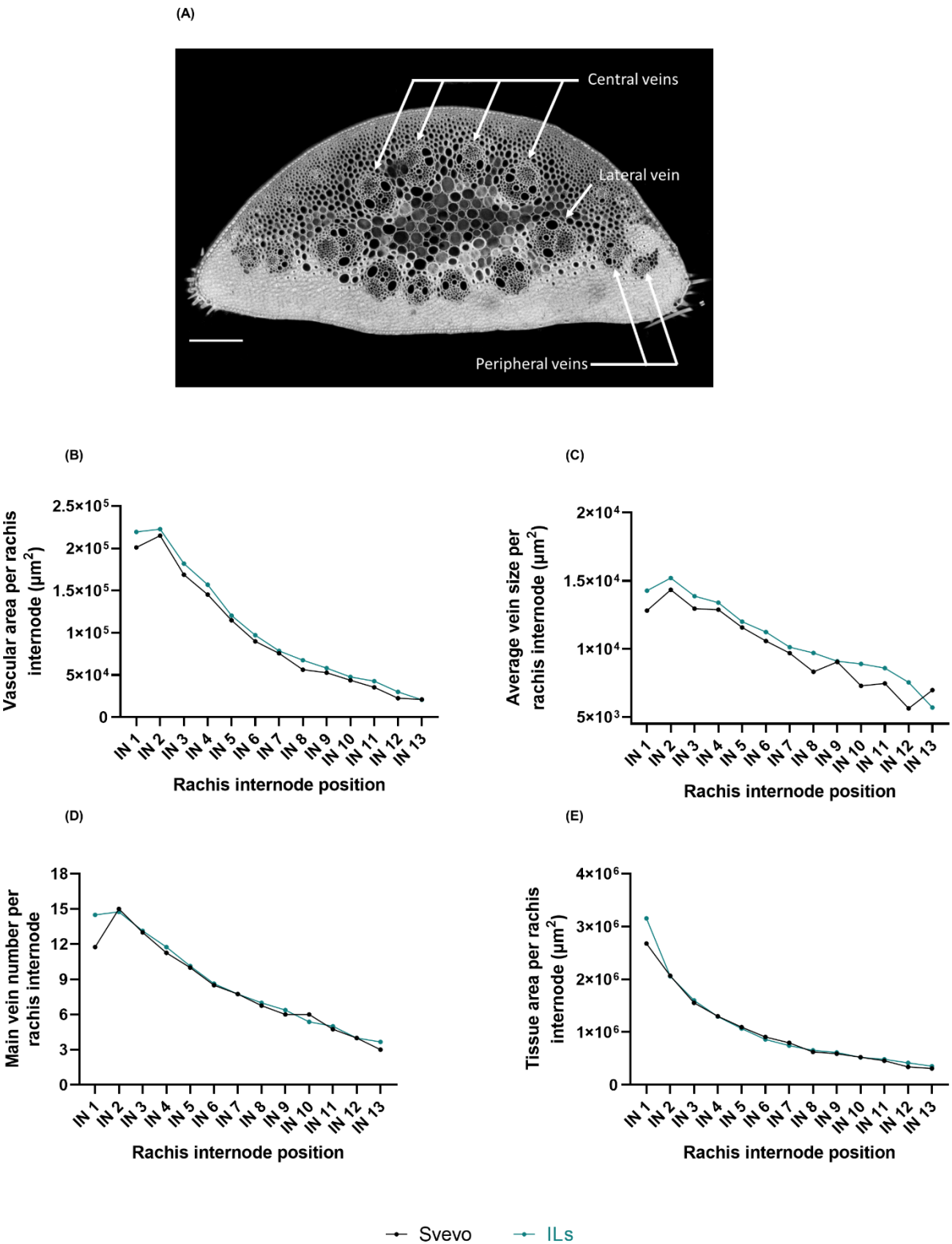


Figure 3.21. Vascular architecture of the lines carrying contrasting alleles at *QSL.ipk-4AL*. (A) representative section depicting central, lateral and peripheral veins from the 3rd rachis internode of a wheat spike. The ILs had a subtle increase in (B) vascular area per rachis

internode and (C) average vein size per rachis internode than Svevo, while the (D) main vein number and total tissue area per rachis internode were higher in the ILs only at the basal part of the spike. Note: Data was collected from 4 spikes of Svevo; ILs: 3 spikes each from IL 34 and IL 40 and two spikes of IL 66.

Nevertheless, our results indicate that longer spikes (Zavitan allele), in general, have larger veins and increased ratio of vascular area to total tissue area, especially in the middle part of the rachis (Figure 3.22 A&B); thus, it might enable increased resource partitioning to the spikelets, a plausible explanation for increased grain yield per spike. Notably, the vascular architecture data points (main vein number & size, total tissue, and vascular area) within various replications of all the tested genotypes were quite consistent.

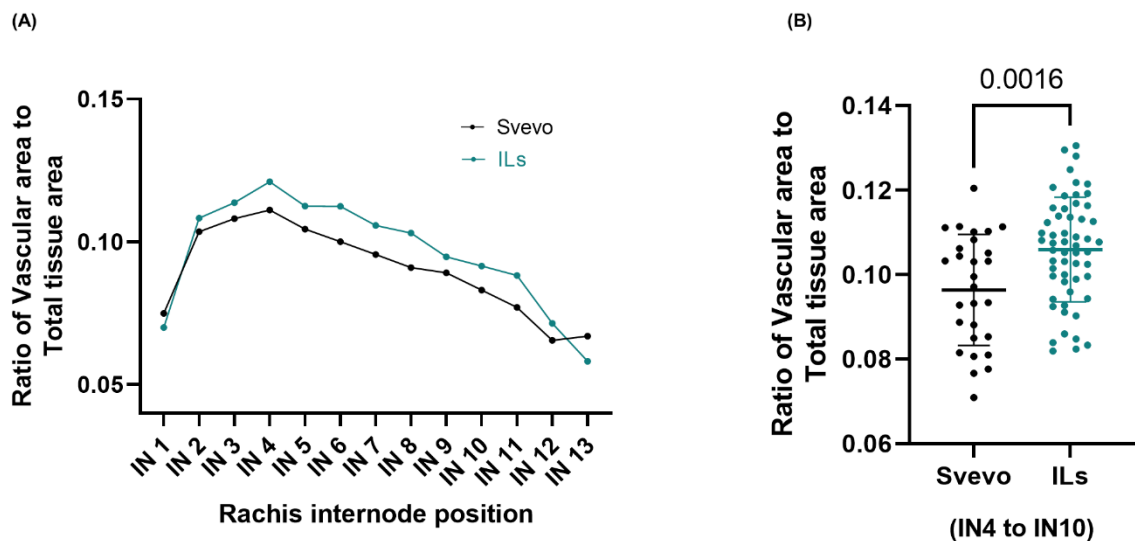


Figure 3.22. The wild emmer introgression within *QSL.ipk-4AL* increased the ratio of vascular area to total tissue area in the middle part of the rachis. (A) Ratio across the rachis and (B) from internode 4 to internode 10 in Svevo and the ILs. Note: Data was collected from 4 spikes of Svevo; ILs: 3 spikes each from IL 34 and IL 40 and two spikes of IL 66.

4. Discussion

4.1 Balancing Grain yield trade-offs in 'Miracle-Wheat'

Over the course of domestication and breeding, grain yield determinants such as grain number and grain weight, but also grain quality traits under both favorable and stressful conditions, were the primary selection targets in all major cereal crops, including wheat (*Triticum* sp.) (McSteen and Kellogg, 2022; Voss-Fels *et al.*, 2019). For instance, the selection of the semi-dwarf *Rht-1* allele was a vital driver of the 'Green Revolution' in wheat (Peng *et al.*, 1999); likewise, the prevalence of the less functional *GNI-A1* allele enabled higher floret fertility in the modern wheat cultivars (Golan *et al.*, 2019; Sakuma *et al.*, 2019). However, as described in *Section 1*, substantial genetic yield gaps [the difference between the genetic yield potential of a crop in a particular environment to that of the potential yield of the current local cultivar] suggest the presence of untapped genetic diversity for enhancing wheat grain yield (Senapati *et al.*, 2022). Grain yield can be optimized by fine-tuning various developmental processes (Mathan *et al.*, 2016) and introducing 'drastic variations' in crop breeding (Abbai *et al.*, 2020; *Section 1.5*). The genetic pathways that coordinate inflorescence architecture are dissected in staple grasses (Kellogg, 2022; Koppolu *et al.*, 2022), which might have relevance for minimizing the genetic yield gap. Here, we considered the case of spike-branching 'Miracle-Wheat' as a potential option for increasing sink strength (more spikelets and grains per spike). However, the genetic analysis of the TRI 984 x CIRNO recombinants revealed a couple of significant limitations.

Firstly, we recorded inconsistencies in the expressivity (degree) of spike-branching (in the RILs that carried similar QTLs/alleles; *Figures 3.6B, 3.7B & 3.8B*). Likewise, large variations in spike-branching intensity (*Figure 3.1E*) and eventually grain number per spike (*Figure 3.1I*) was also observed in TRI 984. Wolde *et al.*, (2021) reported that the expressivity of spike-branching in a particular genotype was higher in the outer rows as opposed to the inner rows of the plot. However, no new QTLs were mapped that specifically explained such differences. One explanation might be that field-grown plants experience competition for various resources, including light (Huber *et al.*, 2021; Postma *et al.*, 2021), especially in the inner rows (Rebetzke *et al.*, 2014). Furthermore, we had two genotypes (three rows each) in 1.5 m² plots in the current study and the neighboring genotype were not the same in all the three replications, which might have affected spike-branching differently due to asymmetric plant-plant competition, where

a particular genotype can have a competitive advantage over its neighboring genotype because its faster growth rate, variations in plant size, leaf and root architecture, among others (Weiner 1990, DeMalach *et al.*, 2016). Hence, future studies investigating the response of various source and sink component traits in high-density monoculture plots or simulated canopy shade (Golan *et al.*, 2022) are required to uncover the genetic framework of plant-plant competition and its effect on spike-branching expressivity.

Next, Poursarebani *et al.*, (2015) found that the *bht-A1* locus increases grain number, but with a grain weight trade-off. Likewise, we also observed considerably smaller grains in the spike-branching genotypes (Figure 3.1J). However, in the current study, the spike-branching phenotype induced by *bht-A1* had no effect on the final grain number (Figures 3.1I&3.6C). Interestingly, Wolde *et al.*, (2021) reported that there was no thousand-grain weight trade-off in the spike-branching Bellaroi x TRI 19165 semi-dwarf RILs and also in the Floradur NILs (semi-dwarf) with supernumerary spikelets (Wolde *et al.*, 2019b); thus, warranting the analysis of source-sink dynamics in the non-canonical spike forms. Here, it is vital to emphasize the relevance of the post-anthesis (yield realization) events, chiefly related to the transfer of assimilates to the previously established sink organs during grain filling (Murchie *et al.*, 2023; Slafer *et al.*, 2023). In this context, the senescence rate might have an impact on grain filling duration (Chapman *et al.*, 2021a; Christopher *et al.*, 2016; Hassan *et al.*, 2021; Kichey *et al.*, 2007; Li *et al.*, 2022), i.e., extended photosynthesis leading to more assimilate production and allocation to the developing grains. However, as described earlier in Section 1.2, the effect of delayed senescence on grain weight is not consistent in wheat. Lichthardt *et al.*, (2020) suggested that a higher sink capacity might be essential to capitalize on the extended photosynthetic period during the grain filling phase. This further establishes the rationale for understanding the genetic and molecular framework of source- and sink-related component traits to enable grain yield gains (Brinton and Uauy, 2019; Reynolds *et al.*, 2022). In the current study, we found that delayed flag leaf, peduncle and spike senescence is associated with higher grain number per spikelet (Figure 3.4D) and grain weight (Figure 3.4E), possibly because of the differences in various sink strength-related traits such as spikelet number per spike (spike-branching) (Figure 3.6B), spike length (Figure 3.13A) and floret number per spikelet (Figure 3.9B) in our RIL population. Hence, the favorable alleles explaining the source-sink dynamics might assist in improving grain number and grain weight in the

spike-branching genotypes. Here, we analyzed the interactions among *bht-A1*, *bht-A3*, and *gpc-B1*; while the *bht-A1* and *bht-A3* loci regulated spike-branching, but also source strength, *gpc-B1* delayed senescence rate and increased thousand-grain weight (Figure 3.12 and Appendix Figure 20). Transcriptional analysis of WT and NAM (GPC) RNAi lines revealed differential regulation of genes related to various processes, including photosynthesis and nitrogen metabolism, during flag leaf senescence (Andleeb *et al.*, 2022). Our preliminary genetic evidence indicates that *gpc-B1* might function independently of the spike-branching associated loci (Appendix Figure 22A&B). In any case, as speculated, the spike-branching RILs with an extended photosynthetic period (delayed senescence) had considerably higher grain yield (per meter row) as opposed to branched spike genotypes that senesced early (Appendix Figure 20G). The stay-green spike-branching RILs had about 11 additional grains per spike (SEM: ± 3.17) (Appendix Figure 20A). However, we believe that the grain number difference might be due to the interaction between floret number and flag leaf senescence, which is mediated by the *bht-A3* locus; here, the CIRNO allele increased florets per spikelet (Figure 3.9B) and delayed flag leaf senescence (Figure 3.7C). We further speculated that the pre-anthesis floret degeneration and the post-anthesis flag leaf senescence might share a common genetic basis thereby primarily affecting the tip of the respective organs, i.e., spikelet meristem/rachilla and flag leaf, respectively. Therefore, it is conceivable that the underlying gene might have a pleiotropic effect on floret degeneration and flag leaf senescence, thus explaining the grain number difference. Recently, enrichment of senescence related transcripts has been reported during pre-anthesis tip degeneration in barley spikes (Shanmugaraj *et al.*, 2023), which further supports our hypothesis. Then in our field experiments conducted at IPK-Gatersleben (2021 and 2022), we found an 8.5% (SEM: $\pm 3.11\%$) increase in average grain weight (Appendix Figure 20B) in the spike-branching genotypes that senesce late as opposed to the early senescing modified spike genotypes. The 2.53% (SEM: $\pm 1.01\%$) rise in grain width (Appendix Figure 21A) majorly contributed to the grain weight difference, as the grain length remained unaffected (Appendix Figure 21B). Incidentally, it was found that grain width increased during wheat evolution under domestication (Gegas *et al.*, 2010). Besides, it might be interesting to evaluate the effect of expansin genes in the spike-branching lines as the ectopic expression of *TaExpA6* increased grain length (Calderini *et al.*, 2021) or alternatively the ancestral

QSL.ipk-4AL allele can be deployed to enhance grain length in spike-branching genotypes (described in *Section 3.5*).

Further, we would like to emphasize certain limitations in our experimental setup: we used relatively small plots (~200 plants per m²) with two genotypes in one plot; therefore, the influence of the border effect ([Rebetzke et al., 2014](#)) cannot be excluded in grain yield per row calculations and besides, the evaluated population are landrace-elite recombinants, that might create another bias in the observed yield increase. Although there is a significant increase in grain number per five spikes and grain weight in the stay-green spike-branching recombinants, the actual yield advantage might be better understood by evaluating the effect in isogenic backgrounds (NILs) and larger plots in multiple environments. In this context, we are developing spike-branching CIRNO NILs for these follow-up experiments. Another trade-off associated with extending the grain filling duration that is not addressed here is its likely impact on grain nutrition profile; the functional *NAM-B1* allele improves grain protein, iron and zinc content by accelerating the senescence process ([Uauy et al., 2006a](#)). Then, the status of the stay-green spike-branching RILs under unfavorable conditions is also beyond the scope of the current study; however, previous reports indicate a positive effect of stay-green phenotypes on wheat grain yield under drought and heat ([Lopes and Reynolds, 2012](#)). Similarly, delay in senescence led to higher grain number and tiller number but lower thousand-grain weight under nitrogen-limiting conditions ([Derkx et al., 2012](#)). In addition, a recent simulation study indicates the advantage of cultivating late-maturing wheat varieties in future climate scenarios ([Minoli et al., 2022](#)), suggesting that a delay in senescence rate might eventually be beneficial for enhancing grain yield.

4.2 Implications of rachis internode length *per se* on grain yield determination in wheat

The rachis, which is the spike-axis, contains recurring structural units called phytomers similar to the culm (stem), however, the rachis internodes are much more compact ([Forster et al., 2007](#)). As mentioned in *Section 1.1*, the rachis has been a primary selection target during wheat domestication and breeding efforts. For instance, the selection of loss-of-function *btr1* allele resulted in the transition from brittle rachis to non-brittle, tough rachis (thickened cell wall in the abscission zone of rachis nodes) in

modern cultivars (Avni *et al.*, 2017). A 2 bp deletion about 290 bp after the start codon caused a premature stop codon in the *btr1-A* of Svevo (modern wheat), while in the *btr1-B*, a 4 kb insertion after 539 bp of the start codon resulted in a longer C-terminus protein sequence in Svevo, compared to wild emmer Zavitan (Avni *et al.*, 2017), leading to a loss-of-function domesticated allele. The introduction of non-brittle rachis is regarded as one of the most important events that assisted wheat domestication by minimizing yield losses due to spikelet shattering.

Likewise, the Q gene (Chr 5A) encoding an AP2-like transcription factor was found to regulate free-threshing character in domesticated wheat (Simons *et al.*, 2006). Besides, it pleiotropically affects many other traits, including spike length (Muramatsu 1963, Kato *et al.*, 1999, Faris *et al.*, 2003, Simons *et al.*, 2006, Zhang *et al.*, 2011). The *q* allele and null mutations result in a longer spear-shaped, speltoid-like spike. It was shown that a single nucleotide polymorphism in the miRNA binding site affected the interaction between miR172 and the domesticated Q allele (Debernardi *et al.*, 2017, Greenwood *et al.*, 2017). Downregulation of miR172 resulted in subcompact spikes and free-threshing grains, while its overexpression led to longer rachis internodes, a reduction in threshability, and increased floret number, suggesting that Q affects both rachis and rachilla elongation (Debernardi *et al.*, 2017, Greenwood *et al.*, 2017). Moreover, the Q homeologue on Chr 5D associated with shorter rachis also had reduced plant height and grains per spike, but with relatively more spikelets per spike and thousand-grain weight (Zeng *et al.*, 2023), while a different SNP at the miRNA binding site resulted in reduced plant height, spike length, grain number and thousand-grain weight (Chen *et al.*, 2015; Zhao *et al.*, 2018). Therefore, the selection of Q locus during domestication not only led to free-threshing grains, but also pleiotropically regulated various agronomic traits.

Besides the known effects induced by the Q locus, other direct influence of rachis length on wheat grain yield determination remains largely elusive. In this context, here we mapped a QTL for spike length – *QSL.ipk-4AL*, where the longer spike allele was also associated with increased grain length and grain number, while not affecting spikelet number per spike (Figures 3.15, 3.17, & 3.20) and plant height (Appendix Figure 23). This finding indicated that the general assumption of a trade-off in resource allocation between internodes and sink organs might not always be true in the case of rachis. Since rachis is the connecting link for resource transport to the developing

spikelets (in juvenile spikes) and grains (during grain filling), an increase in its dimensions might also be translated into larger vascular bundles, as observed in the case of *QSL.ipk-4AL* (Figures 3.21 & 3.22). It is previously known that the peduncle phloem area was the least in diploid wheat, relatively higher in tetraploid wheat, and the highest in hexaploid wheat (Evans *et al.*, 1970). Furthermore, variations were found within similar ploidy levels – the wild emmer wheat had considerably lower phloem area and number of vascular bundles than the two tested durum wheat varieties. They even found that a larger phloem area was associated with an increase in the rate of assimilate import (Evans *et al.*, 1970). These observations suggest that the increase in grain number and grain size during wheat evolution in the wild and under agriculture can at least be partly attributed to the improved vascular architecture *viz.*, more, and larger vascular bundles. Interestingly, in the current study, the wild emmer allele in *QSL.ipk-4AL* showed an increase in relative rachis vascular area (ratio of vascular area to total tissue area) and also average vein size per rachis internode – perhaps, facilitating more resource transport to spikelets; thus, increased grain number (only in optimal light – greenhouse conditions) and grain length (in both optimal light and simulated canopy shade).

While the lower three florets within a spikelet in wheat are directly connected by the principal vascular bundles, the more distal florets are supplied by only the sub-vascular elements (Hanif & Langer, 1972). Hence, a detailed investigation of the rachilla vascular architecture in the lines carrying contrasting alleles at *QSL.ipk-4AL* might strengthen our hypothesis that connects vasculature differences to grain number increase. Moreover, the wild emmer allele had longer grains and more chaff weight, implying bigger spikelets. Thus, a series of spatio-temporal sections of the vascular anatomy during spikelet development might be relevant to explore the implications of resource partitioning dynamics on spikelet size, mediated by contrasting *QSL.ipk-4AL* alleles.

Since the favorable allele of *QSL.ipk-4AL* (longer spikes and increased grain length) has been derived from wild emmer, it most likely implies an uncaptured potential for wheat breeding. The positive effect on grain length was already observed in the Svevo lines carrying the wild emmer introgression in the *QSL.ipk-4AL* interval. In addition, we also evaluated its contribution in TRI 984 x CIRNO RIL population. As described in Section 3.5, the stay-green spike-branching lines carrying the longer spike allele at

QSL.ipk-4AL had higher grain yield per spike than the corresponding non-spike branching RILs (Figure 3.15I), indicating its usefulness for improving 'Miracle-Wheat'-like genotypes.

5. Outlook

5.1 Integrating reductionist approach and genomic selection might improve grain yield gains in spike-branching wheat

The final grain yield is a highly polygenic trait and is the primary target of any breeding program. Broadly, two major strategies are in practice for enhancing grain yield. The first one is a genomic selection (GS) based approach, where the lines with higher 'genomic estimated breeding values (GEBVs)' are forwarded to yield trials (Crossa *et al.*, 2017). Here, the primary focus is on the final plot yield, while the underlying physiological and genetic mechanisms regulating grain yield determination are often ignored. The second strategy is a reductionist approach, where the trait architecture i.e., the factors affecting the yield components and their interactions (for e.g., traits affecting source activity and sink capacity) are first explored, and then the favorable alleles/haplotypes are identified for further use in crop improvement (Bevan *et al.*, 2017; Brinton and Uauy, 2019; Reynolds *et al.*, 2022). Recently, it has been shown that genomic predictions in genebank accessions assisted in shortlisting best parents (unadapted plant genetic resources) for recombining with modern cultivars and the lines derived from such crosses outperformed the local wheat varieties (Schulthess *et al.*, 2022). Conceivably, the selection of parental lines is one of the major factors affecting the genetic gains in a breeding program. In this context, the insights obtained from a reductionist approach might enable identifying an informed set of parental lines (Bevan *et al.*, 2017, Brinton & Uauy, 2019; Brinton *et al.*, 2020). Besides, the GS + *de novo* GWAS model performed better than RR-BLUP and random forest for predicting grain yield-related traits in rice (Spindel *et al.*, 2016), suggesting the benefits of combining marker-trait association data with GS.

This therefore implies that the shortlisted trait-based parents need not themselves be high-yielding *per se*, but should harbor favorable alleles for specific traits that can be rationally combined using GS (Figure 5.1) (hence, parents can be from unadapted sources, such as wild relatives and landraces). Such an approach can capitalize on the favorable major and moderate effect loci (>5% phenotypic variance) identified through genetic analyses, while GS might capture the minor effect alleles. For instance, to improve grain yield gains in spike-branching wheat (Parents 1, 1.1...1.n: high sink number), genotypes harboring favorable alleles for stronger pre-and post-anthesis source activity (Parents 2, 2.1...2.n), increased assimilate remobilization from source to sink (Parents 3, 3.1...3.n) and a set of locally adapted elite cultivars (Parents 4,

4.1...4.n) might be intercrossed to develop a multi-parent advanced generation intercross (MAGIC) population. Such a MAGIC panel represents an array of diverse genotypic combinations of the parents. Eventually, the top performers can be selected based on the presence of favorable alleles (previously known major effect alleles from a reductionist approach and new minor effect alleles identified based on GEBVs) and compared with the grain yield of locally adapted varieties under genuine field conditions. I believe that the proposed experiment might further reduce the yield gap (the difference between potential yield and final yield) and trade-offs in 'Miracle-Wheat'-like genotypes. As spike-branching is not widely used in modern breeding, introducing this as a target trait might offer a new path for wheat improvement.

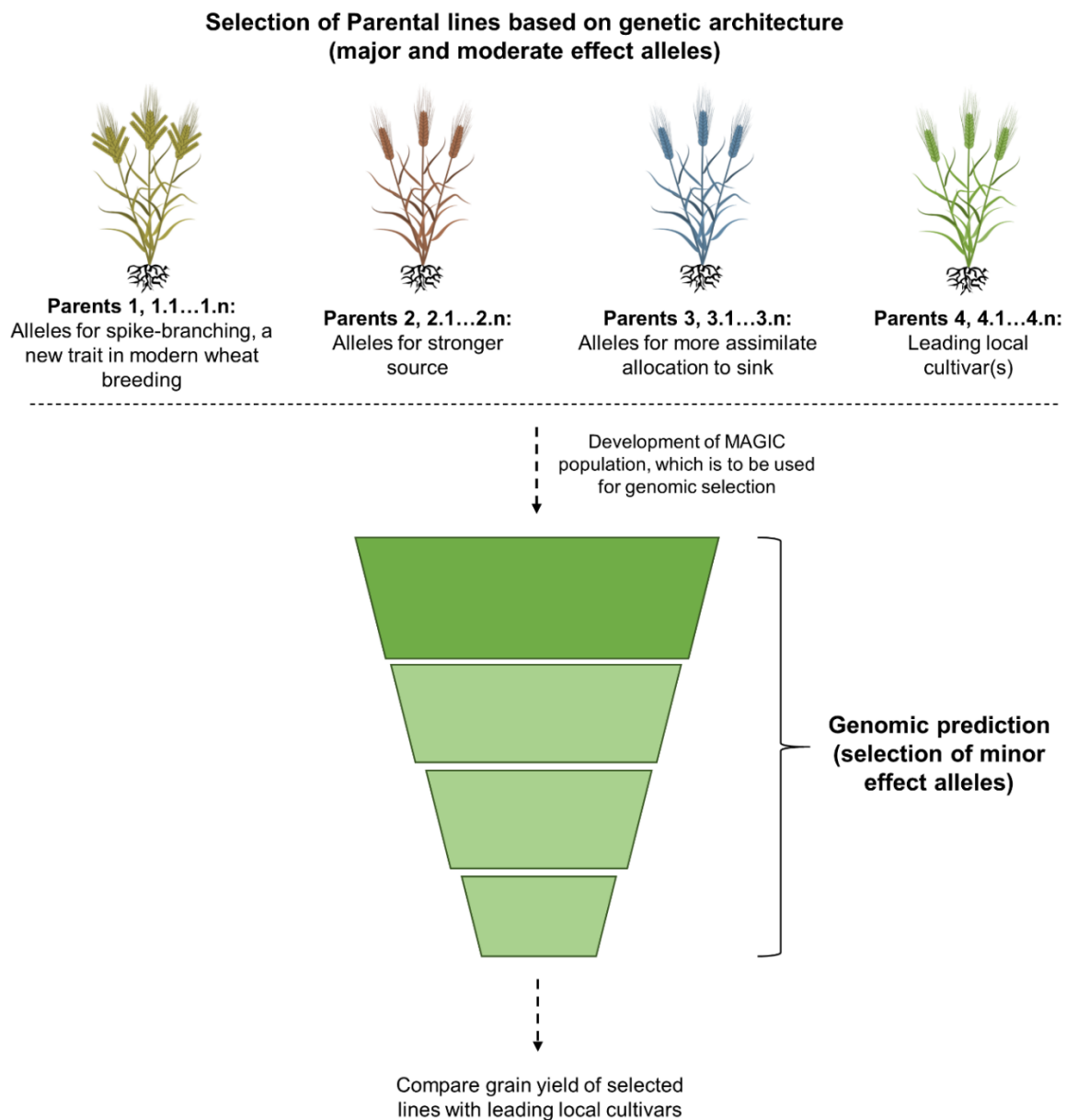


Figure 5.1. Proposed framework for integrating reductionist approach with genomic selection.

Moreover, this strategy can capitalize on the decades of functional genetics efforts for a well-informed GS not only in the case of spike-branching wheat, but also can be extended to other traits in various crops. For instance, over 4000 genes have been functionally characterized in rice (Huang *et al.*, 2022), but only a small number of them are consciously selected in breeding (Abbai *et al.*, 2019; Zhang *et al.*, 2021).

5.2 Identification and functional characterization of the gene underlying *QSL.ipk-4AL*

Based on the fine mapping results (presented in Section 3.5.3), the QTL interval can be narrowed down to a 1.69 Mb region comprising 11 high-confidence genes that are expressed in developing spikes of Zavitan (Table 5.1).

Table 5.1. High confident genes within the *QSL.ipk-4AL* interval that show expression in the developing Zavitan spike.

Gene_Id_Zavitan	Description	start_Zavitan	end_Zavitan
TRIDC4AG054780	Late embryogenesis abundant hydroxyproline-rich glycoprotein	630577424	630580733
TRIDC4AG054790	Late embryogenesis abundant hydroxyproline-rich glycoprotein	630586806	630586922
TRIDC4AG054880	PHD zinc finger protein, putative	631580240	631580320
TRIDC4AG054920	MAN1; Mannan endo-1,4-beta-mannosidase 4	631682321	631682634
TRIDC4AG054940	Uncharacterized protein At1g48350; 50S ribosomal protein L18	631695496	631695514
TRIDC4AG054960	Dirigent protein	631723924	631724258
TRIDC4AG054990	Non-specific phospholipase C	631786010	631786972
TRIDC4AG055020	Katanin p80 WD40 repeat-containing subunit B1 homolog	631882054	631882299
TRIDC4AG055030	N-acetyltransferase	631885193	631885426
TRIDC4AG055050	JmjC and C2H2 Zinc finger protein	631979594	631979776
TRIDC4AG055060	Appr-1-p processing enzyme family protein	632196380	632196397

Among them, TRIDC4AG055050 contains Jumonji C (JmjC) and C2H2 zinc finger domains; a total of 8 amino acid differences were found between the Svevo and Zavitan proteins ([Appendix Figure 24](#)). JmjC domain-containing proteins have been earlier shown to demethylate trimethyl histone 3 lysine 9 (H3K9me) and affect the expression of brassinosteroid (BR) regulated genes in *Arabidopsis thaliana* ([Yu et al., 2008b](#)). Mutations in the JmjC domain of *early flowering 6 (elf6)* and *relative of early flowering 6 (ref6)* displayed differences in flowering time and BR-related phenotypes such as impaired cell elongation and compromised BR-regulated gene expression in *A. thaliana* ([Yu et al., 2008b](#)). As rachis internode elongation is the primary phenotype of *QSL.ipk-4AL*, the JmjC domain-containing protein might be one of the potential candidate genes. However, no significant differences were observed in flowering time between Svevo and the ILs.

Moreover, two genes within the QTL interval might modulate cell wall properties *viz.*, TRIDC4AG05496 (dirigent protein) and TRIDC4AG054920 (MAN1; Mannan endo-1,4-beta-mannosidase 4); in both these cases, amino acid variations were found between the Svevo and Zavitan proteins ([Appendix Figure 25](#) and [Appendix Figure 26](#)). Dirigent proteins were reported to affect the lignin deposition in cell wall ([reviewed by Paniagua et al., 2017](#)). Likewise, mannan hydrolyzing enzymes alter the properties of primary cell wall ([Iglesias-Fernández et al., 2011](#); [Wang et al., 2014b](#)). Hence, it might be worthwhile to check for rachis cell wall composition differences and their implications on cell size in the contrasting genotypes (ancestral vs modern allele).

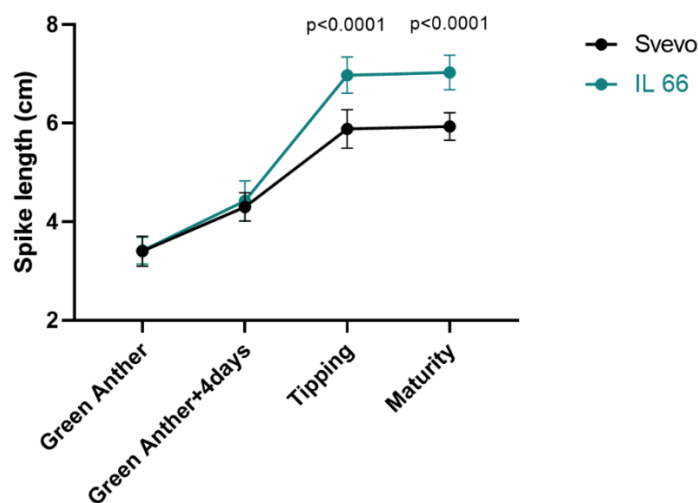


Figure 5.2. Elongation of spike during various developmental stages. The major difference in spike length occurs from GA+4d to Tipping, where IL 66 carrying the wild emmer

introgression within *QSL.ipk-4AL* is longer than Svevo. This analysis was performed using the plants (main culm spike) grown in greenhouse (9 cm square pots, long day condition).

Furthermore, capturing the gene expression variations during rachis elongation might offer additional support in the identification of the underlying gene. It was found that the spike length was similar in both Svevo and IL 66 until green anther+4 days (GA+4d). But, the major difference in spike elongation occurred between GA+4d and the tipping stage (maximum spike length), where IL 66 was considerably longer than Svevo (Figure 5.2); hence, GA, GA+4d, and tipping stages are the key time points for the comparative transcriptome analysis of the developing rachis. Furthermore, the characterization of knock-out mutants (TILLING resource or gene editing) and overexpression lines can confirm the causal gene of *QSL.ipk-4AL*.

6. Summary

Introducing variations in inflorescence architecture, such as the 'Miracle-Wheat' (*Triticum turgidum* convar. *compositum* (L.f.) Filat.) with a branching spike, has relevance for enhancing wheat grain yield. However, in the spike-branching genotypes, the increase in spikelet number is generally not translated into grain yield advantage because of reduced grains per spikelet and shorter grains. Here, we investigated if such trade-offs might be a function of source-sink strength by using 385 RILs developed by intercrossing the spike-branching landrace TRI 984 and CIRNO, an elite durum (*T. durum* L.) cultivar; they were genotyped using the 25K array. About 30 traits affecting sink capacity and post-anthesis source activity were phenotyped under field conditions for two consecutive years and a total of 130 QTLs were mapped. On Chr 5AL, we found a new modifier QTL for spike-branching, *branched head^t 3* (*bh^t-A3*), which was epistatic to the previously known *bh^t-A1* locus and derived from the elite parent. Besides, *bh^t-A3* was associated with more grains per spikelet, a delay in flag leaf senescence rate, and increased grain width, but with a trade-off on grain length.

Interestingly, it was found that some of the QTLs mapped for spike length, including *QSL.ipk-4AL*, affected grain length. The effect of *QSL.ipk-4AL* was confirmed in three different genetic backgrounds in multiple environments and was eventually fine-mapped using a population derived from wild emmer introgression lines and a modern durum cultivar, Svevo. Furthermore, the ancestral allele at *QSL.ipk-4AL* associated with longer rachis and grains, also had an increased ratio of vascular area to total tissue area in rachis and slightly larger rachis vascular bundles, key "interior" architectural traits that might affect resource partitioning to the spikelets. Besides, the longer spike allele at *QSL.ipk-4AL* showed a grain number increase in greenhouse conditions (in pots), but suffered a non-significant reduction in grain number when evaluated under simulated canopy shade (field-like plots in the glasshouse, where the roof is covered with a green LEE122 filter).

Nevertheless, favorable alleles *viz.*, *bh^t-A3*, *grain protein content* (*gpc-B1*) that delayed senescence and *QSL.ipk-4AL* (longer spike and more grain length) increased grain number and grain weight in spike-branching wheat, suggesting that combining both the elite and untapped ancestral alleles affecting sink capacity and post-anthesis source activity is required for its holistic improvement. Overall, findings from the current

thesis provide a genetic framework for increasing yield gains in 'Miracle-Wheat' and also interesting candidate QTLs for further characterization.

7. Zusammenfassung

Die Einführung von Variationen in der Blütenstandsarchitektur, wie z. B. der "Wunderweizen" (*Triticum turgidum* convar. *compositum* (L.f.) Filat.) mit einer verzweigten Ähre, ist für die Steigerung des Kornertrags von Weizen von Bedeutung. Bei den Genotypen mit verzweigten Ähren wird die Zunahme der Ährchenanzahl jedoch im Allgemeinen nicht in einen Vorteil beim Kornertrag umgesetzt, da die Körner pro Ährchen und die Kornlänge reduziert sind. Hier haben wir untersucht, ob solche Effekte von der Stärke der Sinks abhängen, indem wir 385 RILs verwendet haben, die durch Kreuzung der ährenverzweigenden Landrasse TRI 984 und CIRNO, einer Durum-Elitesorte (*T. durum* L.), entstanden sind; sie wurden mit dem 25K-Array genotypisiert. Etwa 30 Merkmale, die die Sink-Kapazität und die Source-Aktivität nach der Blüte beeinflussen, wurden in zwei aufeinander folgenden Jahren unter Feldbedingungen phänotypisiert, und insgesamt wurden 130 QTLs kartiert. Auf Chr 5AL fanden wir einen neuen Modifikator-QTL für die Ährenverzweigung, *branched head^t 3 (bht^t-A3)*, der epistatisch zum bereits bekannten *bht^t-A1*-Locus ist. Außerdem zeigte *bht^t-A3* mehr Körner pro Ährchen, eine Verzögerung der Seneszenzrate der Fahnenblätter und eine größere Kornbreite verbunden, allerdings mit verkürzter Kornlänge.

Interessanterweise wurde festgestellt, dass einige der für die Ährenlänge kartierten QTLs, einschließlich *QSL.ipk-4AL*, auch die Kornlänge beeinflussen. Die Auswirkung von *QSL.ipk-4AL* wurde in drei verschiedenen genetischen Hintergründen in verschiedenen Umgebungen bestätigt und wurde schließlich mit einer Population, die von wilden Emmer-Introgressionslinien und einer modernen Durum-Sorte, Svevo, abgeleitet wurde, feinkartiert. Darüber hinaus wies das Wildallel, *QSL.ipk-4AL*, das mit einer längeren Spindel und längeren Körnern assoziiert ist, auch ein erhöhtes Verhältnis von Gefäßfläche zu Gesamtgewebefläche in der Spindel und etwas größere Gefäßbündel in der Spindel auf - wichtige architektonische Merkmale, die die Verteilung der Ressourcen auf die Ährchen beeinflussen könnten. Außerdem zeigte das Wildallel *QSL.ipk-4AL* mit den längeren Ähren unter Gewächshausbedingungen (in Töpfen) einen Anstieg der Körnerzahl, dies ergab jedoch eine nicht signifikante

Verringerung der Körnerzahl, wenn es unter simulierter Beschattung angebaut wurde (feldähnliche Parzellen im Gewächshaus, bei denen das Dach mit einem grünen LEE122-Filter bedeckt ist).

Dennoch erhöhten günstige Allele, nämlich *bht-A3*, *grain protein content (gpc-B1)*, der die Seneszenz verzögert, und *QSL.ipk-4AL* (längere Ähre und größere Kornlänge) die Kornzahl und das Korngewicht bei ährenverzweigendem Weizen, was darauf hindeutet, dass für eine ganzheitliche Verbesserung sowohl die Kombination von Elite- als auch unerschlossenen Vorfahren-Allelen, die die Sink-Kapazität und die Source-Aktivität nach der Blüte beeinflussen, erforderlich ist. Insgesamt bieten die Ergebnisse der vorliegenden Arbeit einen genetischen Rahmen für die Steigerung der Ertragsgewinne bei 'Miracle-Weizen' und auch interessante Kandidaten-QTLs für eine weitere Charakterisierung.

8. References

- Abbai R, Golan G, Longin CFH, Schnurbusch T.** 2023. Grain yield trade-offs in spike-branching wheat can be mitigated by elite alleles affecting sink capacity and post-anthesis source activity. *Journal of Experimental Botany*, erad373.
- Abbai R, Singh VK, Nachimuthu VV, Sinha P, Selvaraj R, Vipparla AK, Singh AK, Singh UM, Varshney RK, Kumar A.** 2019. Haplotype analysis of key genes governing grain yield and quality traits across 3K RG panel reveals scope for the development of tailor-made rice with enhanced genetic gains. *Plant Biotechnology Journal* **17**, 1612-1622.
- Abbai R, Singh VK, Snowdon RJ, Kumar A, Schnurbusch T.** 2020. Seeking Crops with Balanced Parts for the Ideal Whole. *Trends in Plant Science* **25**, 1189-1193.
- Acreche MM, Slafer GA.** 2009. Grain weight, radiation interception and use efficiency as affected by sink-strength in Mediterranean wheats released from 1940 to 2005. *Field Crops Research* **110**, 98-105.
- Adamski NM, Borrill P, Brinton J, Harrington SA, Marchal C, Bentley AR, Bovill WD, Cattivelli L, Cockram J, Contreras-Moreira B, Ford B, Ghosh S, Harwood W, Hassani-Pak K, Hayta S, Hickey LT, Kanyuka K, King J, Maccaferri M, Naamati G, Pozniak CJ, Ramirez-Gonzalez RH, Sansaloni C, Trevaskis B, Wingen LU, Wulff BBH, Uauy C.** 2020. A roadmap for gene functional characterisation in crops with large genomes: Lessons from polyploid wheat. *eLife* **9**, e55646.
- Allen AM, Winfield MO, Burrige AJ, Downie RC, Benbow HR, Barker GL, Wilkinson PA, Coghill J, Waterfall C, Davassi A.** 2017. Characterization of a Wheat Breeders' Array suitable for high-throughput SNP genotyping of global accessions of hexaploid bread wheat (*Triticum aestivum*). *Plant Biotechnology Journal* **15**, 390-401.
- Amiteye S.** 2021. Basic concepts and methodologies of DNA marker systems in plant molecular breeding. *Heliyon* **7**.
- Andleeb T, Knight E, Borrill P.** 2022. Wheat *NAM* genes regulate the majority of early monocarpic senescence transcriptional changes including nitrogen remobilization genes. *G3: Genes, Genomes, Genetics*.
- Arend D, Lange M, Chen J, Colmsee C, Flemming S, Hecht D, Scholz, U.** 2014. e! DAL-a framework to store, share and publish research data. *BMC Bioinformatics* **15**, 1-13.
- Avni R, Nave M, Barad O, Baruch K, Twardziok SO, Gundlach H, Hale I, Mascher M, Spannagl M, Wiebe K, Jordan KW, Golan G, Deek J, Ben-Zvi B, Ben-Zvi G, Himmelbach A, MacLachlan RP, Sharpe AG, Fritz A, Ben-David R, Budak H, Fahima T, Korol A, Faris JD, Hernandez A, Mikel MA, Levy AA, Steffenson B, Maccaferri M, Tuberosa R, Cattivelli L, Faccioli P, Ceriotti A, Kashkush K, Pourkheirandish M, Komatsuda T, Eilam T, Sela H, Sharon A, Ohad N, Chamovitz DA, Mayer KFX, Stein N, Ronen G, Peleg Z, Pozniak CJ, Akhunov ED, Distelfeld A.** 2017. Wild emmer genome architecture and diversity elucidate wheat evolution and domestication. *Science* **357**, 93-97.

- Avni R, Nave M, Eilam T, Sela H, Alekperov C, Peleg Z, Dvorak J, Korol A, Distelfeld A.** 2014. Ultra-dense genetic map of durum wheat x wild emmer wheat developed using the 90K iSelect SNP genotyping assay. *Molecular Breeding* **34**, 1549-1562.
- Avni R, Zhao R, Pearce S, Jun Y, Uauy C, Tabbita F, Fahima T, Slade A, Dubcovsky J, Distelfeld A.** 2014. Functional characterization of GPC-1 genes in hexaploid wheat. *Planta* **239**, 313-324.
- Bacher H, Zhu F, Gao T, Liu K, Dhatt BK, Awada T, Zhang C, Distelfeld A, Yu H, Peleg Z, Walia H.** 2021. Wild emmer introgression alters root-to-shoot growth dynamics in durum wheat in response to water stress. *Plant Physiology* **187**, 1149-1162.
- Basten CJ, Weir BS, Zeng Z-B.** 2002. QTL Cartographer, version 1.17. Department of Statistics, North Carolina State University, Raleigh, NC.
- Benes B, Guan K, Lang M, Long SP, Lynch JP, Marshall-Colón A, Peng B, Schnable J, Sweetlove LJ, Turk MJ.** 2020. Multiscale computational models can guide experimentation and targeted measurements for crop improvement. *The Plant Journal* **103**, 21-31.
- Bevan MW, Uauy C, Wulff BB, Zhou J, Krasileva K, Clark MD.** 2017. Genomic innovation for crop improvement. *Nature* **543**, 346-354.
- Boden SA, Cavanagh C, Cullis BR, Ramm K, Greenwood J, Jean Finnegan E, Trevaskis B, Swain SM.** 2015. *Ppd-1* is a key regulator of inflorescence architecture and paired spikelet development in wheat. *Nature Plants* **1**, 14016.
- Bonnett OT.** 1966. Inflorescences of maize, wheat, rye, barley, and oats: their initiation and development, University of Illinois, College of Agriculture, Agricultural Experiment Station.
- Borrill P, Fahy B, Smith AM, Uauy C.** 2015. Wheat grain filling is limited by grain filling capacity rather than the duration of flag leaf photosynthesis: a case study using NAM RNAi plants. *PLoS One* **10**, e0134947.
- Borrill P, Harrington SA, Simmonds J, Uauy C.** 2019. Identification of transcription factors regulating senescence in wheat through gene regulatory network modelling. *Plant Physiology* **180**, 1740-1755.
- Borrill P, Ramirez-Gonzalez R, Uauy C.** 2016. expVIP: a customizable RNA-seq data analysis and visualization platform. *Plant Physiology* **170**, 2172-2186.
- Brinton J, Ramirez-Gonzalez RH, Simmonds J, Wingen L, Orford S, Griffiths S, 10 Wheat Genome Project, Haberer G, Spannagl M, Walkowiak S, Pozniak C, Uauy C.** 2020. A haplotype-led approach to increase the precision of wheat breeding. *Communications Biology* **3**, 712.
- Brinton J, Uauy C.** 2019. A reductionist approach to dissecting grain weight and yield in wheat. *Journal of Integrative Plant Biology* **61**, 337-358.
- Calderini DF, Castillo FM, Arenas-M A, Molero G, Reynolds MP, Craze M, Bowden S, Milner MJ, Wallington EJ, Dowle A.** 2021. Overcoming the trade-off between grain weight and number in wheat by the ectopic expression of expansin in developing seeds leads to increased yield potential. *New Phytologist* **230**, 629-640.

Cavanagh CR, Chao S, Wang S, Huang BE, Stephen S, Kiani S, Forrest K, Saintenac C, Brown-Guedira GL, Akhunova A, See D, Bai G, Pumphrey M, Tomar L, Wong D, Kong S, Reynolds M, da Silva ML, Bockelman H, Talbert L, Anderson JA, Dreisigacker S, Baenziger S, Carter A, Korzun V, Morrell PL, Dubcovsky J, Morell MK, Sorrells ME, Hayden MJ, Akhunov E. 2013. Genome-wide comparative diversity uncovers multiple targets of selection for improvement in hexaploid wheat landraces and cultivars. *Proceedings of the National Academy of Sciences* **110**, 8057-8062.

Chang TG, Shi Z, Zhao H, Song Q, He Z, Van Rie J, Den Boer B, Galle A, Zhu XG. 2022. 3dCAP-Wheat: An open-source comprehensive computational framework precisely quantifies wheat foliar, nonfoliar, and canopy Photosynthesis. *Plant Phenomics* **2022**, 9758148.

Chao S, Sharp P, Worland A, Warham E, Koebner R, Gale M. 1989. RFLP-based genetic maps of wheat homoeologous group 7 chromosomes. *Theoretical and Applied Genetics* **78**, 495-504.

Chapman EA, Orford S, Lage J, Griffiths S. 2021a. Delaying or delivering: identification of novel *NAM-1* alleles that delay senescence to extend wheat grain fill duration. *Journal of Experimental Botany* **72**, 7710-7728.

Chapman EA, Orford S, Lage J, Griffiths S. 2021b. Capturing and Selecting Senescence Variation in Wheat. *Frontiers in Plant Science* **12**, 638738.

Chen S, Gao R, Wang H, Wen M, Xiao J, Bian N, Zhang R, Hu W, Cheng S, Bie T. 2015. Characterization of a novel reduced height gene (*Rht23*) regulating panicle morphology and plant architecture in bread wheat. *Euphytica* **203**, 583-594.

Christopher JT, Christopher MJ, Borrell AK, Fletcher S, Chenu K. 2016. Stay-green traits to improve wheat adaptation in well-watered and water-limited environments. *Journal of Experimental Botany* **67**, 5159-5172.

Collard BC, Jahufer M, Brouwer J, Pang ECK. 2005. An introduction to markers, quantitative trait loci (QTL) mapping and marker-assisted selection for crop improvement: the basic concepts. *Euphytica* **142**, 169-196.

Cortes L, Zhang Z, Yu J. 2021. Status and prospects of genome-wide association studies in plants. *The Plant Genome* **14**, e20077.

Crossa J, Pérez-Rodríguez P, Cuevas J, Montesinos-López O, Jarquín D, De Los Campos G, Burgueño J, González-Camacho JM, Pérez-Elizalde S, Beyene Y. 2017. Genomic selection in plant breeding: methods, models, and perspectives. *Trends in Plant Science* **22**, 961-975.

Cui F, Zhang N, Fan X-l, Zhang W, Zhao C-h, Yang L-j, Pan R-q, Chen M, Han J, Zhao X-q. 2017. Utilization of a Wheat660K SNP array-derived high-density genetic map for high-resolution mapping of a major QTL for kernel number. *Scientific Reports* **7**, 3788.

Debernardi JM, Lin H, Chuck G, Faris JD, Dubcovsky J. 2017. microRNA172 plays a crucial role in wheat spike morphogenesis and grain threshability. *Development* **144**, 1966-1975.

- DeMalach N, Zaady E, Weiner J, Kadmon, R.** 2016. Size asymmetry of resource competition and the structure of plant communities. *Journal of Ecology* **104**, 899-910.
- Denison RF.** 2012. Darwinian agriculture: how understanding evolution can improve agriculture. Princeton University Press.
- Derkx AP, Orford S, Griffiths S, Foulkes MJ, Hawkesford MJ.** 2012. Identification of differentially Senescing mutants of wheat and impacts on yield, biomass and nitrogen partitioning. *Journal of Integrative Plant Biology* **54**, 555-566.
- Díaz A, Zikhali M, Turner AS, Isaac P, Laurie DA.** 2012. Copy number variation affecting the *Photoperiod-B1* and *Vernalization-A1* genes is associated with altered flowering time in wheat (*Triticum aestivum*). *PloS one* **7**, e33234.
- Distelfeld A, Avni R, Fischer AM.** 2014. Senescence, nutrient remobilization, and yield in wheat and barley. *Journal of Experimental Botany* **65**, 3783-3798.
- Dixon LE, Greenwood JR, Bencivenga S, Zhang P, Cockram J, Mellers G, Ramm K, Cavanagh C, Swain SM, Boden SA.** 2018. *TEOSINTE BRANCHED1* regulates inflorescence architecture and development in bread wheat (*Triticum aestivum*). *The Plant Cell* **30**, 563-581.
- Dixon LE, Pasquariello M, Badgami R, Levin KA, Poschet G, Ng PQ, Orford S, Chayut N, Adamski NM, Brinton J, Simmonds J, Steuernagel B, Searle IR, Uauy C, Boden SA.** 2022. MicroRNA-resistant alleles of *HOMEODOMAIN-2* modify inflorescence branching and increase grain protein content of wheat. *Science Advances* **8**, eabn5907.
- Dobrovolskaya O, Pont C, Sibout R, Martinek P, Badaeva E, Murat F, Chosson A, Watanabe N, Prat E, Gautier N, Gautier V, Poncet C, Orlov YL, Krasnikov AA, Berges H, Salina E, Laikova L, Salse J.** 2015. *FRIZZY PANICLE* drives supernumerary spikelets in bread wheat. *Plant Physiology* **167**, 189-199.
- Donald CM.** 1968. The breeding of crop ideotypes. *Euphytica* **17**, 385-403.
- Dreccer MF, Wockner KB, Palta JA, McIntyre CL, Borgognone MG, Bourgault M, Reynolds M, Miralles DJ.** 2014. More fertile florets and grains per spike can be achieved at higher temperature in wheat lines with high spike biomass and sugar content at booting. *Functional Plant Biology* **41**, 482-495.
- Dubcovsky J, Dvorak J.** 2007. Genome plasticity a key factor in the success of polyploid wheat under domestication. *Science* **316**, 1862-1866.
- Evans L, Dunstone R, Rawson H, Williams R.** 1970. The phloem of the wheat stem in relation to requirements for assimilate by the ear. *Australian Journal of Biological Sciences* **23**, 743-752.
- Evers JB, Vos J, Andrieu B, Struik PC.** 2006. Cessation of tillering in spring wheat in relation to light interception and red : far-red ratio. *Annals of Botany* **97**, 649-658.
- Fahy B, Siddiqui H, David LC, Powers SJ, Borrill P, Uauy C, Smith AM.** 2018. Final grain weight is not limited by the activity of key starch-synthesising enzymes during grain filling in wheat. *Journal of Experimental Botany* **69**, 5461-5475.
- FAO 2022.** Agricultural production statistics. 2000–2021. FAOSTAT Analytical Brief Series No. 60. Rome. <https://doi.org/10.4060/cc3751en>

FAO, IFAD, UNICEF, WFP and WHO. 2023. The State of Food Security and Nutrition in the World 2023. Urbanization, agrifood systems transformation and healthy diets across the rural–urban continuum. Rome, FAO. <https://doi.org/10.4060/cc3017en>

FAOSTAT 2023: <https://www.fao.org/faostat/en/#data/QCL>

Faris JD, Fellers JP, Brooks SA, Gill BS. 2003. A bacterial artificial chromosome contig spanning the major domestication locus *Q* in wheat and identification of a candidate gene. *Genetics* **164**, 311-321.

Ferrante A, Savin R, Slafer GA. 2013. Floret development and grain setting differences between modern durum wheats under contrasting nitrogen availability. *Journal of Experimental Botany* **64**, 169-184.

Fischer R, Stockman Y. 1986. Increased kernel number in Norin 10-derived dwarf wheat: evaluation of the cause. *Functional Plant Biology* **13**, 767-784.

Fischer R. 2011. Wheat physiology: a review of recent developments. *Crop and Pasture Science* **62**, 95-114.

Forster BP, Franckowiak JD, Lundqvist U, Lyon J, Pitkethly I, Thomas WT. 2007. The barley phytomer. *Annals of Botany* **100**, 725-733.

Gaju O, Allard V, Martre P, Snape J, Heumez E, LeGouis J, Moreau D, Bogard M, Griffiths S, Orford S. 2011. Identification of traits to improve the nitrogen-use efficiency of wheat genotypes. *Field Crops Research* **123**, 139-152.

Gegas VC, Nazari A, Griffiths S, Simmonds J, Fish L, Orford S, Sayers L, Doonan JH, Snape JW. 2010. A genetic framework for grain size and shape variation in wheat. *The Plant Cell* **22**, 1046-1056.

Ghosh S, Watson A, Gonzalez-Navarro OE, Ramirez-Gonzalez RH, Yanes L, Mendoza-Suarez M, Simmonds J, Wells R, Rayner T, Green P, Hafeez A, Hayta S, Melton RE, Steed A, Sarkar A, Carter J, Perkins L, Lord J, Tester M, Osbourn A, Moscou MJ, Nicholson P, Harwood W, Martin C, Domoney C, Uauy C, Hazard B, Wulff BBH, Hickey LT. 2018. Speed breeding in growth chambers and glasshouses for crop breeding and model plant research. *Nature Protocols* **13**, 2944-2963.

Golan G, Abbai R, Schnurbusch T. 2022. Exploring the trade-off between individual fitness and community performance of wheat crops using simulated canopy shade. *Plant, Cell & Environment*.

Golan G, Ayalon I, Perry A, Zimran G, Ade-Ajayi T, Mosquna A, Distelfeld A, Peleg Z. 2019. *GNI-A1* mediates trade-off between grain number and grain weight in tetraploid wheat. *Theoretical and Applied Genetics* **132**, 2353-2365.

Grassini P, Eskridge KM, Cassman KG. 2013. Distinguishing between yield advances and yield plateaus in historical crop production trends. *Nature Communications* **4**, 2918.

Greenwood JR, Finnegan EJ, Watanabe N, Trevaskis B, Swain SM. 2017. New alleles of the wheat domestication gene *Q* reveal multiple roles in growth and reproductive development. *Development* **144**, 1959-1965.

- Guo Z, Chen D, Alqudah AM, Röder MS, Ganal MW, Schnurbusch T.** 2017. Genome-wide association analyses of 54 traits identified multiple loci for the determination of floret fertility in wheat. *New Phytologist* **214**, 257-270.
- Guo Z, Liu G, Röder MS, Reif JC, Ganal MW, Schnurbusch T.** 2018a. Genome-wide association analyses of plant growth traits during the stem elongation phase in wheat. *Plant Biotechnology Journal* **16**, 2042-2052.
- Guo Z, Schnurbusch T.** 2015. Variation of floret fertility in hexaploid wheat revealed by tiller removal. *Journal of Experimental Botany* **66**, 5945-5958.
- Guo Z, Slafer GA, Schnurbusch T.** 2016. Genotypic variation in spike fertility traits and ovary size as determinants of floret and grain survival rate in wheat. *Journal of Experimental Botany* **67**, 4221-4230.
- Guo Z, Zhao Y, Röder MS, Reif JC, Ganal MW, Chen D, Schnurbusch T.** 2018b. Manipulation and prediction of spike morphology traits for the improvement of grain yield in wheat. *Scientific Reports* **8**, 14435.
- Hanif M, Langer RHM.** 1972. The vascular system of the spikelet in wheat (*Triticum aestivum*). *Annals of Botany* **36**, 721-727.
- Harrington SA, Overend LE, Cobo N, Borrill P, Uauy C.** 2019. Conserved residues in the wheat (*Triticum aestivum*) NAM-A1 NAC domain are required for protein binding and when mutated lead to delayed peduncle and flag leaf senescence. *BMC Plant Biology* **19**, 407.
- Hassan MA, Yang M, Rasheed A, Tian X, Reynolds M, Xia X, Xiao Y, He Z.** 2021. Quantifying senescence in bread wheat using multispectral imaging from an unmanned aerial vehicle and QTL mapping. *Plant Physiology* **187**, 2623-2636.
- Hickey LT, A NH, Robinson H, Jackson SA, Leal-Bertioli SCM, Tester M, Gao C, Godwin ID, Hayes BJ, Wulff BBH.** 2019. Breeding crops to feed 10 billion. *Nature Biotechnology* **37**, 744-754.
- Huang BE, Verbyla KL, Verbyla AP, Raghavan C, Singh VK, Gaur P, Leung H, Varshney RK, Cavanagh CR.** 2015. MAGIC populations in crops: current status and future prospects. *Theoretical and Applied Genetics* **128**, 999-1017.
- Huang F, Jiang Y, Chen T, Li H, Fu M, Wang Y, Xu Y, Li Y, Zhou Z, Jia L, Ouyang Y, Yao W.** 2022. New data and new features of the funRiceGenes (functionally characterized rice genes) database: 2021 Update. *Rice* **15**, 23.
- Huber M, Nieuwendijk NM, Pantazopoulou CK, Pierik R.** 2021. Light signalling shapes plant–plant interactions in dense canopies. *Plant, Cell & Environment* **44**, 1014-1029.
- Hyles J, Bloomfield MT, Hunt JR, Trethowan RM, Trevaskis B.** 2020. Phenology and related traits for wheat adaptation. *Heredity* **125**, 417-430.
- Iglesias-Fernández R, Rodríguez-Gacio MC, Barrero-Sicilia C, Carbonero P, and Matilla A.** 2011. Three endo- β -mannanase genes expressed in the micropylar endosperm and in the radicle influence germination of *Arabidopsis thaliana* seeds. *Planta* **233**, 25-36.
- IWGSC.** 2018. Shifting the limits in wheat research and breeding using a fully annotated reference genome. *Science* **361**, eaar7191.

Jaganathan D, Bohra A, Thudi M, Varshney RK. 2020. Fine mapping and gene cloning in the post-NGS era: advances and prospects. *Theoretical and Applied Genetics* **133**, 1791-1810.

Jansen RC, Stam P. 1994. High resolution of quantitative traits into multiple loci via interval mapping. *Genetics* **136**, 1447-1455.

Jia J, Zhao S, Kong X, Li Y, Zhao G, He W, Appels R, Pfeifer M, Tao Y, Zhang X, Jing R, Zhang C, Ma Y, Gao L, Gao C, Spannagl M, Mayer KF, Li D, Pan S, Zheng F, Hu Q, Xia X, Li J, Liang Q, Chen J, Wicker T, Gou C, Kuang H, He G, Luo Y, Keller B, Xia Q, Lu P, Wang J, Zou H, Zhang R, Xu J, Gao J, Middleton C, Quan Z, Liu G, Wang J, International Wheat Genome Sequencing C, Yang H, Liu X, He Z, Mao L, Wang J. 2013. *Aegilops tauschii* draft genome sequence reveals a gene repertoire for wheat adaptation. *Nature* **496**, 91-95.

Jones N, Ougham H, Thomas H. 1997. Markers and mapping: we are all geneticists now. *New Phytologist* **137**, 165-177.

Kato K, Miura H, Sawada S. 1999. QTL mapping of genes controlling ear emergence time and plant height on chromosome 5A of wheat. *Theoretical and Applied Genetics* **98**, 472-477.

Kellogg EA. 2022. Genetic control of branching patterns in grass inflorescences. *The Plant Cell* **34**, 2518-2533.

Kichey T, Hirel B, Heumez E, Dubois F, Le Gouis J. 2007. In winter wheat (*Triticum aestivum* L.), post-anthesis nitrogen uptake and remobilisation to the grain correlates with agronomic traits and nitrogen physiological markers. *Field Crops Research* **102**, 22-32.

Kirby E, Appleyard M. 1984. *Cereal development guide*, 2nd edn. Stoneleigh: National Agricultural Centre Arable Unit.

Kislev ME. 1980. *Triticum parvicoccum* sp. Nov., the oldest naked wheat. *Israel Journal of Botany* **28**, 95-107.

Kislev ME. 1984. Emergence of wheat agriculture. *Paléorient* 61-70.

KOKUBUN M. 1988. Design and examination of soybean ideotypes. *Growth* **3**, 13-23.

Koppolu R, Chen S, Schnurbusch T. 2022. Evolution of inflorescence branch modifications in cereal crops. *Current Opinion in Plant Biology* **65**, 102168.

Koppolu R, Schnurbusch T. 2019. Developmental pathways for shaping spike inflorescence architecture in barley and wheat. *Journal of Integrative Plant Biology* **61**, 278-295.

Krasileva KV, Vasquez-Gross HA, Howell T, Bailey P, Paraiso F, Clissold L, Simmonds J, Ramirez-Gonzalez RH, Wang X, Borrill P, Fosker C, Ayling S, Phillips AL, Uauy C, Dubcovsky J. 2017. Uncovering hidden variation in polyploid wheat. *Proceedings of the National Academy of Sciences* **114**, 913-921.

Lander ES, Botstein D. 1989. Mapping mendelian factors underlying quantitative traits using RFLP linkage maps. *Genetics* **121**, 185-199.

Lander ES, Green P, Abrahamson J, Barlow A, Daly MJ, Lincoln SE, Newberg LA. 1987. MAPMAKER: an interactive computer package for constructing primary

genetic linkage maps of experimental and natural populations. *Genomics* **1**, 174-181.

Levy AA, Feldman M. 2022. Evolution and origin of bread wheat. *The Plant Cell* **34**, 2549-2567.

Li H, Liu H, Hao C, Li T, Liu Y, Wang X, Yang Y, Zheng J, Zhang X. 2022. The auxin response factor TaARF15-A1 negatively regulates senescence in common wheat (*Triticum aestivum* L.). *Plant Physiology* **2**, 1254-1271.

Lichthardt C, Chen T-W, Stahl A, Stützel H. 2020. Co-evolution of sink and source in the recent breeding history of winter wheat in Germany. *Frontiers in Plant Science* **10**, 1771.

Liu Y-G, Tsunewaki K. 1991. Restriction fragment length polymorphism (RFLP) analysis in wheat. II. Linkage maps of the RFLP sites in common wheat. *The Japanese Journal of Genetics* **66**, 617-633.

Lopes MS, Reynolds MP. 2012. Stay-green in spring wheat can be determined by spectral reflectance measurements (normalized difference vegetation index) independently from phenology. *Journal of Experimental Botany* **63**, 3789-3798.

Luo MC, Gu YQ, Puiu D, Wang H, Twardziok SO, Deal KR, Huo N, Zhu T, Wang L, Wang Y, McGuire PE, Liu S, Long H, Ramasamy RK, Rodriguez JC, Van SL, Yuan L, Wang Z, Xia Z, Xiao L, Anderson OD, Ouyang S, Liang Y, Zimin AV, Perteau G, Qi P, Bennetzen JL, Dai X, Dawson MW, Muller HG, Kugler K, Rivarola-Duarte L, Spannagl M, Mayer KFX, Lu FH, Bevan MW, Leroy P, Li P, You FM, Sun Q, Liu Z, Lyons E, Wicker T, Salzberg SL, Devos KM, Dvorak J. 2017. Genome sequence of the progenitor of the wheat D genome *Aegilops tauschii*. *Nature* **551**, 498-502.

Maccaferri M, Harris NS, Twardziok SO, Pasam RK, Gundlach H, Spannagl M, Ormanbekova D, Lux T, Prade VM, Milner SG, Himmelbach A, Mascher M, Bagnaresi P, Faccioli P, Cozzi P, Lauria M, Lazzari B, Stella A, Manconi A, Gnocchi M, Moscatelli M, Avni R, Deek J, Biyiklioglu S, Frascaroli E, Corneti S, Salvi S, Sonnante G, Desiderio F, Marè C, Crosatti C, Mica E, Özkan H, Kilian B, De Vita P, Marone D, Joukhadar R, Mazzucotelli E, Nigro D, Gadaleta A, Chao S, Faris JD, Melo ATO, Pumphrey M, Pecchioni N, Milanese L, Wiebe K, Ens J, MacLachlan RP, Clarke JM, Sharpe AG, Koh CS, Liang KYH, Taylor GJ, Knox R, Budak H, Mastrangelo AM, Xu SS, Stein N, Hale I, Distelfeld A, Hayden MJ, Tuberosa R, Walkowiak S, Mayer KFX, Ceriotti A, Pozniak CJ, Cattivelli L. 2019. Durum wheat genome highlights past domestication signatures and future improvement targets. *Nature Genetics* **51**, 885-895.

Maccaferri M, Ricci A, Salvi S, Milner SG, Noli E, Martelli PL, Casadio R, Akhunov E, Scalabrin S, Vendramin V, Ammar K, Blanco A, Desiderio F, Distelfeld A, Dubcovsky J, Fahima T, Faris J, Korol A, Massi A, Mastrangelo AM, Morgante M, Pozniak C, N'Diaye A, Xu S, Tuberosa R. 2015. A high-density, SNP-based consensus map of tetraploid wheat as a bridge to integrate durum and bread wheat genomics and breeding. *Plant Biotechnology Journal* **13**, 648-663.

Marcussen T, Sandve SR, Heier L, Spannagl M, Pfeifer M, IWGSC, Jakobsen KS, Wulff BBH, Steuernagel B, Mayer KFX, Olsen O-A. 2014. Ancient hybridizations among the ancestral genomes of bread wheat. *Science* **345**, 1250092.

- Mastrangelo AM, Cattivelli L.** 2021. What Makes Bread and Durum Wheat Different? *Trends in Plant Science* **26**, 677-684.
- Mathan J, Bhattacharya J, Ranjan A.** 2016. Enhancing crop yield by optimizing plant developmental features. *Development* **143**, 3283-3294.
- Mazzucotelli E, Sciara G, Mastrangelo AM, Desiderio F, Xu SS, Faris J, Hayden MJ, Tricker PJ, Ozkan H, Echenique V, Steffenson BJ, Knox R, Niane AA, Udupa SM, Longin FCH, Marone D, Petruzzino G, Corneti S, Ormanbekova D, Pozniak C, Roncallo PF, Mather D, Able JA, Amri A, Braun H, Ammar K, Baum M, Cattivelli L, Maccaferri M, Tuberosa R, Bassi FM.** 2020. The Global Durum Wheat Panel (GDP): An International Platform to Identify and Exchange Beneficial Alleles. *Frontiers in Plant Science* **11**.
- Mcfadden ES, Sears ER.** 1946. The origin of *Triticum spelta* and its free-threshing hexaploid relatives. *Journal of Heredity* **37**, 81-89.
- McSteen P, Kellogg EA.** 2022. Molecular, cellular, and developmental foundations of grass diversity. *Science* **377**, 599-602.
- Miller P, Lanier W, Brandt S.** 2001. Using growing degree days to predict plant stages. Ag/Extension Communications Coordinator, Communications Services, Montana State University-Bozeman, Bozeman, MO.
- Minoli S, Jägermeyr J, Asseng S, Urfels A, Müller C.** 2022. Global crop yields can be lifted by timely adaptation of growing periods to climate change. *Nature Communications* **13**, 1-10.
- Molero G, Joynson R, Pinera-Chavez FJ, Gardiner LJ, Rivera-Amado C, Hall A, Reynolds MP.** 2019. Elucidating the genetic basis of biomass accumulation and radiation use efficiency in spring wheat and its role in yield potential. *Plant Biotechnology Journal* **17**, 1276-1288.
- Molero G, Reynolds MP.** 2020. Spike photosynthesis measured at high throughput indicates genetic variation independent of flag leaf photosynthesis. *Field Crops Research* **255**, 107866.
- Moncur MW.** 1981. Floral initiation in field crops: An atlas of scanning electron micrographs. Division of Land Use Research, CSIRO.
- Muramatsu M.** 1963. Dosage effect of the spelta gene q of hexaploid wheat. *Genetics* **48**, 469.
- Murchie EH, Reynolds M, Slafer GA, Foulkes MJ, Acevedo-Siaca L, McAusland L, Sharwood R, Griffiths S, Flavell RB, Gwyn J, Sawkins M, Carmo-Silva E.** 2023. A 'wiring diagram' for source strength traits impacting wheat yield potential. *Journal of Experimental Botany* **74**, 72-90.
- Nalam VJ, Vales MI, Watson CJW, Kianian SF, Riera-Lizarazu O.** 2006. Map-based analysis of genes affecting the brittle rachis character in tetraploid wheat (*Triticum turgidum* L.). *Theoretical and Applied Genetics* **112**, 373-381.
- Nave M, Avni R, Cakir E, Portnoy V, Sela H, Pourkheirandish M, Ozkan H, Hale I, Komatsuda T, Dvorak J, Distelfeld A.** 2019. Wheat domestication in light of haplotype analyses of the *Brittle rachis 1* genes (*BTR1-A* and *BTR1-B*). *Plant Science* **285**, 193-199.

Niu KX, Chang CY, Zhang MQ, Guo YT, Yan Y, Sun HJ, Zhang GL, Li XM, Gong YL, Ding CH, Wang ML, Ni Z, Sun Q, & Gou JY. 2023. Suppressing *ASPARTIC PROTEASE 1* prolongs photosynthesis and increases wheat grain weight. *Nature Plants* **9**, 965-977.

Ostrander EA, Wang G-D, Larson G, Vonholdt BM, Davis BW, Jagannathan V, Hitte C, Wayne RK, Zhang Y-P. 2019. Dog10K: an international sequencing effort to advance studies of canine domestication, phenotypes and health. *National Science Review* **6**, 810-824.

Paniagua C, Bilkova A, Jackson P, Dabravolski S, Riber W, Didi V, Houser J, Gigli-Bisceglia N, Wimmerova M, Budínská E, Hamann T, Hejatko J. 2017. Dirigent proteins in plants: modulating cell wall metabolism during abiotic and biotic stress exposure. *Journal of Experimental Botany* **68**, 3287-3301.

Peng J, Richards DE, Hartley NM, Murphy GP, Devos KM, Flintham JE, Beales J, Fish LJ, Worland AJ, Pelica F, Sudhakar D, Christou P, Snape JW, Gale MD, Harberd NP. 1999. 'Green revolution' genes encode mutant gibberellin response modulators. *Nature* **400**, 256-261.

Percival J (1921) *The wheat plant: a monograph*. Duckworth, London

Poland JA, Brown PJ, Sorrells ME, Jannink J-L. 2012. Development of high-density genetic maps for barley and wheat using a novel two-enzyme genotyping-by-sequencing approach. *PLoS One* **7**, e32253.

Postma JA, Hecht VL, Hikosaka K, Nord EA, Pons TL, Poorter H. 2021. Dividing the pie: A quantitative review on plant density responses. *Plant, Cell & Environment* **44**, 1072-1094.

Potapov P, Turubanova S, Hansen MC, Tyukavina A, Zalles V, Khan A, Song XP, Pickens A, Shen Q, Cortez J. 2022. Global maps of cropland extent and change show accelerated cropland expansion in the twenty-first century. *Nature Food* **3**, 19-28.

Poursarebani N, Seidensticker T, Koppolu R, Trautewig C, Gawronski P, Bini F, Govind G, Rutten T, Sakuma S, Tagiri A, Wolde GM, Youssef HM, Battal A, Ciannamea S, Fusca T, Nussbaumer T, Pozzi C, Borner A, Lundqvist U, Komatsuda T, Salvi S, Tuberosa R, Uauy C, Sreenivasulu N, Rossini L, Schnurbusch T. 2015. The genetic basis of composite spike form in barley and 'Miracle-Wheat'. *Genetics* **201**, 155-165.

Ramírez-González RH, Borrill P, Lang D, Harrington SA, Brinton J, Venturini L, Davey M, Jacobs J, van Ex F, Pasha A, Khedikar Y, Robinson SJ, Cory AT, Florio T, Concia L, Juery C, Schoonbeek H, Steuernagel B, Xiang D, Ridout CJ, Chalhoub B, Mayer KFX, Benhamed M, Latrasse D, Bendahmane A, IWGSC, Wulff BBH, Appels R, Tiwari V, Datla R, Choulet F, Pozniak CJ, Provart NJ, Sharpe AG, Paux E, Spannagl M, Bräutigam A, Uauy C. 2018. The transcriptional landscape of polyploid wheat. *Science* **361**, eaar6089.

Rawson H. 1970. Spikelet number, its control and relation to yield per ear in wheat. *Australian Journal of Biological Sciences* **23**, 1-16.

Rebetzke GJ, Fischer RTA, Van Herwaarden AF, Bonnett DG, Chenu K, Rattey AR, Fettell NA. 2014. Plot size matters: Interference from intergenotypic competition in plant phenotyping studies. *Functional Plant Biology* **41**, 107-118.

- Reynolds M, Pellegrineschi A, Skovmand B.** 2005. Sink-limitation to yield and biomass: a summary of some investigations in spring wheat. *Annals of Applied Biology* **146**, 39-49.
- Reynolds M, Slafer G, Foulkes J, Griffiths S, Murchie E, Carmo-Silva E, Asseng S, Chapman S, Sawkins M, Gwyn J, Flavell R.** 2022. A wiring diagram to integrate physiological traits of wheat yield potential. *Nature Food* **3**, 318-324.
- Risch N.** 1992. Genetic Linkage: Interpreting Lod Scores. *Science* **255**, 803-804.
- Röder MS, Korzun V, Wendehake K, Plaschke J, Tixier M-H, Leroy P, Ganal MW.** 1998. A Microsatellite Map of Wheat. *Genetics* **149**, 2007-2023.
- Roychowdhury R, Zilberman O, Chandrasekhar K, Curzon AY, Nashef K, Abbo S, Slafer GA, Bonfil DJ, Ben-David R.** 2023. Pre-anthesis spike growth dynamics and its association to yield components among elite bread wheat cultivars (*Triticum aestivum* L. spp.) under Mediterranean climate. *Field Crops Research* **298**, 108948.
- Sadras V, Alston J, Aphalo P, Connor D, Denison RF, Fischer T, Gray R, Hayman P, Kirkegaard J, Kirchmann H.** 2020. Making science more effective for agriculture. *Advances in Agronomy* **163**, 153-177.
- Sakuma S, Golan G, Guo Z, Ogawa T, Tagiri A, Sugimoto K, Bernhardt N, Brassac J, Mascher M, Hensel G, Ohnishi S, Jinno H, Yamashita Y, Ayalon I, Peleg Z, Schnurbusch T, Komatsuda T.** 2019. Unleashing floret fertility in wheat through the mutation of a homeobox gene. *Proceedings of the National Academy of Sciences* **116**, 5182-5187.
- Sakuma S, Schnurbusch T.** 2020. Of floral fortune: tinkering with the grain yield potential of cereal crops. *New Phytologist* **225**, 1873-1882.
- Schindelin J, Arganda-Carreras I, Frise E, Kaynig V, Longair M, Pietzsch T, Preibisch S, Rueden C, Saalfeld S, Schmid B.** 2012. Fiji: an open-source platform for biological-image analysis. *Nature Methods* **9**, 676-682.
- Schlötterer C.** 2004. The evolution of molecular markers — just a matter of fashion? *Nature Reviews Genetics* **5**, 63-69.
- Schulthess AW, Kale SM, Liu F, Zhao Y, Philipp N, Rembe M, Jiang Y, Beukert U, Serfling A, Himmelbach A, Fuchs J, Oppermann M, Weise S, Boeven PHG, Schacht J, Longin CFH, Kollers S, Pfeiffer N, Korzun V, Lange M, Scholz U, Stein N, Mascher M, Reif JC.** 2022. Genomics-informed prebreeding unlocks the diversity in genebanks for wheat improvement. *Nature Genetics* **54**, 1544-1552.
- Scott MF, Ladejobi O, Amer S, Bentley AR, Biernaskie J, Boden SA, Clark M, Dell'Acqua M, Dixon LE, Filippi CV, Fradgley N, Gardner KA, Mackay IJ, Donal O'Sullivan D, Percival-Alwyn L, Roorkiwal M, Singh RK, Thudi M, Varshney RK, Venturini L, Whan A, Cockram J, Mott R.** 2020. Multi-parent populations in crops: a toolbox integrating genomics and genetic mapping with breeding. *Heredity* **125**, 396-416.
- Sears ER** (1954) The aneuploids of common wheat. *Missouri Agricultural Experiment Station Research Bulletin* **572**, 1–58
- Senapati N, Semenov MA, Halford NG, Hawkesford MJ, Asseng S, Cooper M, Ewert F, van Ittersum MK, Martre P, Olesen JE, Reynolds M, Rötter RP,**

- Webber H.** 2022. Global wheat production could benefit from closing the genetic yield gap. *Nature Food* **3**, 532-541.
- Serrago RA, Alzueta I, Savin R, Slafer GA.** 2013. Understanding grain yield responses to source–sink ratios during grain filling in wheat and barley under contrasting environments. *Field Crops Research* **150**, 42-51.
- Shanmugaraj N, Rajaraman J, Kale S, Kamal R, Huang Y, Thirulogachandar V, Garibay-Hernández A, Budhagatapalli N, Tandron Moya YA, Hajirezaei MR, Rutten T, Hensel G, Melzer M, Kumlehn J, von Wirén N, Mock H, & Schnurbusch T.** 2023. Multilayered regulation of developmentally programmed pre-anthesis tip degeneration of the barley inflorescence. *The Plant Cell* **11**, 3973-4001.
- Sharma JS, Running KLD, Xu SS, Zhang Q, Peters Haugrud AR, Sharma S, McClean PE, Faris JD.** 2019. Genetic analysis of threshability and other spike traits in the evolution of cultivated emmer to fully domesticated durum wheat. *Molecular Genetics and Genomics* **294**, 757-771.
- Shaw LM, Turner AS, Laurie DA.** 2012. The impact of photoperiod insensitive Ppd-1a mutations on the photoperiod pathway across the three genomes of hexaploid wheat (*Triticum aestivum*). *The Plant Journal* **71**, 71-84.
- Sierra-Gonzalez A, Molero G, Rivera-Amado C, Babar MA, Reynolds MP, Foulkes MJ.** 2021. Exploring genetic diversity for grain partitioning traits to enhance yield in a high biomass spring wheat panel. *Field Crops Research* **260**, 107979.
- Simons KJ, Fellers JP, Trick HN, Zhang Z, Tai YS, Gill BS, Faris JD.** 2006. Molecular characterization of the major wheat domestication gene Q. *Genetics* **172**, 547-555.
- Slafer G.** 2003. Genetic basis of yield as viewed from a crop physiologist's perspective. *Annals of Applied Biology* **142**, 117-128.
- Slafer GA, Foulkes MJ, Reynolds MP, Murchie EH, Carmo-Silva E, Flavell R, Gwyn J, Sawkins M, Griffiths S.** 2023. A 'wiring diagram' for sink strength traits impacting wheat yield potential. *Journal of Experimental Botany* **74**, 40-71.
- Spindel JE, Begum H, Akdemir D, Collard B, Redoña E, Jannink JL, McCouch S.** 2016. Genome-wide prediction models that incorporate de novo GWAS are a powerful new tool for tropical rice improvement. *Heredity* **116**, 395-408.
- Springer N.** 2010. Shaping a better rice plant. *Nature Genetics* **42**, 475-476.
- Stam P.** 1993. Construction of integrated genetic linkage maps by means of a new computer package: Join Map. *The Plant Journal* **3**, 739-744.
- Sun C, Dong Z, Zhao L, Ren Y, Zhang N, Chen F.** 2020. The Wheat 660K SNP array demonstrates great potential for marker-assisted selection in polyploid wheat. *Plant biotechnology Journal* **18**, 1354-1360.
- Tanno K-i, Willcox G.** 2006. How Fast Was Wild Wheat Domesticated? *Science* **311**, 1886-1886.
- Trevaskis B, Bagnall DJ, Ellis MH, Peacock WJ, Dennis ES.** 2003. MADS box genes control vernalization-induced flowering in cereals. *Proceedings of the National Academy of Sciences* **100**, 13099-13104.

- Tschermak E.** 1914. Die Verwertung der Bastardierung für phylogenetische Fragen in der Getreidegruppe. *Zeitschr. f. Pflanzenzüchtung.* **2**, 291-312.
- Uauy C, Distelfeld A, Fahima T, Blechl A, Dubcovsky J.** 2006a. A NAC gene regulating senescence improves grain protein, zinc, and iron content in wheat. *Science* **314**, 1298-1301.
- Uauy C, Brevis JC, Dubcovsky J.** 2006b. The high grain protein content gene *Gpc-B1* accelerates senescence and has pleiotropic effects on protein content in wheat. *Journal of Experimental Botany* **57**, 2785-2794.
- Varshney RK, Bohra A, Yu J, Graner A, Zhang Q, Sorrells ME.** 2021. Designing Future Crops: Genomics-Assisted Breeding Comes of Age. *Trends Plant Science* **26**, 631-649.
- Voorrips RE.** 2002. MapChart: software for the graphical presentation of linkage maps and QTLs. *Journal of Heredity* **93**, 77-78.
- Voss-Fels KP, Stahl A, Wittkop B, Lichthardt C, Nagler S, Rose T, Chen T-W, Zetzsche H, Seddig S, Majid Baig M.** 2019. Breeding improves wheat productivity under contrasting agrochemical input levels. *Nature Plants* **5**, 706-714.
- Waddington S, Cartwright P, Wall P.** 1983. A quantitative scale of spike initial and pistil development in barley and wheat. *Annals of Botany* **51**, 119-130.
- Wallace JG, Rodgers-Melnick E, Buckler ES.** 2018. On the road to breeding 4.0: unraveling the good, the bad, and the boring of crop quantitative genomics. *Annual Review of Genetics* **52**, 421-444.
- Wang S, Wong D, Forrest K, Allen A, Chao S, Huang BE, Maccaferri M, Salvi S, Milner SG, Cattivelli L.** 2014a. Characterization of polyploid wheat genomic diversity using a high-density 90 000 single nucleotide polymorphism array. *Plant Biotechnology Journal* **12**, 787-796.
- Wang Y, Vilaplana F, Brumer H, Aspeborg H.** 2014b. Enzymatic characterization of a glycoside hydrolase family 5 subfamily 7 (GH5_7) mannanase from *Arabidopsis thaliana*. *Planta* **239**, 653-665.
- Watson A, Ghosh S, Williams MJ, Cuddy WS, Simmonds J, Rey MD, Asyraf Md Hatta M, Hinchliffe A, Steed A, Reynolds D, Adamski NM, Breakspear A, Korolev A, Rayner T, Dixon LE, Riaz A, Martin W, Ryan M, Edwards D, Batley J, Raman H, Carter J, Rogers C, Domoney C, Moore G, Harwood W, Nicholson P, Dieters MJ, DeLacy IH, Zhou J, Uauy C, Boden SA, Park RF, Wulff BBH, Hickey LT.** 2018. Speed breeding is a powerful tool to accelerate crop research and breeding. *Nature Plants* **4**, 23-29.
- Weiner J.** 1990. Asymmetric competition in plant populations. *Trends in Ecology and Evolution* **5**, 360-364.
- Weiner J.** 2019. Looking in the wrong direction for higher-yielding crop genotypes. *Trends in Plant Science* **24**, 927-933.
- Wendler N, Mascher M, Nöh C, Himmelbach A, Scholz U, Ruge-Wehling B, Stein N.** 2014. Unlocking the secondary gene-pool of barley with next-generation sequencing. *Plant Biotechnology Journal* **12**, 1122-1131.

- Whingwiri E, Kuo J, Stern W.** 1981. The vascular system in the rachis of a wheat ear. *Annals of Botany* **48**, 189-202.
- Winfield MO, Allen AM, Burrige AJ, Barker GL, Benbow HR, Wilkinson PA, Coghill J, Waterfall C, Davassi A, Scopes G, Pirani A, Webster T, Brew F, Bloor C, King J, West C, Griffiths S, King I, Bentley AR, Edwards KJ** 2016. High-density SNP genotyping array for hexaploid wheat and its secondary and tertiary gene pool. *Plant Biotechnology Journal* **14**, 1195-1206.
- Wolde GM, Trautewig C, Mascher M, Schnurbusch T.** 2019a. Genetic insights into morphometric inflorescence traits of wheat. *Theoretical and Applied Genetics* **132**, 1661-1676.
- Wolde GM, Mascher M, Schnurbusch T.** 2019b. Genetic modification of spikelet arrangement in wheat increases grain number without significantly affecting grain weight. *Molecular Genetics and Genomics* **294**, 457-468.
- Wolde GM, Schreiber M, Trautewig C, Himmelbach A, Sakuma S, Mascher M, Schnurbusch T.** 2021. Genome-wide identification of loci modifying spike-branching in tetraploid wheat. *Theoretical and Applied Genetics* **134**, 1925-1943.
- Wuest SE, Niklaus PA.** 2018. A plant biodiversity effect resolved to a single chromosomal region. *Nature Ecology & Evolution* **2**, 1933-1939.
- Yan L, Loukoianov A, Tranquilli G, Helguera M, Fahima T, Dubcovsky J.** 2003. Positional cloning of the wheat vernalization gene *VRN1*. *Proceedings of the National Academy of Sciences* **100**, 6263-6268.
- Yan Y, Wang LM, Guo TY, Ding HC, Niu XK, Li XM., Sun C, Dong Z, Cui D, Rasheed A, Hao C, Zhang X, Guo G, Ni Z, Sun Q, Chen F, Guo JY.** 2023. HSP90.2 promotes CO₂ assimilation rate, grain weight and yield in wheat. *Plant Biotechnology Journal* **21**, 1229-1239.
- Yu J, Holland JB, McMullen MD, Buckler ES.** 2008a. Genetic Design and Statistical Power of Nested Association Mapping in Maize. *Genetics* **178**, 539-551.
- Yu X, Li L, Li L, Guo M, Chory J, Yin Y.** 2008b. Modulation of brassinosteroid-regulated gene expression by Jumonji domain-containing proteins ELF6 and REF6 in *Arabidopsis*. *Proceedings of the National Academy of Sciences* **105**, 7618-7623.
- Zadoks J, Chang T, Konzak C.** 1974. Decimal code for the growth-stages of cereals. *Weed Res.* **14**, 415-421.
- Zeng V, Uauy C, Chen Y.** 2023. Identification of a novel SNP in the miR172 binding site of Q homoeolog *AP2L-D5* is associated with spike compactness and agronomic traits in wheat (*Triticum aestivum* L.). *bioRxiv*
- Zeng ZB.** 1994. Precision mapping of quantitative trait loci. *Genetics* **136**, 1457-1468.
- Zhang F, Wang C, Li M, Cui Y, Shi Y, Wu Z, Hu Z, Wang W, Xu J, Li Z.** 2021. The landscape of gene–CDS–haplotype diversity in rice: Properties, population organization, footprints of domestication and breeding, and implications for genetic improvement. *Molecular Plant* **14**, 787-804.
- Zhang J, Xiong H, Burguener GF, Vasquez-Gross H, Liu Q, Debernardi JM, Akhunova A, Garland-Campbell K, Kianian SF, Brown-Guedira G, Pozniak C,**

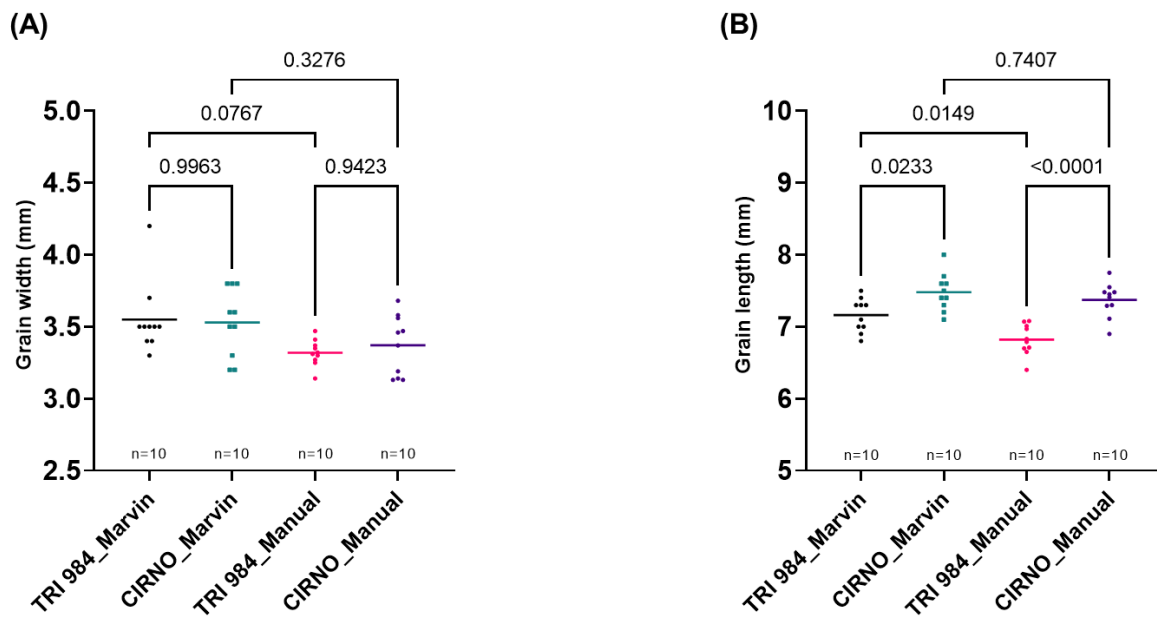
Faris JD, Akhunov E, Dubcovsky J. 2023. Sequencing 4.3 million mutations in wheat promoters to understand and modify gene expression. *Proceedings of the National Academy of Sciences* **120**, e2306494120.

Zhang Z, Belcram H, Gornicki P, Charles M, Just J, Huneau C, Magdelenat G, Couloux A, Samain S, Gill BS. 2011. Duplication and partitioning in evolution and function of homoeologous Q loci governing domestication characters in polyploid wheat. *Proceedings of the National Academy of Sciences* **108**, 18737-18742.

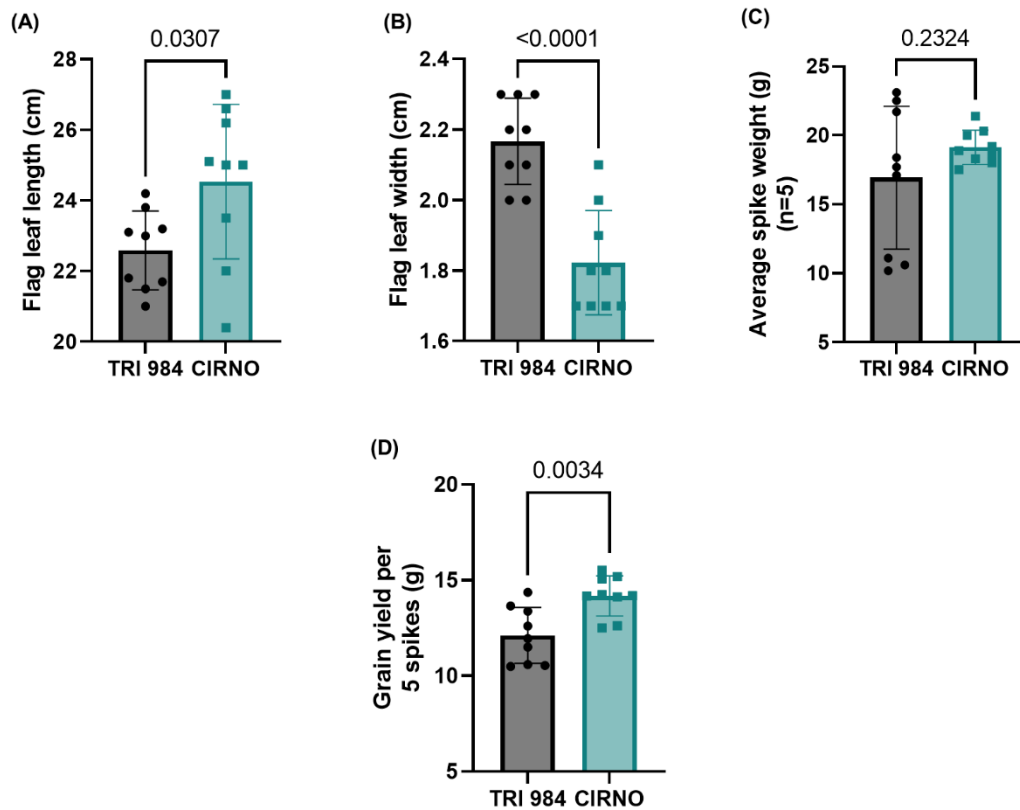
Zhao G, Zou C, Li K, Wang K, Li T, Gao L, Zhang X, Wang H, Yang Z, Liu X, Jiang W, Mao L, Kong X, Jiao Y, Jia J. 2017. The *Aegilops tauschii* genome reveals multiple impacts of transposons. *Nature Plants* **3**, 946-955.

Zhu C, Gore M, Buckler ES, Yu J. 2008. Status and prospects of association mapping in plants. *The Plant Genome* **1**.

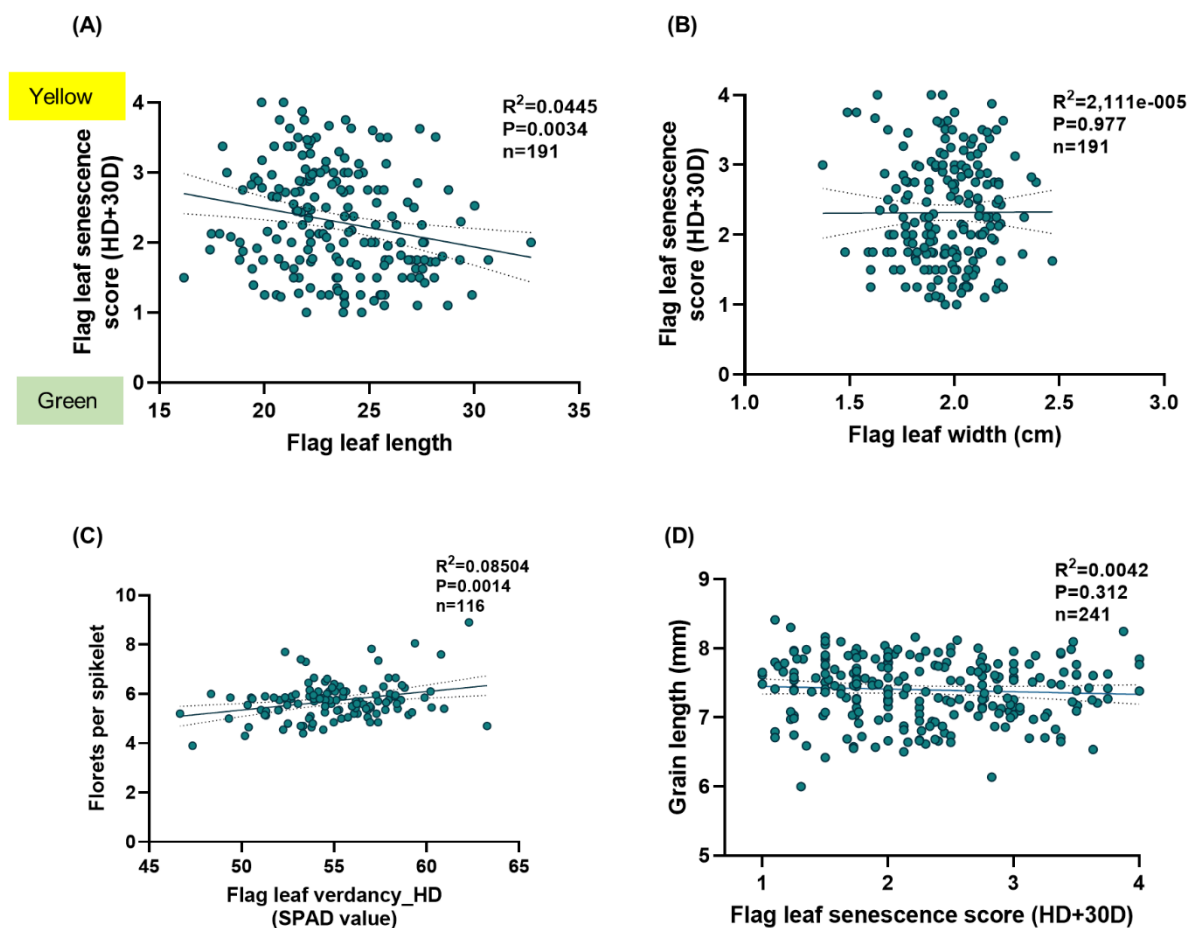
9. Appendix



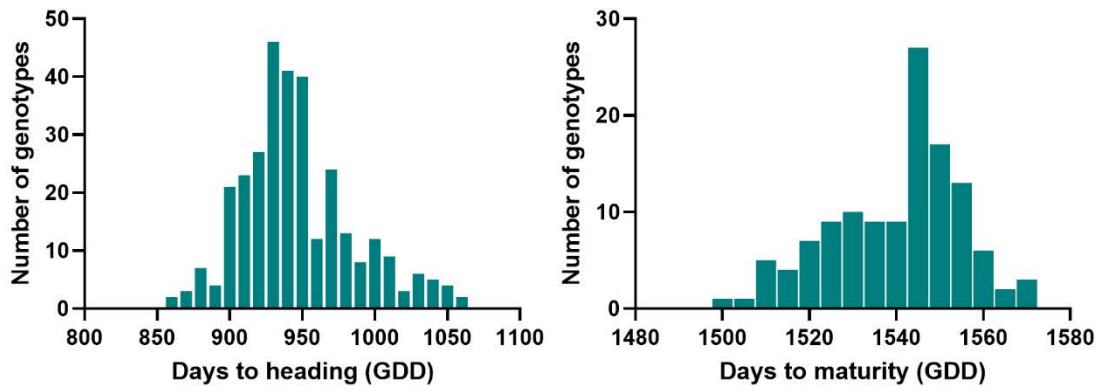
Appendix Figure 1. Validation of Marvin results. (A) The grain width and (B) grain length results obtained from the Marvin grain analyzer were confirmed manually using a Vernier caliper. Although there was a difference in absolute values, the trend between the parental lines remained the same; thus, it might not affect the QTL mapping analysis. Note: Data obtained from field grown plants was used for the analysis in (A-B).



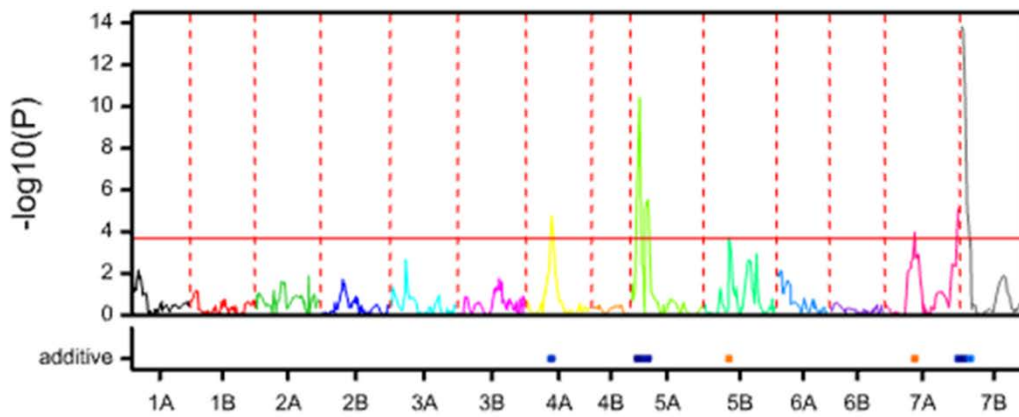
Appendix Figure 2. TRI 984 vs CIRNO. (A) Flag leaf length, (B) Flag leaf width, (C) Average spike weight and (D) Grain yield per 5 spikes. Note: Data obtained from field grown plants was used for the analysis in (A-D).



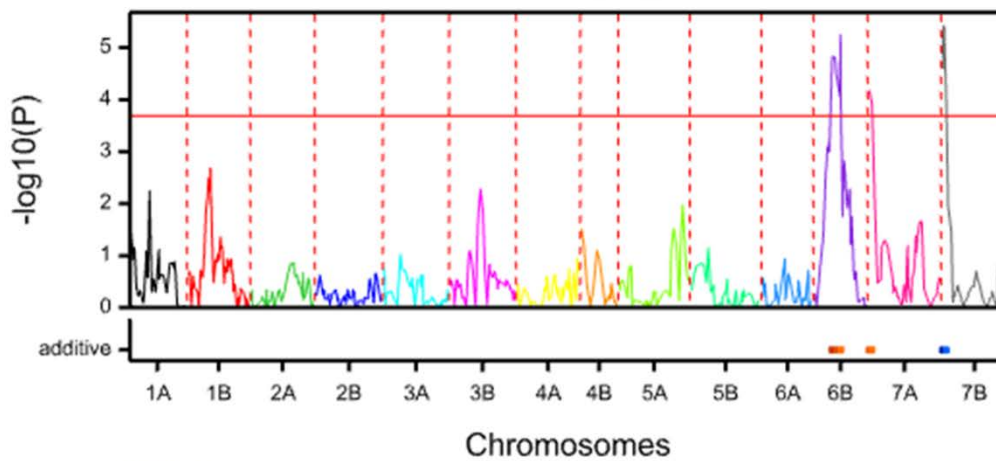
Appendix Figure 3. Relationship between various traits across the population. (A) Flag leaf length vs Flag leaf senescence, (B) Flag leaf width vs Flag leaf senescence, (C) Flag leaf verdancy at heading vs Florets per spikelet, (D) Flag leaf senescence vs Grain length. Note: Data obtained from field grown plants was used for the analysis in (A-D).



Days to heading



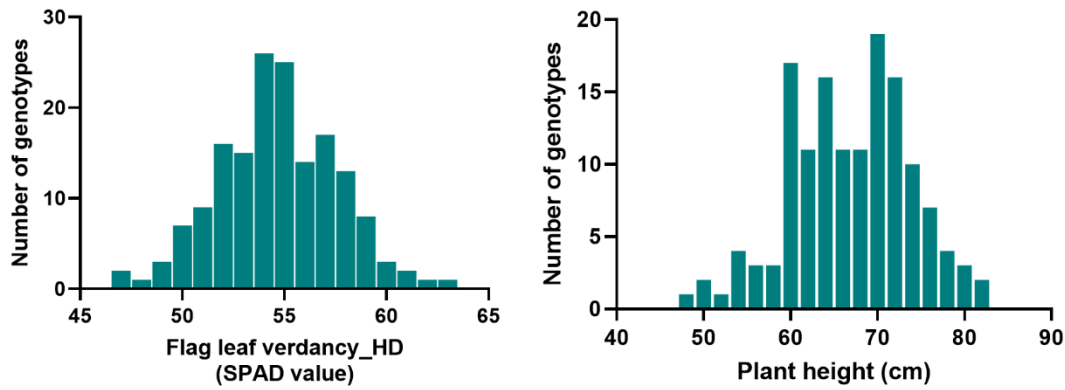
Days to maturity



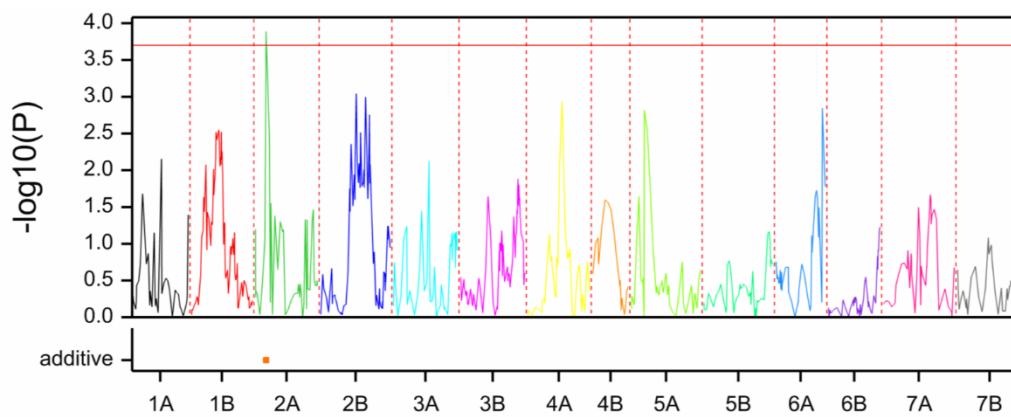
QTL effects:
additive (blue=Parent 1 ; yellow-red=Parent 2)

Appendix Figure 4. Phenotypic distribution and composite interval mapping of days to heading and days to maturity in TRI 984x CIRNO RILs.

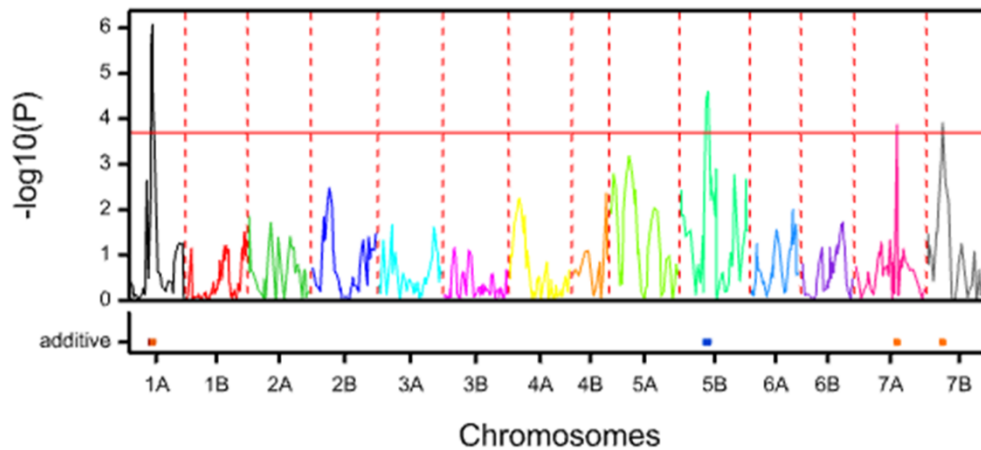
Note: Parent 1: TRI 984 and Parent 2: CIRNO.



Flag leaf verdancy at heading



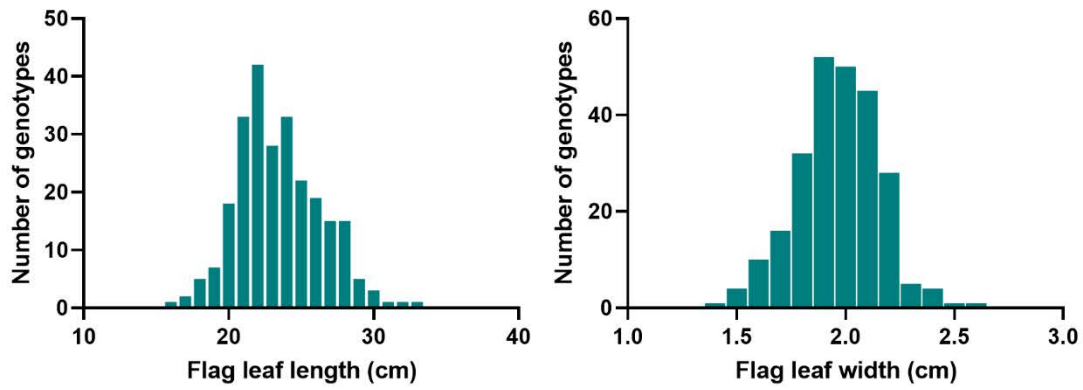
Plant height



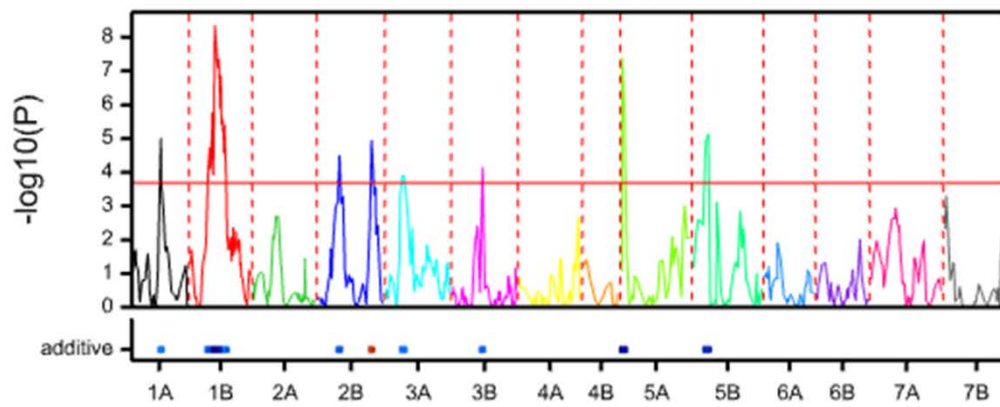
QTL effects:
additive (blue=Parent 1 ; yellow-red=Parent 2)

Appendix Figure 5. Phenotypic distribution and composite interval mapping of flag leaf verdancy at heading and plant height in TRI 984x CIRNO RILs.

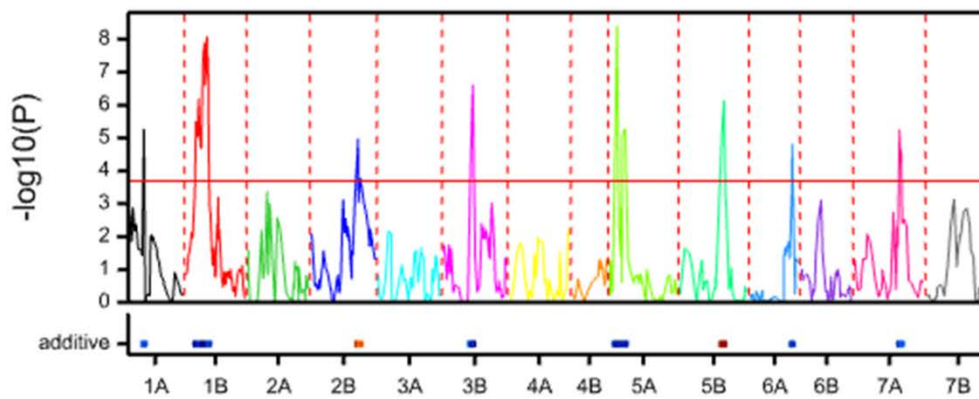
Note: For plant height, only the lines with semi-dwarf *Rht-B1* were used for QTL mapping. Parent 1: TRI 984 and Parent 2: CIRNO.



Flag leaf length



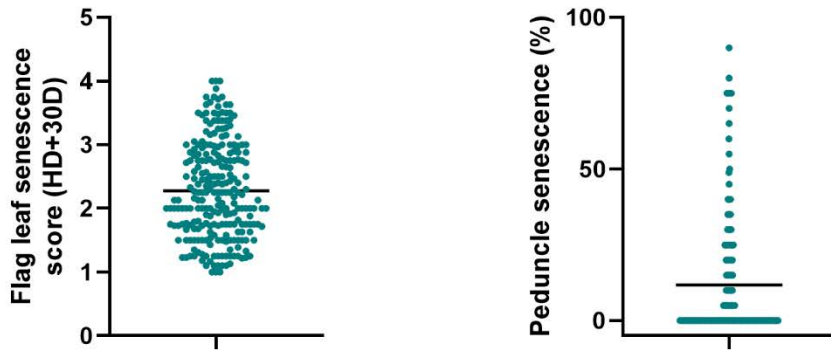
Flag leaf width



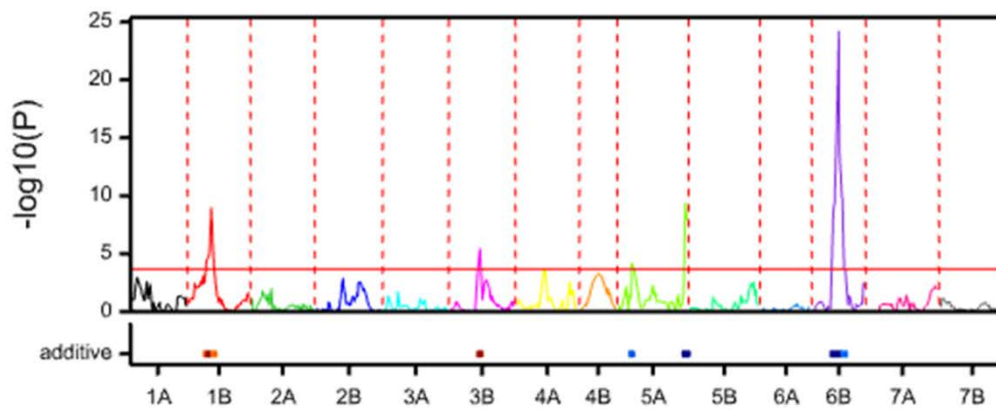
Chromosomes

QTL effects:
additive (blue=Parent 1 ; yellow-red=Parent 2)

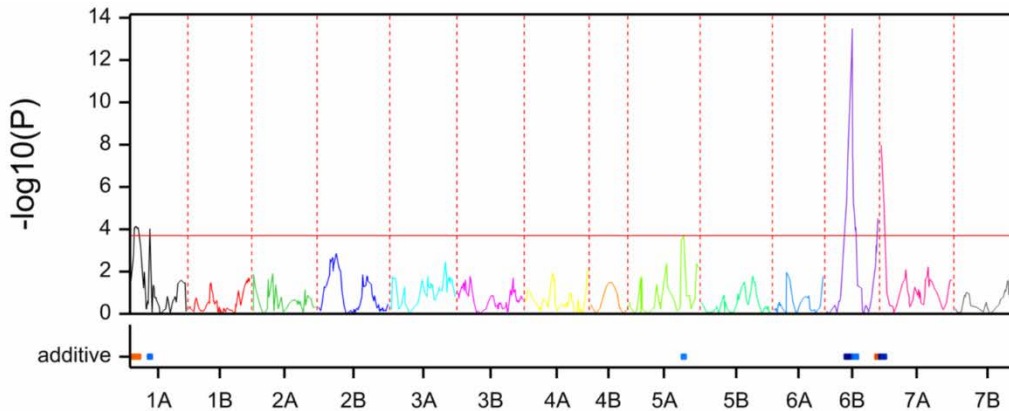
Appendix Figure 6. Phenotypic distribution and composite interval mapping of flag leaf length and flag leaf width in TRI 984x CIRNO RILs.
Note: Parent 1: TRI 984 and Parent 2: CIRNO.



Flag leaf senescence



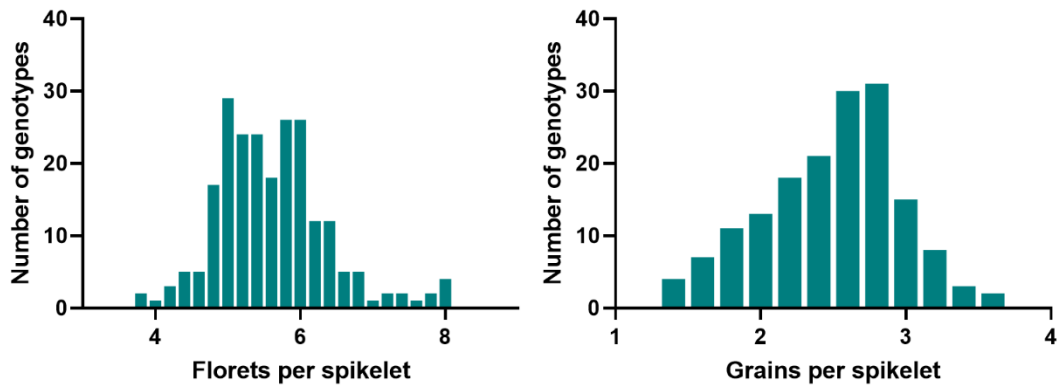
Peduncle senescence



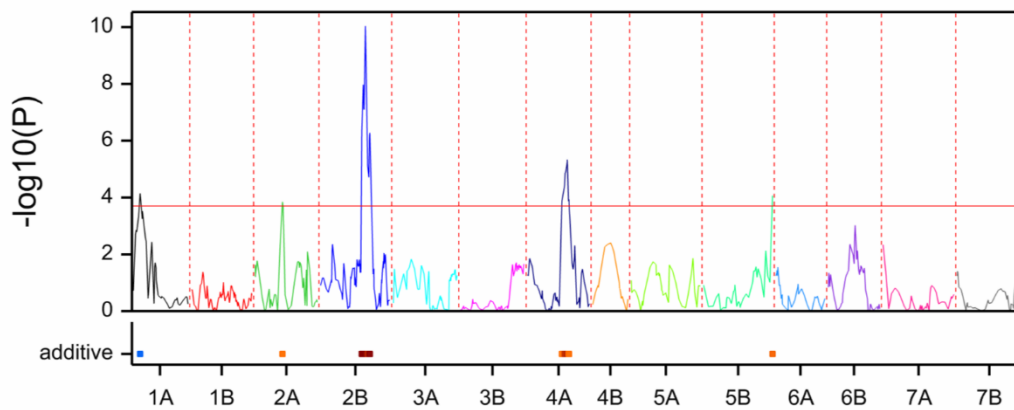
Chromosomes

QTL effects:
additive (blue=Parent 1 ; yellow-red=Parent 2)

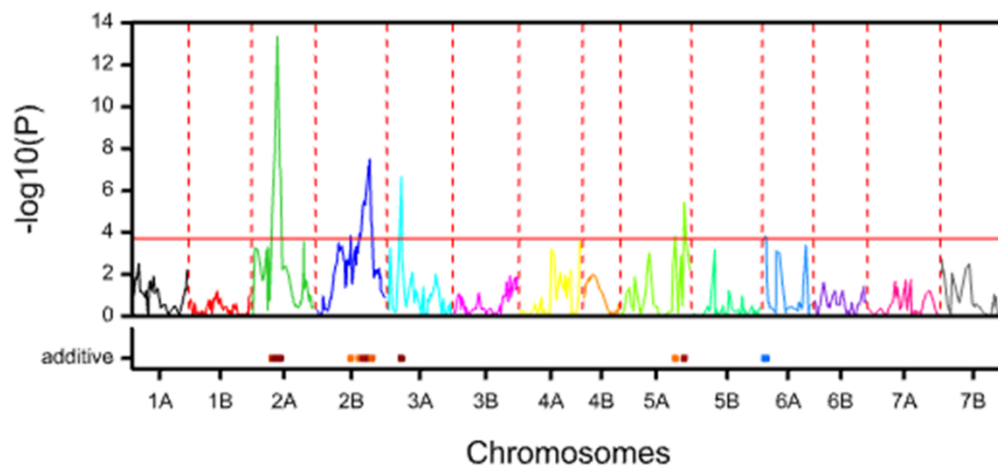
Appendix Figure 7. Phenotypic distribution and composite interval mapping of flag leaf senescence and peduncle senescence in TRI 984xCIIRNO RILs.
Note: Parent 1: TRI 984 and Parent 2: CIIRNO.



Florets per spikelet



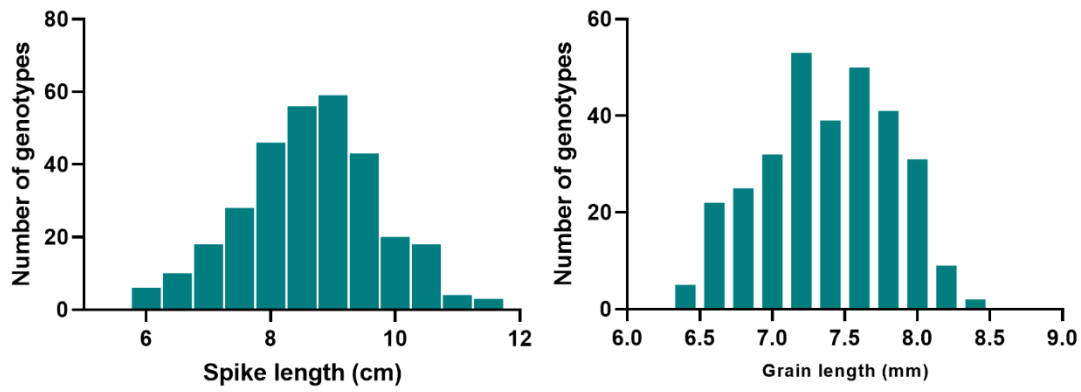
Grains per spikelet



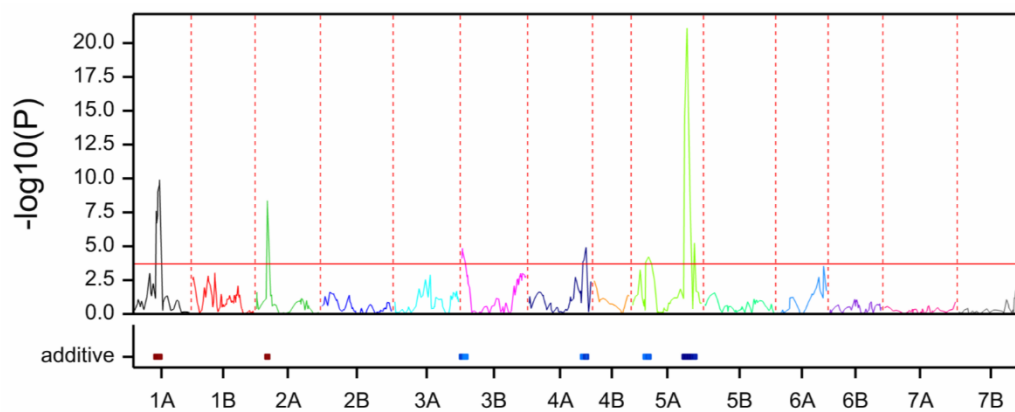
QTL effects:
additive (blue=Parent 1 ; yellow-red=Parent 2)

Appendix Figure 8. Phenotypic distribution and composite interval mapping of florets per spikelet and grains per spikelet in TRI 984x CIRNO RILs.

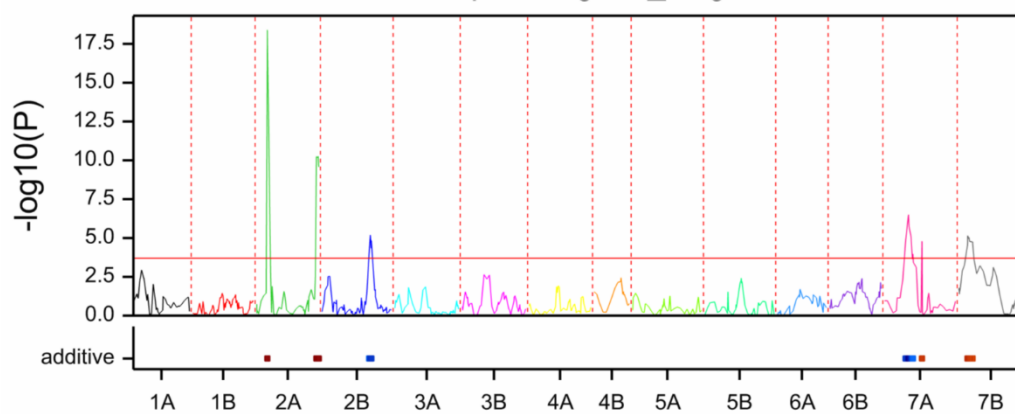
Note: The lines with spike-branching were excluded for the analysis of florets and grains per spikelet, Parent 1: TRI 984 and Parent 2: CIRNO.



Spike length



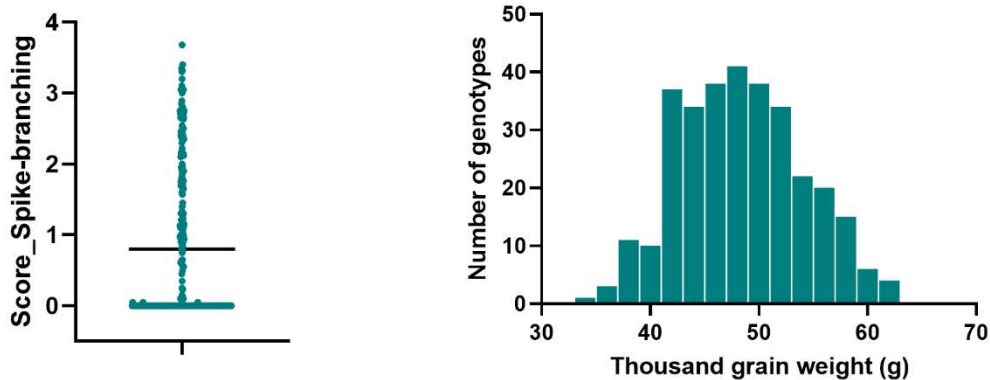
Grain length



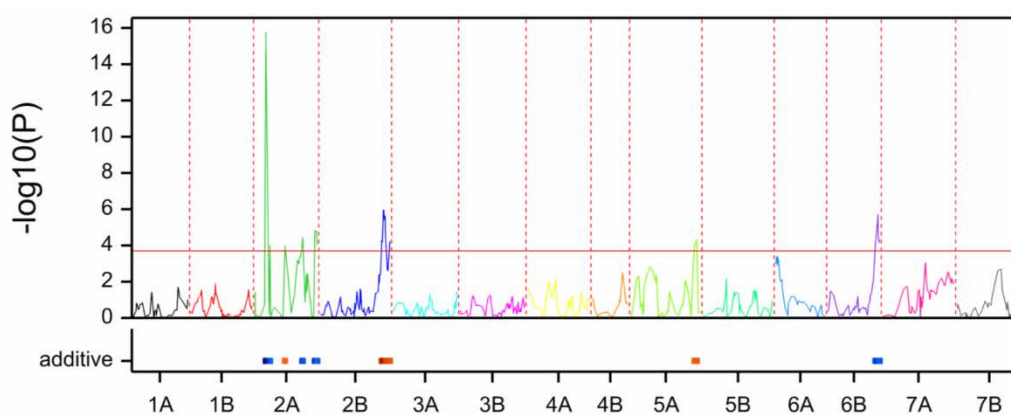
Chromosomes

QTL effects:
additive (blue=Parent 1 ; yellow-red=Parent 2)

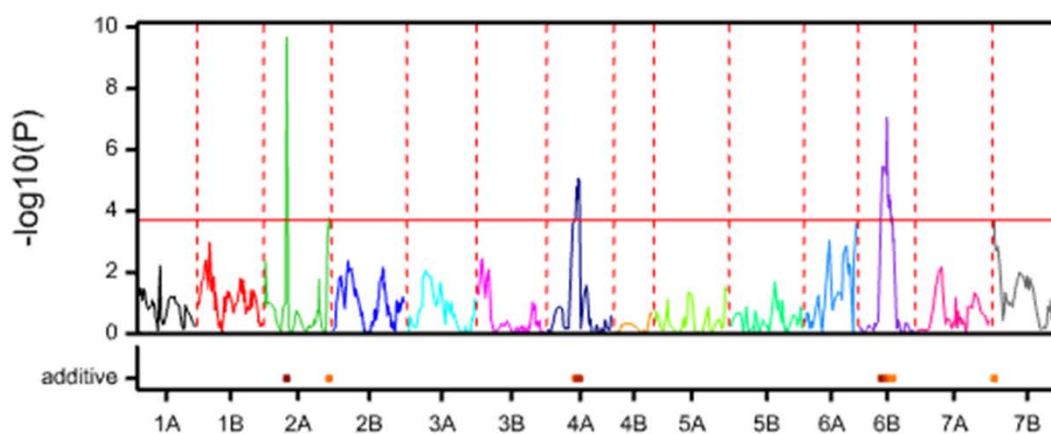
Appendix Figure 9. Phenotypic distribution and composite interval mapping of spike length and grain length in TRI 984x CIRNO RILs.
Note: Parent 1: TRI 984 and Parent 2: CIRNO.



Spike-branching



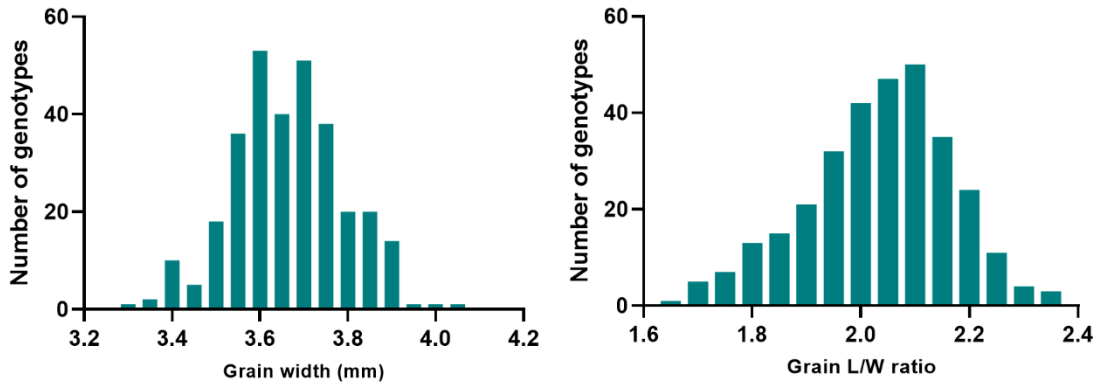
Thousand grain weight



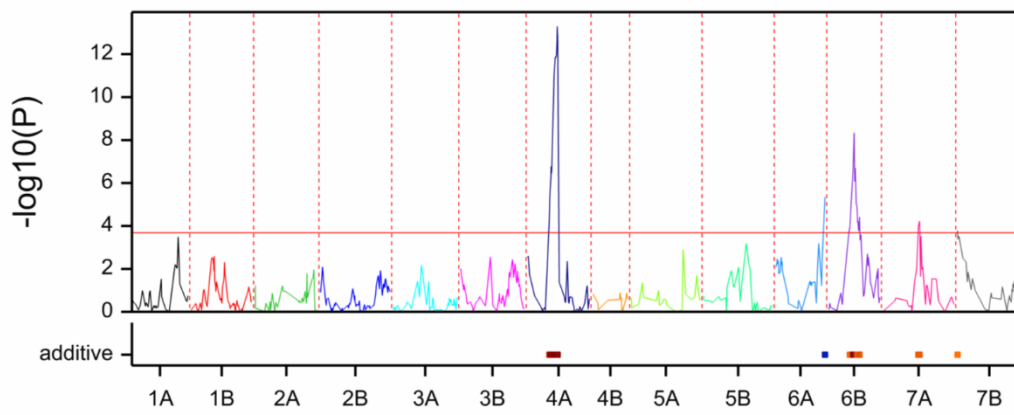
Chromosomes

QTL effects:
additive (blue=Parent 1 ; yellow-red=Parent 2)

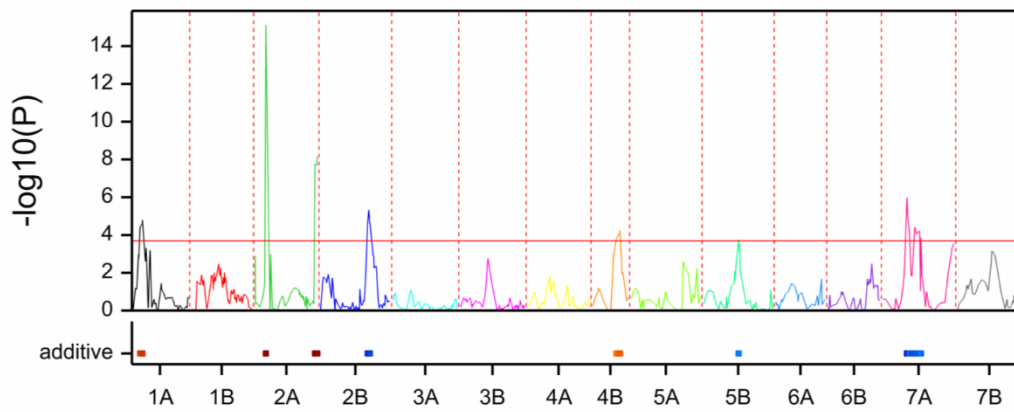
Appendix Figure 10. Phenotypic distribution and composite interval mapping of spike-branching and thousand-grain weight in TRI 984x CIRNO RILs.
Note: Parent 1: TRI 984 and Parent 2: CIRNO.



Grain width



Grain L/W ratio

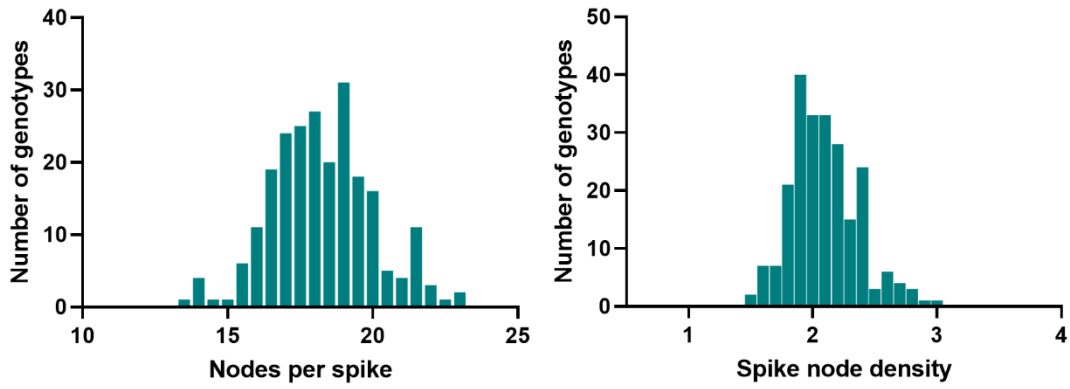


Chromosomes

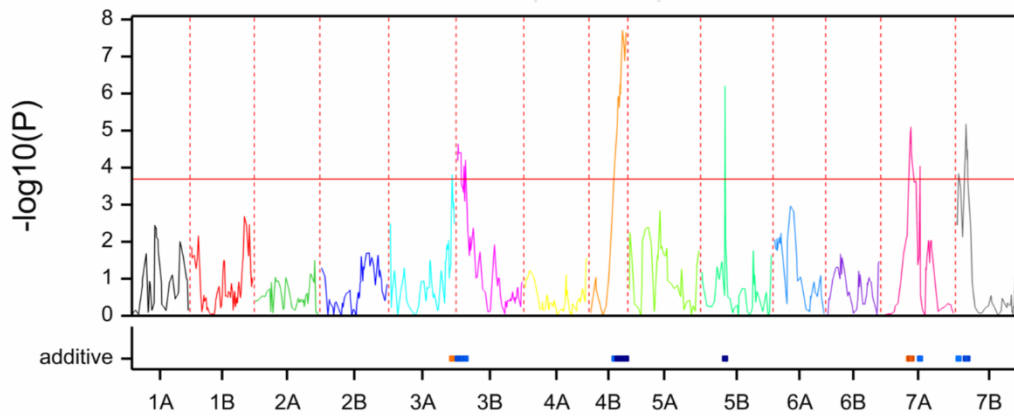
QTL effects:
additive (blue=Parent 1 ; yellow-red=Parent 2)

Appendix Figure 11. Phenotypic distribution and composite interval mapping of grain width and grain L/W (length/width) ratio in TRI 984x CIRNO RILs.

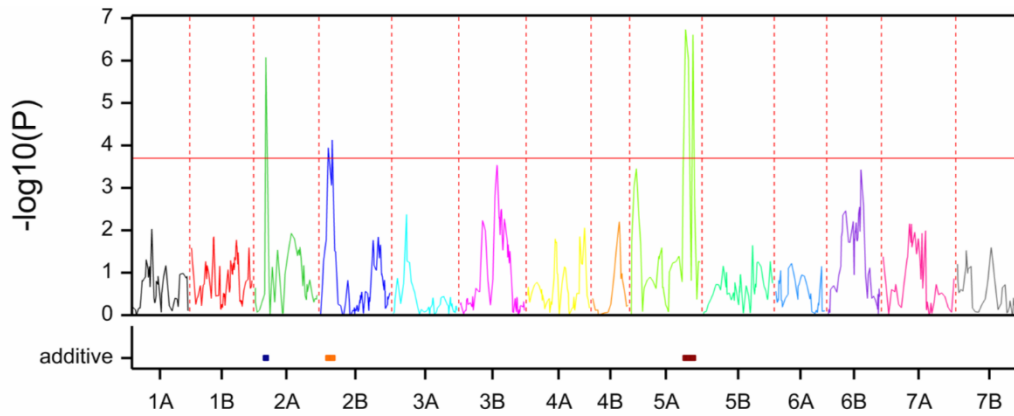
Note: Parent 1: TRI 984 and Parent 2: CIRNO.



Nodes per spike (central rachis)



Spike node density



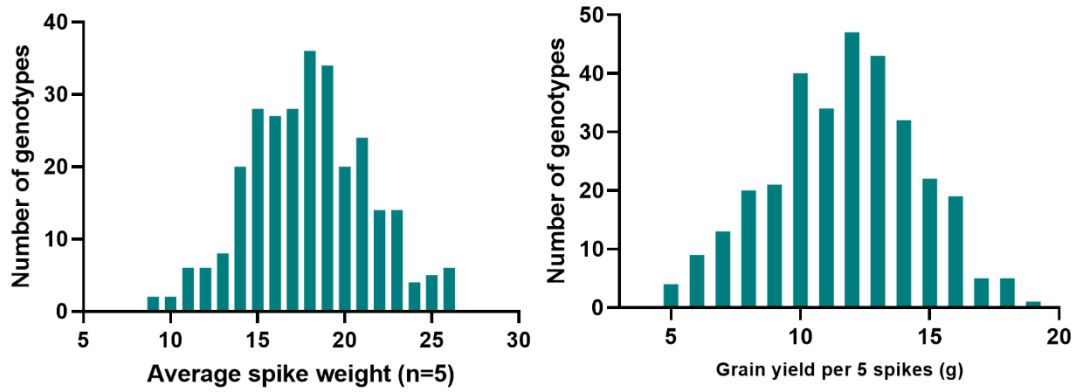
Chromosomes

QTL effects:

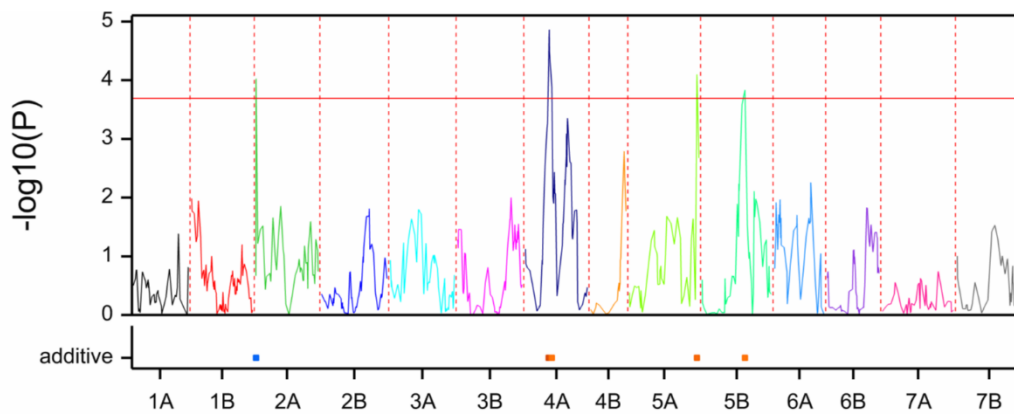
additive (blue=Parent 1 ; yellow-red=Parent 2)

Appendix Figure 12. Phenotypic distribution and composite interval mapping of nodes per spike and spike node density in TRI 984x CIRNO RILs.

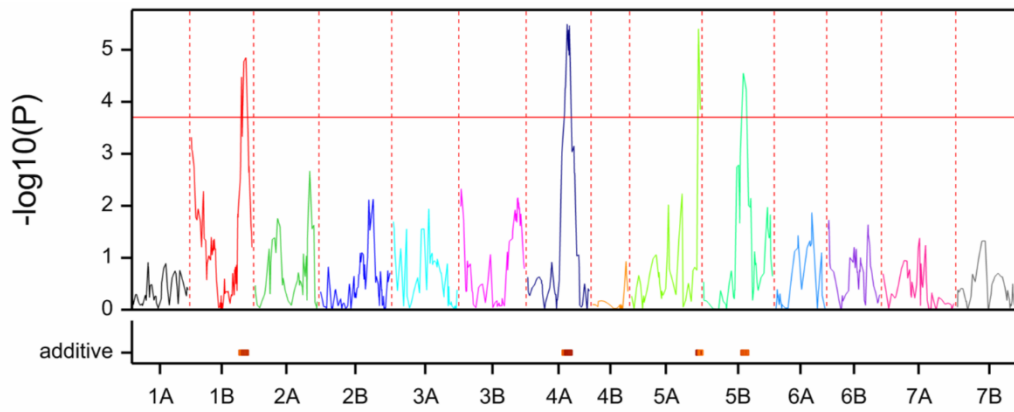
Note: The lines with spike-branching were excluded for the analysis of nodes per spike and spike node density, Parent 1: TRI 984 and Parent 2: CIRNO.



Average spike weight



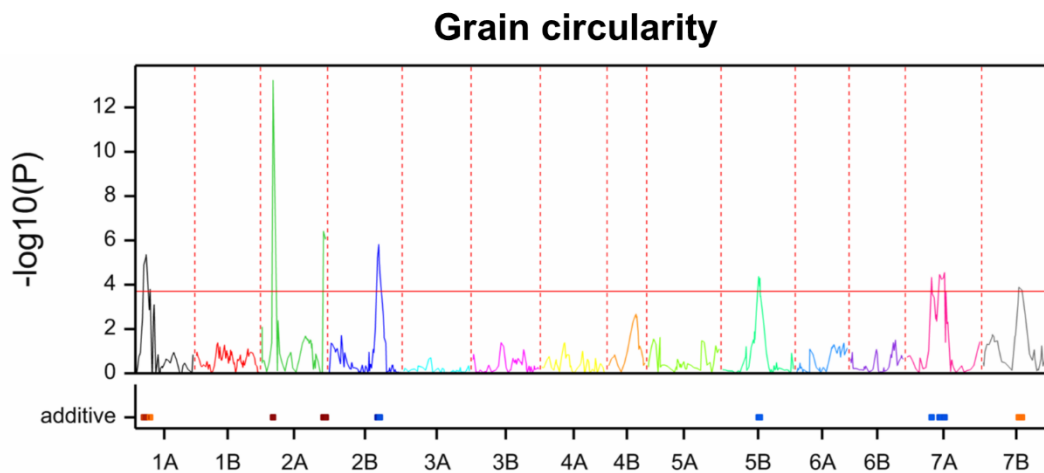
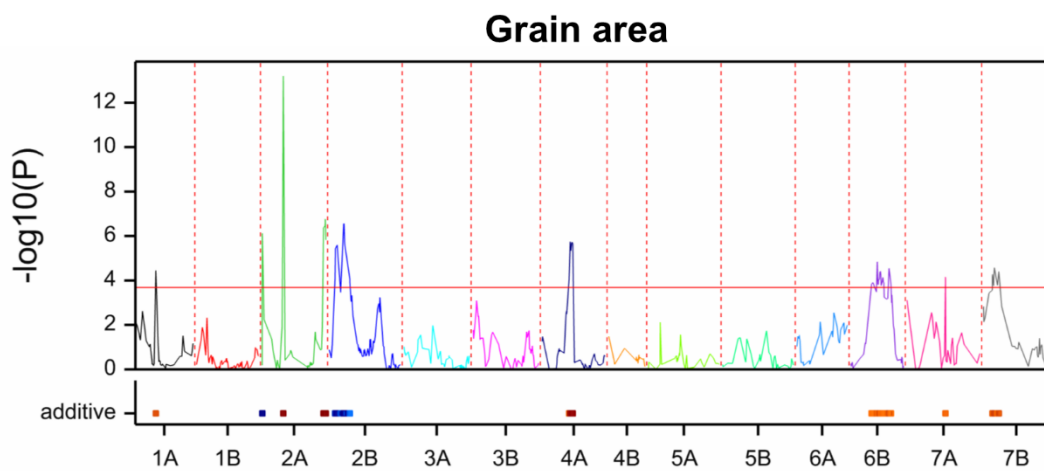
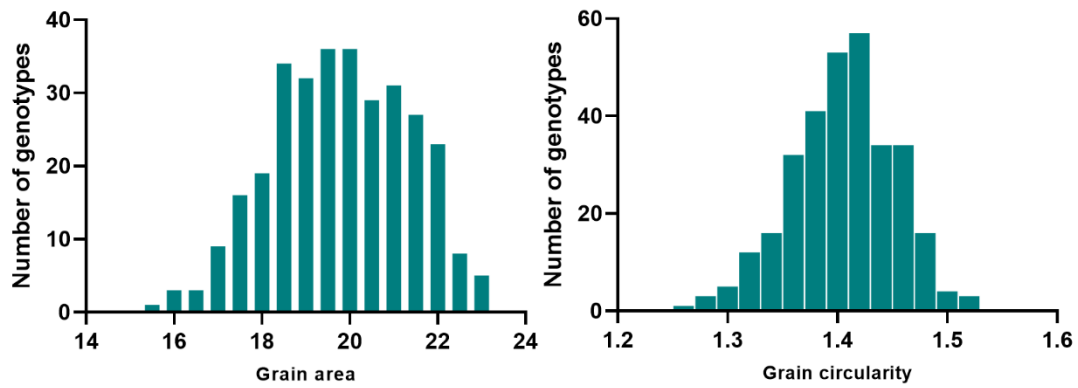
Grain weight per spike



Chromosomes

QTL effects:
additive (blue=Parent 1 ; yellow-red=Parent 2)

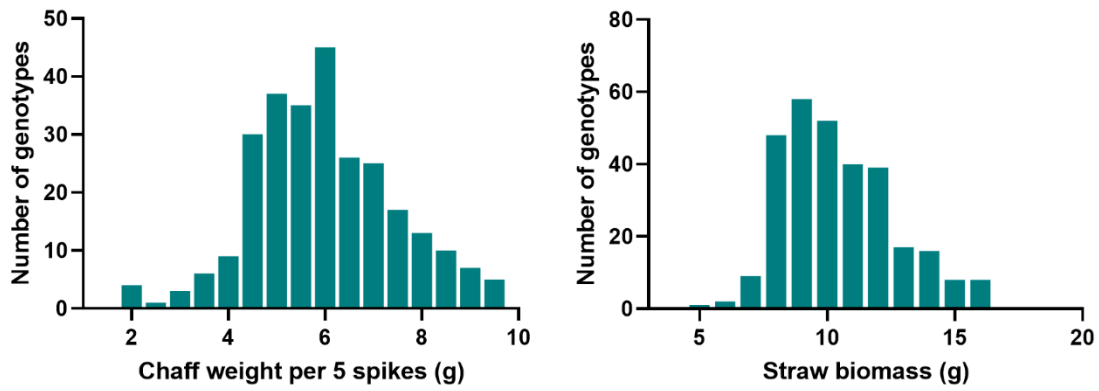
Appendix Figure 13. Phenotypic distribution and composite interval mapping of average spike weight and grain weight per spike in TRI 984x CIRNO RILs.
Note: Parent 1: TRI 984 and Parent 2: CIRNO.



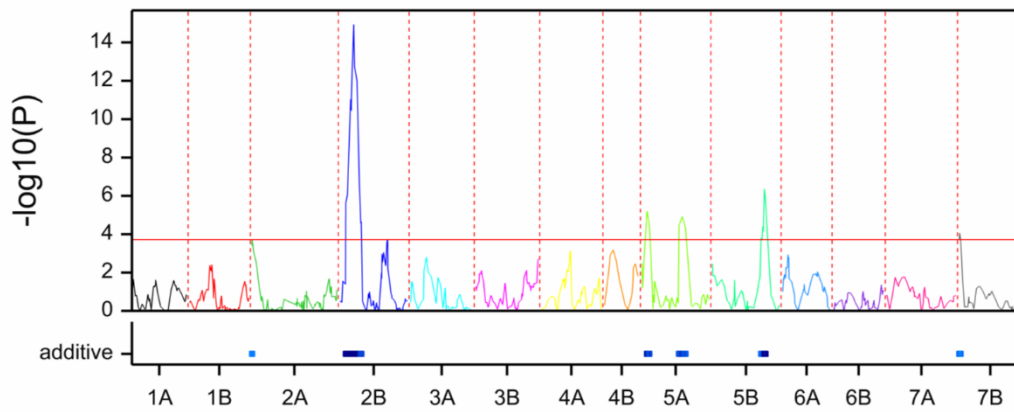
Chromosomes

QTL effects:
 additive (blue=Parent 1 ; yellow-red=Parent 2)

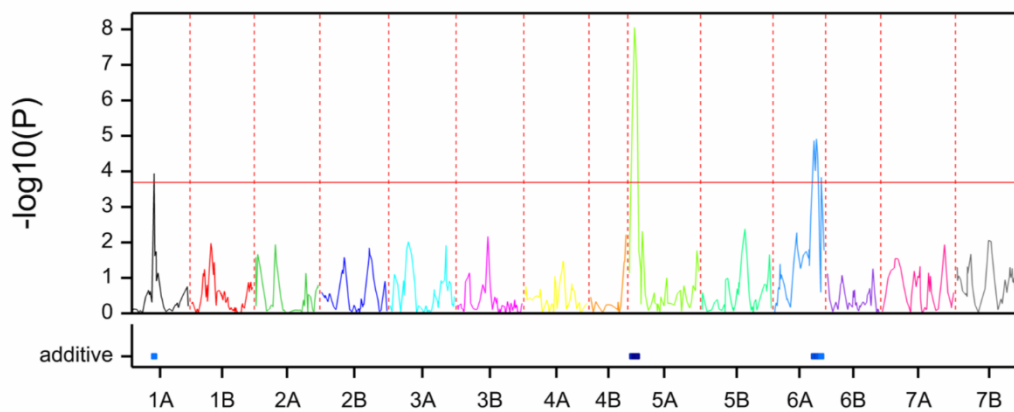
Appendix Figure 14. Phenotypic distribution and composite interval mapping of grain area and grain circularity in TRI 984x CIRNO RILs. Note: Parent 1: TRI 984 and Parent 2: CIRNO.



Spike chaff weight



Straw biomass



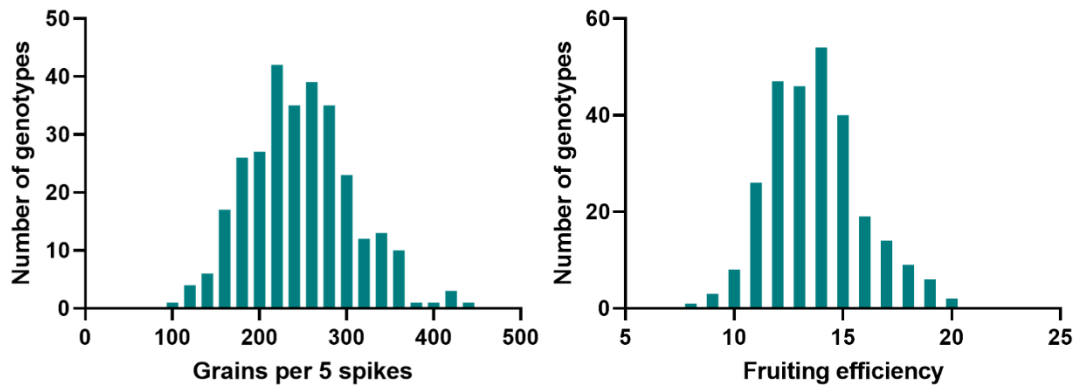
Chromosomes

QTL effects:

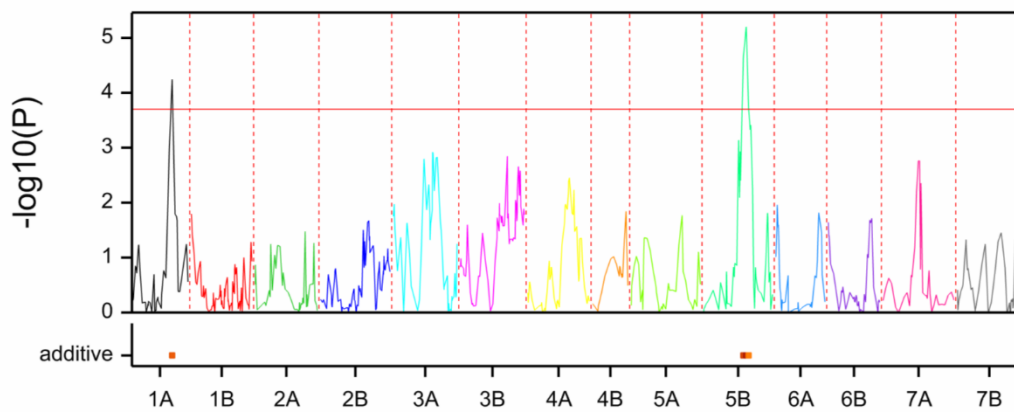
additive (blue=Parent 1 ; yellow-red=Parent 2)

Appendix Figure 15. Phenotypic distribution and composite interval mapping of spike chaff weight and straw biomass in TRI 984x CIRNO RILs.

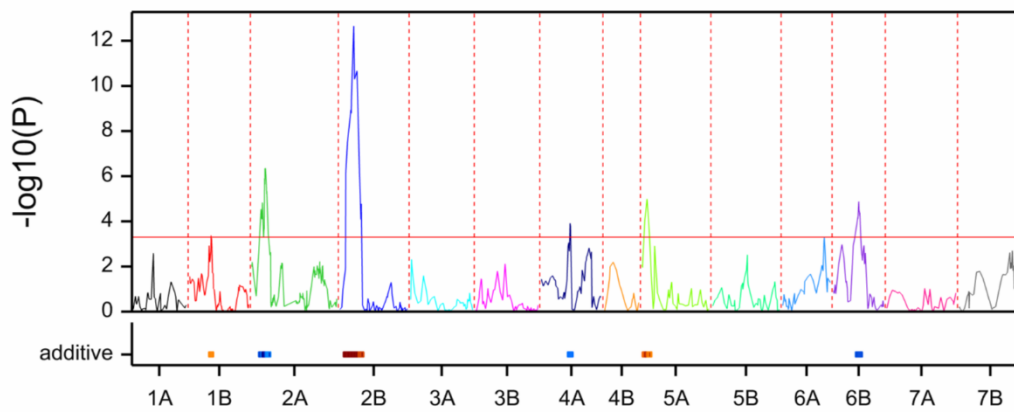
Note: Parent 1: TRI 984 and Parent 2: CIRNO.



Grains per spike



Fruiting efficiency

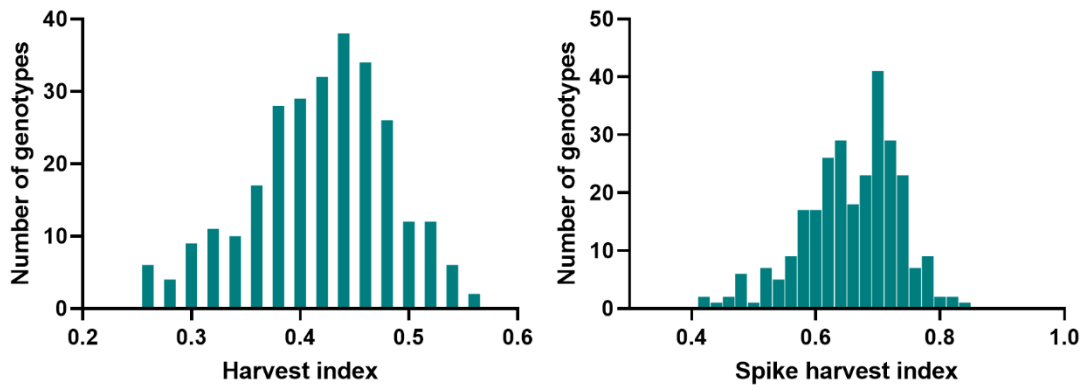


Chromosomes

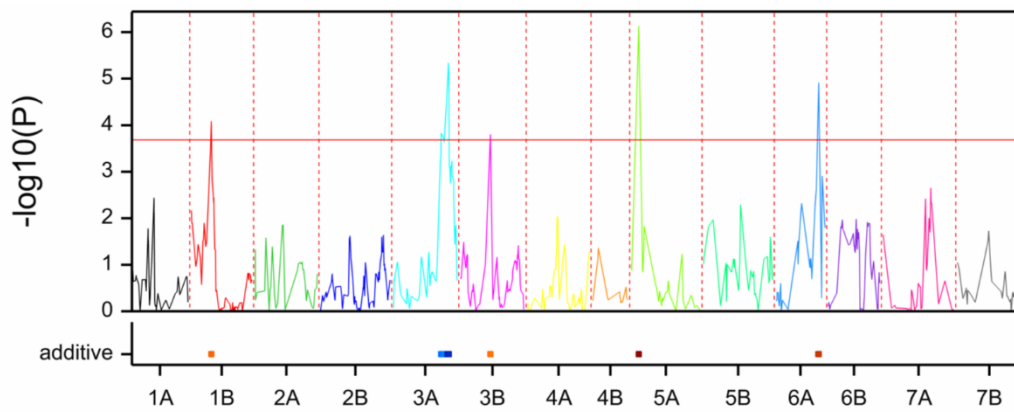
QTL effects:

additive (blue=Parent 1 ; yellow-red=Parent 2)

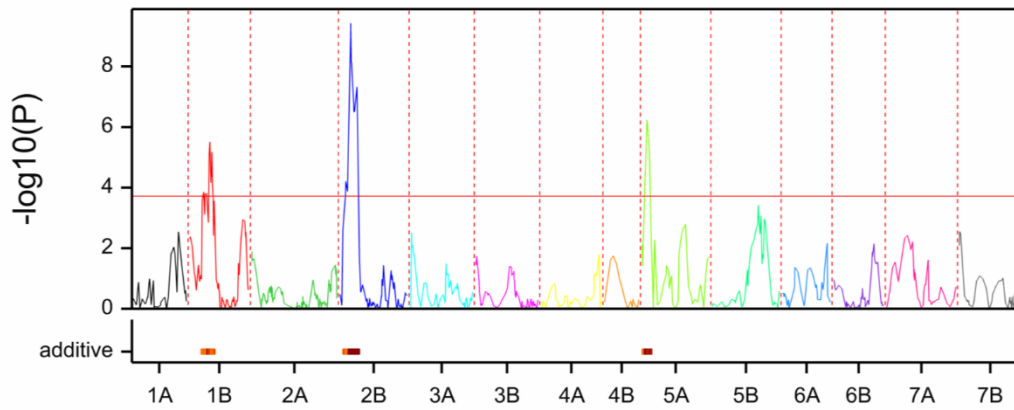
Appendix Figure 16. Phenotypic distribution and composite interval mapping of grains per spike and fruiting efficiency in TRI 984x CIRNO RILs.
 Note: Parent 1: TRI 984 and Parent 2: CIRNO.



Harvest Index



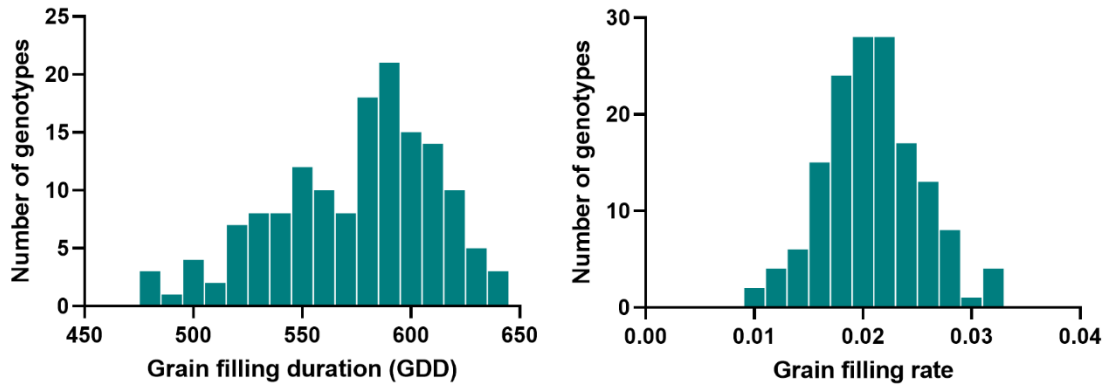
Spike harvest index



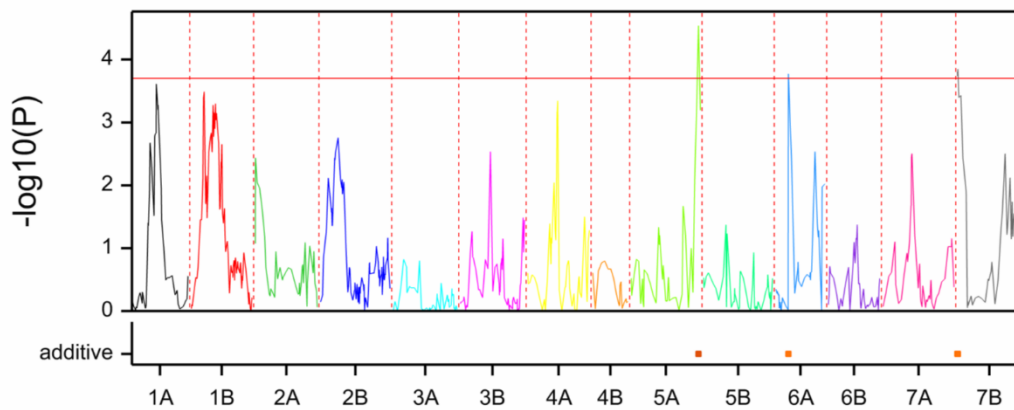
Chromosomes

QTL effects:
additive (blue=Parent 1 ; yellow-red=Parent 2)

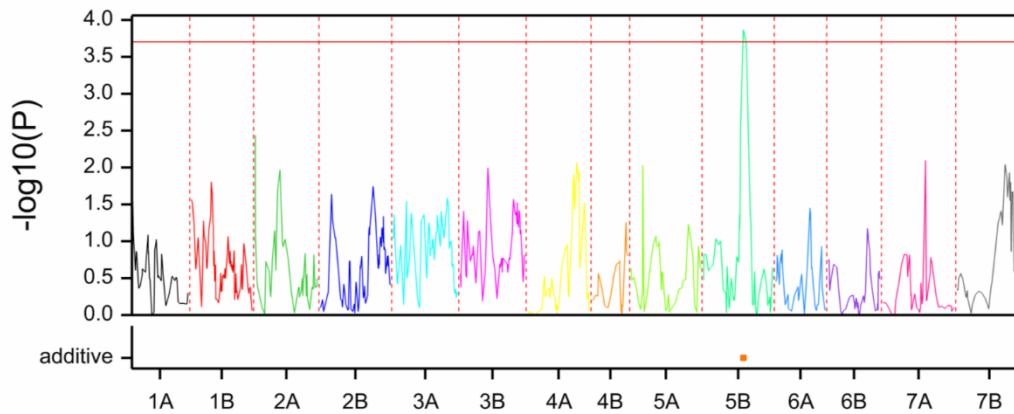
Appendix Figure 17. Phenotypic distribution and composite interval mapping of harvest index and spike harvest index in TRI 984x CIRNO RILs.
Note: Parent 1: TRI 984 and Parent 2: CIRNO.



Grain filling duration



Grain filling rate



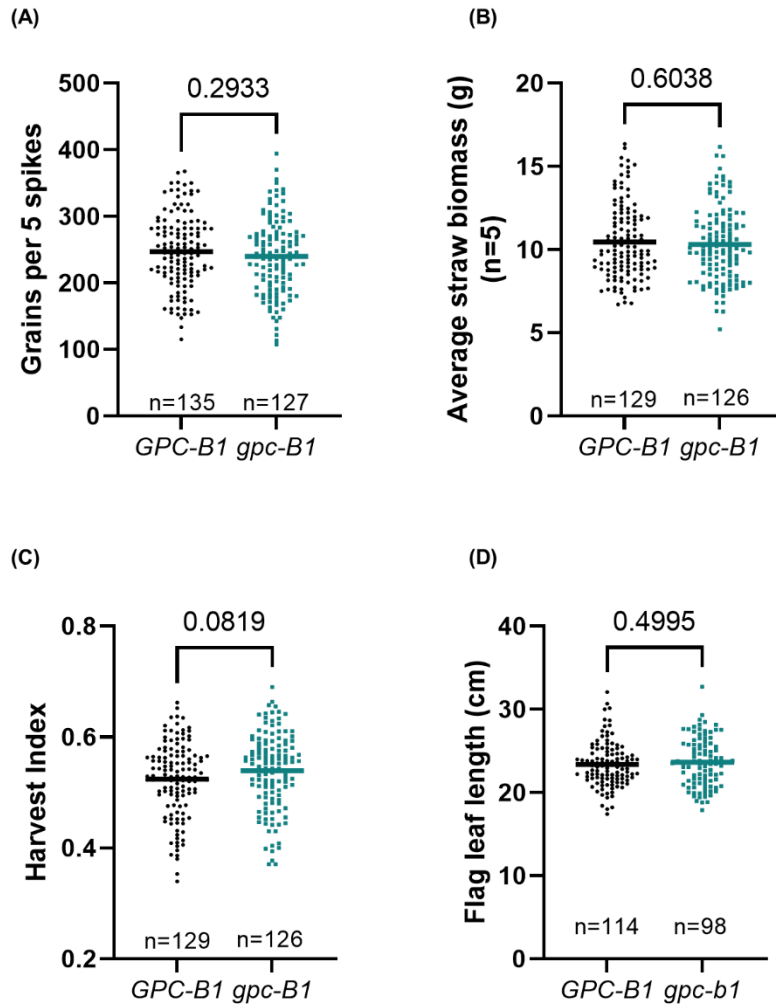
Chromosomes

QTL effects:

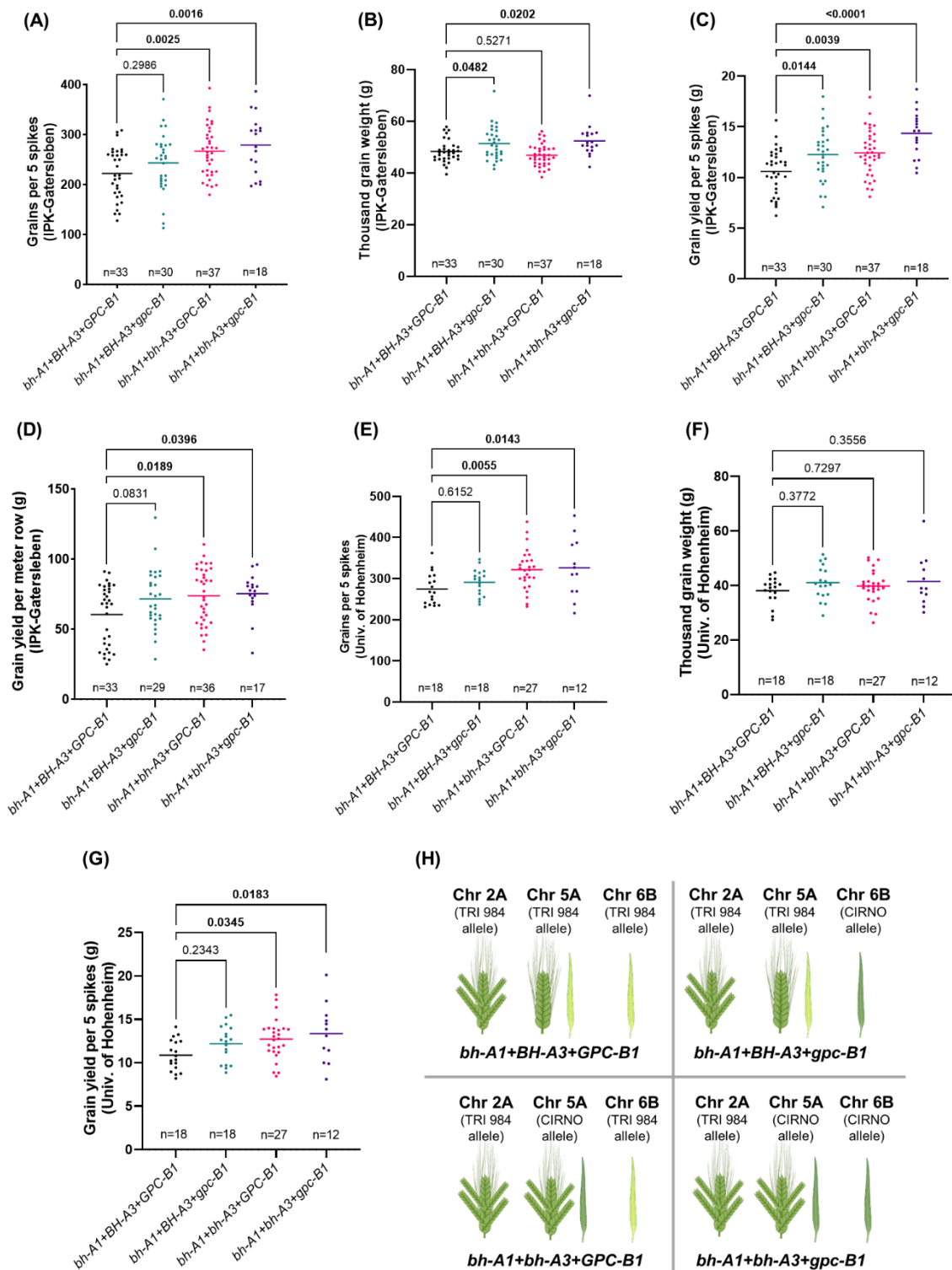
additive (blue=Parent 1 ; yellow-red=Parent 2)

Appendix Figure 18. Phenotypic distribution and composite interval mapping of grain filling duration and grain filling rate in TRI 984x CIRNO RILs.

Note: Parent 1: TRI 984 and Parent 2: CIRNO.

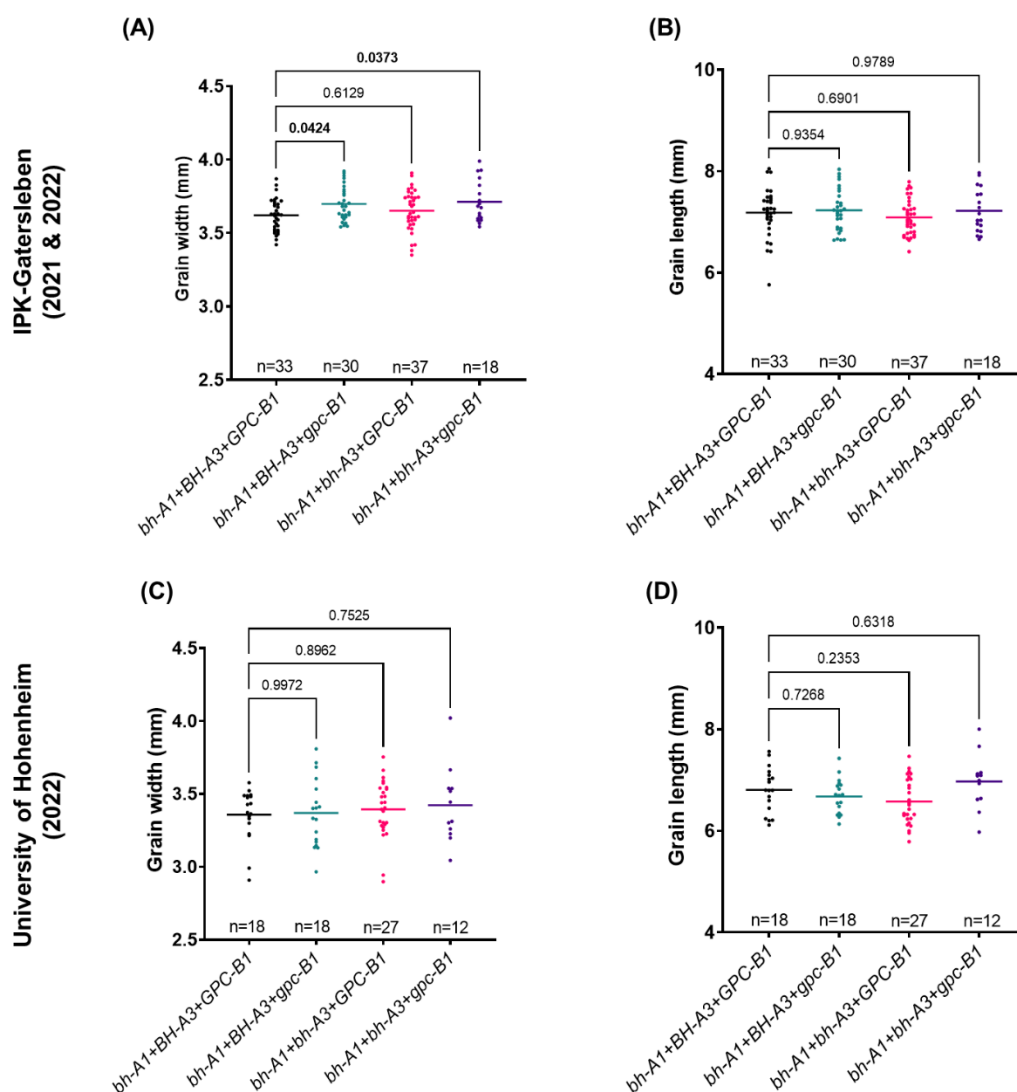


Appendix Figure 19. *gpc-B1* does not influence (A) Grains per 5 spikes, (B) Straw biomass, (C) Harvest index and (D) Flag leaf length. Note: Data obtained from field grown plants was used for the analysis in (A-D).



Appendix Figure 20. *bh^t-A1*, *bh^t-A3*, and *gpc-B1* balance the grain yield trade-offs in spike-branching recombinants. The RILs with various combinations of alleles were phenotyped at IPK-Gatersleben (2021 & 2022) and the University of Hohenheim (2022). At IPK, the spike-branching RILs that senesce late (*bh^t-A1+bh^t-A3+gpc-B1*) had (A) higher grain number per 5 spikes; (B) increased thousand-grain weight at IPK, (C) more grain yield per five spikes and (D) Finally, grain yield per meter row was also higher in the stay-green spike-branching RILs (calculated only at IPK). Likewise, at Hohenheim, (E) we observed more grains per five spikes,

(F) but no change in thousand-grain weight; eventually, (G) there was an increase in grain yield per spike. (H) pictorial depiction of the various allelic combinations that are analyzed in (A-G). Note: In (A-G), one-way ANOVA followed by Dunnett's test was used to determine the statistical significance. All the comparisons are made with respect to '*bh^t-A1+BH^t-A3+GPC-B1*' allelic combination, and the corresponding P-values are displayed in all the graphs (significant ones are in bold). Data obtained from field grown plants was used for the analysis in (A-G). The image (H) is partly created using biorender (<https://biorender.com/>). *bh^t-A1+BH^t-A3+GPC-B1*: Recombinants with one locus for spike-branching and two loci for accelerated senescence; *bh^t-A1+BH^t-A3+gpc-B1*: Recombinants with one locus each for spike-branching and delayed senescence; *bh^t-A1+bh^t-A3+GPC-B1*: Recombinants with two loci for spike-branching, while carrying one locus for delayed senescence; *bh^t-A1+bh^t-A3+gpc-B1*: Recombinants with two loci each for spike-branching and delayed senescence.



Appendix Figure 21. Genetic interaction among *bh^t-A1*, *bh^t-A3* and *gpc-B1*. The effect of various allele combinations at IPK (A) Grain width, (B) Grain length and at University of Hohenheim (C) Grain width, (D) Grain length. Note: Data obtained from field grown plants was used for the analysis in (A-D).

Zavitan	1	MPDDVPGVTSPMVYIGMLFSWFAWHIEDHELHSLNFLTHTGAPKTWYAVPGDRAAELEEVI	60
Svevo	1	60
Zavitan	61	RVHGYGGNPDRLASLAVLGEKTTLMSPEVIVAAGLPCCRLVQHPGEFVVTFRAYHVGFS	120
Svevo	61	120
Zavitan	121	HGFNCGEAANFATPQWLKFAKEAAVRRAMNYLPMLSHQQLLYLLAVSFISRTPRELLYG	180
Svevo	121	180
Zavitan	181	IRTSRLRDRRKEERELLKKREFLQDMISENELLC AFLKKKLIENAVLWEPDLLPSSTALH	240
Svevo	181 V	240
Zavitan	241	SCSSGPKAPLKVDDVHSIESVPKENSSSSDDIASRAGIQPKCMSMDSKSSDAMSAAEAQKL	300
Svevo	241	300
Zavitan	301	DTDTDDGDLPFDLSIDSGSLTCVACGILGFPMAILQPSKKALEDMSLVDIERFKLNCE	360
Svevo	301	360
Zavitan	361	KENHSNAIPCSPPDSISGHPVIAKRPSSPVAQSNFSHQNAESDKDGVLDGPLLPHNSA	420
Svevo	361	420
Zavitan	421	HSCNSENTLNP GINTETTETKIP SARFGIEFSKQTGRGDIDAQATESCGNTVDWNITSAF	480
Svevo	421 T	480
Zavitan	481	VRPRIFCLQHALEIEELLEGGGAHALIICHADYTKLKALAI SIAEEIEFQDCKDVPLA	540
Svevo	481 G	540
Zavitan	541	NASKSDLHLINISIDDEGYKEDERDWTQMG LNMKYFAKLRKETPGCQEQPPLSFWKRLD	600
Svevo	541	600
Zavitan	601	ISDKPSPISVVPNLKWLRRARTPYRVVGYAASRNATVGPDVVSPAVTKAEMGTSGNAYE	660
Svevo	601 R	660
Zavitan	661	NAKEQRTGEQDAPLEPSRLQEADDVADMHTCSEDIDQDMHCLIGSKRQRTAEQNAPLQPS	720
Svevo	661 A	720
Zavitan	721	RLQEADDVDMHMCSDNDQDMHRLIGIPVAAA EYPMTHQVCEGTVSVSTCELDDLVSAS	780
Svevo	721 T M	780
Zavitan	781	TSDDPICS AHSQDSPGVSDDF TTEQQCVQSD ELTSSVAMSAQQFLVDGSM TAEDSSNHEN	840
Svevo	781 S	840
Zavitan	841	LGSYNTSECKDKQLQVQQEQENIELCNNAGRNLAAAVQVNSGHFGDKAVNLKSAIPTES	900
Svevo	841	900
Zavitan	901	QHEYPKRDAIVLEGMQAALTTVVS GENRNSVNT ELD SLGILLGALAEESILADVP GKDEV	960
Svevo	901	960
Zavitan	961	DDASLTMLTASIDQSAGDV AHNEVIETSSSSV GASISCKGRTL SNLASD GSLRIQNAEI	1020
Svevo	961	1020
Zavitan	1021	QNKQENAE EVGAWNCQGLKNSRGILDSSANSLSDTGKSSGTPKAYQPDILSR SIGSSKRR	1080
Svevo	1021 T	1080
Zavitan	1081	SIICYVRRKRKQKRKRESELSTNSQSF GSFARAPCERLRPRR KPAVIEEPAEQIETAKP	1140
Svevo	1081	1140
Zavitan	1141	SAAATKGKR SKVVELFQCEIDFCDMTFESRAELRAHERNIC TDESCGKRFQSHKY LKRHQ	1200
Svevo	1141	1200
Zavitan	1201	CVHRDERPFKCPWDGCGMTFKWLWAQTEHIRVHTGERPYECSVPDCGQTFRYVSDYSRHR	1260
Svevo	1201	1260
Zavitan	1261	RKFNHY	1266
Svevo	1261	1266

Appendix Figure 24. Comparison of protein sequences of TRIDC4AG055050 (JmjC and C2H2 Zinc finger protein) between Zavitan and Svevo. The amino acid variations are indicated in red.

Zavitan	1	MAKGAVTLLVLFVTL SAVSQAQLQHGPGRHRTLSHGHRRSADRAAPTHLHFFFHDTVSGAS	60
Svevo	1 M P	60
Zavitan	61	PSAVRVVGPADPSSRTFFGMVNVMDPLTEGPDPGSAAVGRAQGLYMGADQAE LGFLQTM	120
Svevo	61	120
Zavitan	121	NLVLTSGPYNGSTLAVLGRNCPLTDVREMPVVGTTGAFRFARGYAQARTH WLD FKTDAT	180
Svevo	121	180
Zavitan	181	VEYDVVVMH	189
Svevo	181	189

Appendix Figure 25. Comparison of protein sequences of TRIDC4AG054960 (Dirigent protein) between Zavitan and Svevo. The amino acid variations are indicated in red.

Zavitan	MRPRPPADLVVGLFVLAVLVVVPWHAAAAGDGGGMVRTDGTRFVAGDGDRTVYLSGFNA	60
Svevo D L	60
Zavitan	YWLMEASDPSRRGGVVSFRQAAAHGLNLARTWAFSDGGDRPLQSSPSVYHEDMFQGLD	120
Svevo	120
Zavitan	FVVAEARRHGIYLLCLTNFDDFGGKRQYVQWAREDVAAGAGAHNLT SADDFDNTLVK	180
Svevo	180
Zavitan	SYYKNHVKTVLTRVNTVSGVAYRDDPAIFGWELMNEPRCGADPTGAMVQAWVEEMAPYLK	240
Svevo	240
Zavitan	AIDAAHLVTAGLEGFYGDGAHESKELNPWGIYYGTNFVATHQAAGIDFATIHLYPDVWLW	300
Svevo	300
Zavitan	GSTADQQARFRNWTASHVSDTHRHLRKPLLVT EY GKFLWEEGGENATSATQRRDRFLGT	360
Svevo	360
Zavitan	VLDAIYESASRGGPLVGGAFWQLLLDGDGMDALKDGYQIVLPEDARAASIISDHSEKMAE	420
Svevo	420
Zavitan	LSEQDAAESGRRTTRKIGSFGS WDGTHPYVQRFLIRFVSL LRSVSSLFGPM	471
Svevo V	471

Appendix Figure 26. Comparison of protein sequences of TRIDC4AG054920 (MAN1; Mannan endo-1,4-beta-mannosidase 4) between Zavitan and Svevo. The amino acid variations are indicated in red.

Appendix Table 1. Summary of the QTLs mapped in TRI 984 x CIRNO population.

Chromosome	Trait	Start (cM)	Position (cM)	End (cM)	Phenotypic variance (%)	High value allele	Additive effect
Chr 1A	Peduncle senescence	6.034	19.6	33.166	5.954	CIRNO	4.81
Chr 1A	Florets per spikelet	9.324	24.3	39.276	5.533	TRI984	0.202
Chr 1A	Grain circularity	18.165	31.1	44.035	6.173	CIRNO	0.012
Chr 1A	Grain lb ratio	18.236	31.1	43.964	6.199	CIRNO	0.03
Chr 1A	Plant height	66.126	71.71	77.294	12.457	CIRNO	2.53
Chr 1A	Spike length	68.257	77.5	86.743	8.067	CIRNO	0.321
Chr 1A	Grains per spike	115.234	119.4	123.566	16.245	CIRNO	19.925
Chr 1B	Harvest index	27.071	59.2	91.329	3.447	CIRNO	0.011
Chr 1B	Spike harvest index	49.395	61.5	73.605	6.497	CIRNO	0.03
Chr 1B	Flag leaf width	45.005	64.4	83.795	4.261	TRI984	0.038
Chr 1B	Fruiting efficiency	0	65.3	179.9	1.946	CIRNO	0.303
Chr 1B	Flag leaf senescence	55.6	66.19	76.78	7.221	CIRNO	0.221
Chr 1B	Flag leaf length	64.749	72.7	80.651	9.153	TRI984	0.841
Chr 1B	Grain weight per spike	150.812	162	173.188	6.911	CIRNO	0.753
Chr 2A	Average Spike weight	0	0.44	18.033	4.935	TRI984	0.762
Chr 2A	Spike chaff weight	0	0.5	44.689	3.007	TRI984	0.298
Chr 2A	Spike length	18.912	31.3	43.688	6.381	CIRNO	0.285
Chr 2A	Flag leaf verdancy_Heading	22.577	31.3	40.023	8.466	CIRNO	0.812
Chr 2A	Grain circularity	23.844	31.3	38.756	9.67	CIRNO	0.015
Chr 2A	Spike node density	24.471	31.3	38.129	10.431	TRI984	0.092
Chr 2A	Spike branching	27.395	31.3	35.205	17.244	TRI984	0.438

Chromosome	Trait	Start (cM)	Position (cM)	End (cM)	Phenotypic variance (%)	High value allele	Additive effect
Chr 2A	Thousand-grain weight	21.772	32	42.228	10.154	CIRNO	1.816
Chr 2A	Grain lb ratio	28.582	35.5	42.418	13.199	CIRNO	0.049
Chr 2A	Grain length	30.721	35.7	40.679	13.403	CIRNO	0.169
Chr 2A	Fruiting efficiency	31.117	41.3	51.483	7.453	TRI984	0.593
Chr 2A	Grain area	38.636	44	49.364	10.032	CIRNO	0.494
Chr 2A	Grains per spikelet	69.318	73.3	77.282	17.885	CIRNO	0.237
Chr 2A	Florets per spikelet	69.041	80.6	92.159	6.735	CIRNO	0.223
Chr 2A	Spike branching	0	140.9	183.9	1.54	TRI984	0.131
Chr 2A	Spike branching	0	177.1	183.9	1.802	TRI984	0.141
Chr 2A	Grain circularity	166.759	177.1	183.9	7.361	CIRNO	0.013
Chr 2A	Thousand-grain weight	156.16	182.4	183.9	3.837	CIRNO	1.116
Chr 2A	Grain area	164.622	182.4	183.9	4.9	CIRNO	0.345
Chr 2A	Grain length	173.323	182.4	183.9	8.19	CIRNO	0.132
Chr 2A	Grain lb ratio	173.283	183.9	183.9	7.206	CIRNO	0.036
Chr 2B	Spike harvest index	27.201	32.8	38.399	12.426	CIRNO	0.028
Chr 2B	Spike node density	18.031	34.3	50.569	5.213	CIRNO	0.065
Chr 2B	Grain area	26.677	41.8	56.923	5.494	TRI984	0.366
Chr 2B	Fruiting efficiency	37.13	41.8	46.47	14.634	CIRNO	0.831
Chr 2B	Spike chaff weight	39.261	41.8	44.339	25.822	TRI984	0.873
Chr 2B	Flag leaf length	41.587	63.9	86.213	4.224	TRI984	0.571
Chr 2B	Florets per spikelet	127.306	133	138.694	12.243	CIRNO	0.301
Chr 2B	Grains per spikelet	85.933	139.6	193.267	2.823	CIRNO	0.082

Chromosome	Trait	Start (cM)	Position (cM)	End (cM)	Phenotypic variance (%)	High value allele	Additive effect
Chr 2B	Grain circularity	115.163	143.2	171.237	3.698	TRI984	0.009
Chr 2B	Grain lb ratio	117.736	143.2	168.664	3.903	TRI984	0.026
Chr 2B	Grain length	122.919	143.2	163.481	4.487	TRI984	0.098
Chr 2B	Flag leaf width	117.408	145.5	173.592	3.695	CIRNO	0.034
Chr 2B	Flag leaf length	154.428	177.6	200.772	4.127	CIRNO	0.565
Chr 2B	Spike branching	99.716	186.4	206	2.574	CIRNO	0.169
Chr 3A	Flag leaf length	0	53	189.1	2.393	TRI984	0.43
Chr 3A	Harvest index	152.021	163.2	174.379	6.916	TRI984	0.016
Chr 3A	Nodes per spike	89.168	182.6	189.08	2.554	CIRNO	0.105
Chr 3B	Nodes per spike	0	1.39	21.336	4.536	TRI984	0.368
Chr 3B	Spike length	0	1.4	31.451	3.565	TRI984	0.213
Chr 4A	Average Spike weight	56.982	70.31	83.638	6.034	CIRNO	0.842
Chr 4A	Days to heading	46.406	71.06	95.714	3.977	TRI984	7.674
Chr 4A	Grain area	62.419	81.3	100.181	4.704	CIRNO	0.338
Chr 4A	Thousand-grain weight	70.305	86.8	103.295	5.162	CIRNO	1.295
Chr 4A	Fruiting efficiency	55.357	87.4	119.443	3.452	TRI984	0.404
Chr 4A	Grain width	82.6	87.4	92.2	14.257	CIRNO	0.049
Chr 4A	Grain weight per spike	103.927	117	130.073	6.123	CIRNO	0.709
Chr 4A	Florets per spikelet	107.155	117.2	127.245	7.536	CIRNO	0.236
Chr 4A	Spike length	140.097	168.6	182.8	3.666	TRI984	0.216
Chr 4B	Nodes per spike	79.734	93.88	104.51	5.771	TRI984	0.415
Chr 5A	Flag leaf length	0	1.2	9.775	8.588	TRI984	0.815

Chromosome	Trait	Start (cM)	Position (cM)	End (cM)	Phenotypic variance (%)	High value allele	Additive effect
Chr 5A	Straw Biomass	12.861	15.12	17.379	28.86	TRI984	0.864
Chr 5A	Spike chaff weight	0	15.13	36.179	4.381	TRI984	0.36
Chr 5A	Fruiting efficiency	7.794	15.13	22.466	9.806	CIRNO	0.681
Chr 5A	Spike harvest index	10.56	15.13	19.7	14.925	CIRNO	0.031
Chr 5A	Days to heading	14.405	22.06	29.715	9.454	TRI984	11.832
Chr 5A	Harvest index	0	22.1	46.596	3.992	CIRNO	0.012
Chr 5A	Flag leaf width	16.652	22.1	27.548	12.734	TRI984	0.064
Chr 5A	Flag leaf senescence	15.189	38.18	61.171	4.147	TRI984	0.167
Chr 5A	Spike length	32.49	47.03	61.57	5.654	TRI984	0.268
Chr 5A	Nodes per spike	73.184	84.14	95.096	7.027	CIRNO	0.458
Chr 5A	Peduncle senescence	142.106	161.2	180.294	4.669	TRI984	4.259
Chr 5A	Spike node density	156.179	161.2	166.221	13.704	CIRNO	0.106
Chr 5A	Spike length	157.395	161.2	165.005	17.661	TRI984	0.474
Chr 5A	Spike branching	153.006	194.7	205.1	3.073	CIRNO	0.185
Chr 5A	Grain weight per spike	186.065	199.4	205.1	6.032	CIRNO	0.703
Chr 5A	Grain filling duration	189.941	199.4	205.1	7.915	CIRNO	10.573
Chr 5A	Grains per spikelet	192.141	199.4	205.1	9.894	CIRNO	0.154
Chr 5A	Average Spike weight	180.859	199.41	205.12	4.76	CIRNO	0.748
Chr 5A	Flag leaf senescence	192.314	199.41	205.12	10.091	TRI984	0.261
Chr 5B	Days to heading	23.326	69.27	115.214	2.966	CIRNO	6.627
Chr 5B	Plant height	74.071	81.99	89.909	9.184	TRI984	2.173
Chr 5B	Grain circularity	52.646	103.6	154.554	2.867	TRI984	0.008

Chromosome	Trait	Start (cM)	Position (cM)	End (cM)	Phenotypic variance (%)	High value allele	Additive effect
Chr 5B	Grain weight per spike	106.631	117.65	128.669	6.995	CIRNO	0.758
Chr 5B	Grain filling rate	112.449	117.65	122.851	13.275	CIRNO	0.002
Chr 5B	Average Spike weight	103.74	126.16	148.58	4.211	CIRNO	0.704
Chr 5B	Grains per spike	118.876	126.2	133.524	7.819	CIRNO	15.491
Chr 5B	Spike chaff weight	133.383	158.3	183.217	3.952	TRI984	0.342
Chr 5B	Florets per spikelet	191.808	204.3	204.3	6.34	CIRNO	0.216
Chr 6A	Grains per spikelet	0.000	2.800	39.167	3.253	TRI984	0.101
Chr 6A	Straw Biomass	115.566	123.2	130.834	9.476	TRI984	0.495
Chr 6A	Harvest index	77.674	127.2	145.7	2.892	CIRNO	0.01
Chr 6A	Flag leaf width	115.685	127.2	138.715	6.756	TRI984	0.046
Chr 6A	Grain width	132.445	145.7	145.7	6.059	TRI984	0.032
Chr 6B	Grain area	0	76.6	152.6	1.618	CIRNO	0.198
Chr 6B	Fruiting efficiency	63.477	76.6	89.723	6.106	TRI984	0.537
Chr 6B	Thousand-grain weight	66.775	76.6	86.425	7.673	CIRNO	1.578
Chr 6B	Grain width	67.712	76.6	85.488	8.335	CIRNO	0.038
Chr 6B	Peduncle senescence	72.712	76.6	80.488	17.312	TRI984	8.202
Chr 6B	Days to maturity	71.448	76.61	81.772	13.365	CIRNO	6.587
Chr 6B	Flag leaf senescence	74.74	76.61	78.48	34.605	TRI984	0.483
Chr 6B	Grain area	0	110.5	152.6	1.385	CIRNO	0.184
Chr 6B	Spike branching	0	147.5	152.6	2.472	TRI984	0.166
Chr 6B	Peduncle senescence	112.4	152.6	152.6	2.464	CIRNO	2.464
Chr 7A	Grain circularity	0	71	210.6	2.234	TRI984	0.007

Chromosome	Trait	Start (cM)	Position (cM)	End (cM)	Phenotypic variance (%)	High value allele	Additive effect
Chr 7A	Grain lb ratio	30.487	71	111.513	3.108	TRI984	0.024
Chr 7A	Grain length	51.941	71	90.059	4.674	TRI984	0.1
Chr 7A	Days to heading	48.248	82.67	117.092	3.335	CIRNO	7.028
Chr 7A	Grain circularity	0	108.3	210.6	2.212	TRI984	0.007
Chr 7A	Grain width	59.077	108.3	157.523	2.898	CIRNO	0.022
Chr 7A	Grain length	60.721	111.1	161.479	2.877	CIRNO	0.078
Chr 7A	Plant height	115.256	126.02	136.784	7.127	CIRNO	1.914
Chr 7A	Flag leaf width	125.974	136.5	147.026	7.256	TRI984	0.048
Chr 7A	Days to heading	189.262	210.65	210.65	4.337	TRI984	8.014
Chr 7B	Grain width	0	0.5	48.022	2.932	CIRNO	0.022
Chr 7B	Thousand-grain weight	0	0.5	31.17	3.528	CIRNO	1.07
Chr 7B	Days to heading	0	1.36	6.498	13.422	TRI984	14.098
Chr 7B	Grain filling duration	0	1.4	7.03	12.367	CIRNO	13.215
Chr 7B	Spike chaff weight	0	1.4	189.7	2.274	TRI984	0.259
Chr 7B	Days to maturity	0.174	4.48	8.786	15.759	TRI984	7.152
Chr 7B	Grain area	0	31.7	66.794	3.306	CIRNO	0.284
Chr 7B	Plant height	34.441	44.66	54.879	7.432	CIRNO	1.954
Chr 7B	Nodes per spike	79.365	90.38	101.395	6.997	CIRNO	0.457
Chr 7B	Grain lb ratio	0	102.4	189.7	2.277	CIRNO	0.02
Chr 7B	Grain circularity	48.387	102.4	156.413	2.818	CIRNO	0.008
Chr 7B	Spike length	150.168	188.3	189.7	3.187	TRI984	0.201

Appendix Table 2. Details of the mapped QTLs

Trait	1A	1B	2A	2B	3A	3B	4A	4B	5A	5B	6A	6B	7A	7B
Spike-branching			3	1					1			1		
Nodes per spike					1	1		1	1					1
Spike length	1	1				1	1		2					1
Spike node density			1	1					1					
Days to heading (HD)							1		1	1			2	1
Flag leaf SPAD_HD			1											
Flag leaf length		1		2	1				1					
Flag leaf width		1		1					1		1		1	
Florets per spikelet	1		1	1			1			1				
Grains per spikelet			1	1			1		1					
Grains per spike	1									1				
Flag leaf senescence		1							2			1		
Peduncle senescence	1								1			2		
Days to maturity												1		1
Grain filling duration									1					1
Grain filling rate										1				
Plant height	1									1			1	1
Straw biomass									1		1			
Average spike weight			1				1		1	1				
Grain weight per spike		1					1		1	1				
Thousand-grain weight			2				1					1		1
Grain length			2	1									2	
Grain width							1				1	1	1	1
Grain area			2	1			1					2		1
Grain l/b	1		2	1									1	1
Grain circularity	1		2	1						1			2	1
Harvest index		1			1				1		1			
Fruiting efficiency		1	1	1			1		1			1		
Spike chaff weight			1	1					1	1				1
Spike harvest index		1		1					1					

Appendix Table 3. Wild emmer introgression patterns in the ILs. Green boxes indicate the presence of Zavitan introgression in that particular chromosome. Based on [Bacher et al., 2021](#) with minor modifications.

IL / Chr.	% Zavitan genome	Introgressions													
		1A	1B	2A	2B	3A	3B	4A	4B	5A	5B	6A	6B	7A	7B
IL 34	4.15														
IL 66	6.87														
IL 40	3.12														
IL 74	3.14														
IL 18	3.60							Het							
IL 82	14.02														

Note: The Zavitan introgression at *QSL.ipk-4AL* in IL 18 was heterozygous when originally genotyped.

Appendix Table 4. List of PCR primers used for fine mapping *QSL.ipk-4AL*

No	Primer ID	Sequence (5' to 3')	Zavitan start position (Mbp)	Zavitan allele size (bp)	Svevo allele size (bp)
1	4AQLT_1.3_F	ACTACATTCTCTTACCTGTGGCA	627.36	259	231
	4AQLT_1.3_R	CCGAGATTGCATTACTTCTCTCAT			
2	4AQLT_1.4.1_F	GGACCTGCAATGTTAAGCTTGA	628.33	230	284
	4AQLT_1.4.1_R	ATTTTGCCAACCTGCGAGTG			
3	TRIDC4AG054470_F	CACAATGCTGGAAAAAGCAG	628.64	199	178
	TRIDC4AG054470_R	GTCATATTGCGAGCCAGGTT			
4	4AQLT_2.1.1_F	CTCGATTTACGTGCCGTACA	629.59	238	220
	4AQLT_2.1.1_R	GCCTCGCCGGATTTTCAGTAA			
5	4AQLT_2.2.1_F	AGCAACTAATTGTGCCGGGA	630.41	205	158
	4AQLT_2.2.1_R	CGTTCTCCACGTTCTCTCT			
6	4AQLT_2_F	TTGTTCCCTGGTTCCATCTC	630.57	257	283
	4AQLT_2_R	TCCTAGGGTGTGGTTAGGTTTC			
7	4A_632.26_F	GGCAATTCAGGGCAAATAGA	632.26	307	349
	4A_632.26_R	TGCTTTTGGCTGTCCTGTAA			
8	4A_633.52_F	AAGGAAGCAACCCAACCCC	633.52	216	240
	4A_633.52_R	TCCATTGGGCCCGGAGTG			

10. Abbreviations

%	Percent
°C	degree Celsius
bp	base pair
Chr	Chromosome
CIM	Composite Interval Mapping
cM	Centimorgan
FAO	The Food and Agriculture Organization
g	Gram
GH	Greenhouse
GWAS	Genome-Wide Association Study
ILs	Introgression lines
Mbp	Megabase pairs
mm	Millimeter
ng	Nanogram
NILs	Nearly isogenic lines
PCR	Polymerase Chain Reaction
p-value	Probability value
QTL	Quantitative Trait Locus
R ²	Coefficient of determination
RILs	Recombinant inbred lines
SIM	Simple Interval Mapping
SNP	Single Nucleotide Polymorphism
t ha ⁻¹	Tonnes per hectare
µl	Microliter
µm	Micrometer

11. Curriculum Vitae

Name: Ragavendran Abbai

Gender: Male

ORCID: 0000-0002-5712-910X

Education & Research experience

Doctoral student

August 2019 to present

Martin Luther University Halle-Wittenberg, Germany and Leibniz Institute of Plant Genetics and Crop Plant Research (IPK), Germany

Thesis title: Genetic cornerstones of grain yield determination in spike-branching wheat (*Triticum turgidum* L.)

Supervisor: Prof. Dr. Thorsten Schnurbusch

Publications:

1. **Abbai, R.***, Golan, G., Longin, F.H., and Schnurbusch, T.* (2024). Grain yield trade-offs in spike-branching wheat can be mitigated by elite alleles affecting sink capacity and post-anthesis source activity. *J Exp Bot* 75 (1), pp. 88-102 (*Joint corresponding author)
2. Golan, G., **Abbai, R.** and Schnurbusch, T. (2023). Exploring the trade-off between individual fitness and community performance of wheat crops using simulated canopy shade. *Plant Cell Environ* 46(10), pp. 3144-3157
3. **Abbai, R.***, Singh, V.K., Snowdon, R.J., Kumar, A. and Schnurbusch, T.* (2020). Seeking Crops with Balanced parts for the ideal whole. *Trends Plant Sci* 25(12), pp. 1189-1193 (*Joint corresponding author)

Oral presentations:

1. **Source-Sink strength determines grain yield in 'Miracle-Wheat'**. MonoGram network meeting, University of Reading, UK (2023)
2. **Unravelling the genetics of grain yield potential in wheat**. *From Seed to Pasta IV*, Bologna, Italy (2022)
3. **Genetics of trait trade-offs in wheat**. *CEPLAS-IPK summer school* on "Translational plant biodiversity research", Kloster Steinfeld, Germany (2022)
4. **Balanced Parts for the Ideal Whole**. Virtual training program on "Breeding Innovation for Crop Improvement to Enhance Genetic Gains", *International Rice Research Institute* (virtual; 2021)

Posters:

1. **Balanced parts for the ideal whole**. MonoGram network meeting (virtual; 2021)

2. **Seeking cereal crops with balanced parts for the ideal whole.** PSSC 2021 (virtual)
3. **Agroecological genetics and genomics for food-nutritional security in changing climate.** 22nd EMBL PhD symposium: The Roaring 20's, EMBL, Heidelberg, Germany (2020)

Research Fellow

November 2017 to July 2019

International Rice Research Institute (IRRI), South Asia Hub, Hyderabad, India

Supervisors: Dr. Arvind Kumar and Dr. Vikas Kumar Singh

Selected Publications:

1. Sinha, P., Singh, V.K., Saxena, R.K., Khan, A.W., **Abbai, R.**, Chitikineni, A., Desai, A., Molla, J., Upadhyaya, H.D., Kumar, A. and Varshney, R.K., (2020). Superior haplotypes for haplotype-based breeding for drought tolerance in pigeonpea (*Cajanus cajan* L.). *Plant Biotechnol J* 18(12), pp. 2482-2490
2. Sagare, D.B., **Abbai, R.**, Jain, A., Jayadevappa P.K., Dixit, S., Singh, A.K., Challa, V., Alam, S., Singh, U.M., Yadav, S., et al. (2020) More and more of less and less: Is genomics-based breeding of dry direct-seeded rice (DDSR) varieties the need of hour? *Plant Biotechnol J* 18(11), pp. 2173-86
3. **Abbai, R.**[†], Singh, V.K.[†], Nachimuthu, V.V., Sinha, P., Selvaraj, R., Vipparla, A.K., Singh, A.K., Singh, U.M., Varshney, R.K. and Kumar, A. (2019). Haplotype analysis of key genes governing grain yield and quality traits across 3K RG panel reveals scope for the development of tailor-made rice with enhanced genetic gains. *Plant Biotechnol J* 17(8), pp.1612-1622 ([†]Equal contribution)

M.Sc.

August 2015 to August 2017

Kyung Hee University, South Korea

Major: Biotechnology; CGPA: 4.265/4.3

Thesis title: Silica nanoparticles enhance the tolerance of *Panax ginseng* Meyer against the root rot causing fungus, *Ilyonectria mors-panacis* by regulating sugar efflux into apoplast

Supervisor: Prof. Dr. Deok Chun Yang

Selected Publications:

1. Farh, M.E.A., Kim, Y.J., **Abbai, R.**, Singh, P., Jung, K.H., Kim, Y.J. and Yang, D.C. (2020). Pathogenesis strategies and regulation of ginsenosides by two species of *Ilyonectria* in *Panax ginseng*: power of speciation. *J. Ginseng Res* 44(2), pp.332-340
2. **Abbai, R.**, Kim, Y.J., Mohanan, P., Farh, M.E.A., Mathiyalagan, R., Yang, D.U., Rangaraj, S., Venkatachalam, R., Kim, Y.J. and Yang, D.C. (2019). Silicon confers protective effect against ginseng root rot by regulating sugar efflux into apoplast. *Sci Rep* 9(1), pp.1-10

Patents:

1. Agent for preventing or treating Ginseng root rot ([KR1020180083032](#))
2. Composition for manufacturing metal nanoparticles comprising Siberian ginseng extract and uses thereof ([KR1020180036951](#))

B.Tech.

June 2011 to April 2015

Tamil Nadu Agricultural University, India

Major: Biotechnology

Project: Pyramiding of QTLs conferring tolerance against drought, salinity and submergence in rice

Supervisor: Prof. Dr. Raveendran Muthurajan

CGPA: 8.5/10

Publications:

1. Muthu, V., **Abbai, R.**, Nallathambi, J., Rahman, H., Ramasamy, S., Kambale, R., Thulasinathan, T., Ayyenar, B. and Muthurajan, R. (2020). Pyramiding QTLs controlling tolerance against drought, salinity, and submergence in rice through marker assisted breeding. *PLoS one* 15(1), p.e0227421
2. **Abbai, R.**[†], Rajagopalan, V.R.[†], Nallathambi, J.S., Dubey, H., Selvaraj, S., Varalakshmi, B.C., Mohan, S., Kumar, J., Maheswari, U., Muthurajan, R., *et al.* (2016). Proteomic analysis of compatible and incompatible interactions of wheat with *Puccinia triticina*. *Physiol Mol Plant Pathol* 96, pp.36-46 (†Equal contribution)

Awards

- **Netaji-Subash International Fellowship** (*Not Availed*), Indian Council of Agricultural Research (2019)
- **Best thesis award** (M.Sc. research), Kyung Hee University (2017)
- **President Scholarship**, Kyung Hee University, South Korea (2015-2017)
- **Student Research fellow**, Indian Academy of Sciences: IASc-INSA-NASI (2014)

Complete Publication list:

<https://scholar.google.com/citations?user=V3ELU7oAAAAJ>



12. Eidesstattliche Erklärung/Declaration under Oath

Ich erkläre an Eides statt, dass ich die Arbeit selbstständig und ohne fremde Hilfe verfasst, keine anderen als die von mir angegebenen Quellen und Hilfsmittel benutzt und die den benutzten Werken wörtlich oder inhaltlich entnommenen Stellen als solche kenntlich gemacht habe.

I declare under penalty of perjury that this thesis is my own work entirely and has been written without any help from other people. I used only the sources mentioned and included all the citations correctly both in word or content.

Datum / Date

*Unterschrift des Antragstellers /
Signature of the applicant*